Discrimination of Mobile Supramolecular Chirality:

Acylative Molecular Transformation by Organocatalysis

(可動性超分子キラリティーの識別:有機触媒を用いたアシル化による分子変換)

2015

Ayumi Imayoshi

(今吉 亜由美)

Table of Contents

Abbreviation

Ac	acetyl
Aq.	aqueous
Boc	*tert*-butyloxycarbonyl
Bu	butyl
^{t}Bu	*tert*-butyl
Bz	benzoyl
cat.	catalyst
CD	circular dichroism
COSY	correlation spectroscopy
dba	dibenzylideneacetone
DCC	*N,N'*-dicyclohexylcarbodiimide
de	diastereomeric excess
DEPT	distorsionless enhancement by polarization transfer
DFT	density functional theory
DMAP	4-dimethylaminopyridine 4-dimethylaminopyridine
DMF	*N*,*N*-dimethylformamide
DMSO	dimethylsulfoxide
dppp	1,3-bis(diphenylphosphino)propane
ee	enantiomeric excess
e.g.	for example
ent	enantio-
eq.	equivalent
Et	ethyl
h	hour
HMBC	heteronuclear multiple bond coherence
HMQC	heteronuclear multiple quantum correlation
HPLC	high performance liquid chromatography
HRMS	high resolution mass spectrometer
IBX	2-iodoxybenzoyc acid
^{i}Pr	isopropyl
IR	infrared
Me	methyl
m.p.	melting point
NMR	nuclear magnetic resonance
Ns	2-nitrobenzenesulfonyl
o-	ortho-
p-	para-
PPTS	pyridinium *p*-toluenesulfonate
PPY	4-pyrrolidinopyridine

PTLC	preparative thin-layer chromatography
rt	room temperature
sat.	saturated
s factor	selectivity factor
SM	starting material
TD-DFT	time-dependent-density functional theory
tert	tertially
Tf	trifluoromethanesulfonyl
THF	tetrahydrofuran
THP	tetrahydropyrane
TLC	thin-layer chromatography
TS	transition state
Ts	*p*-toluenesulfonyl
UV	ultraviolet
VCD	vibrational circular dichroism
XPhos	2-dicyclohexylphosphino-2′,4′,6′-triisopropylbiphenyl
ZPE	zero-point energy
1D	one dimension
2D	two dimensions

Theoretical Section

Preface

Organic chemists create new products, explore mechanisms, and control compounds at the molecular level, thereby contribute to macro-scale subjects such as material, medicinal, biological, and environmental subjects. Figure 1 shows the map of relationships among scientific paradigms (*1*, *2*). Since organic chemistry is a fundamental science that treats origin of all phenomena and functions at the molecular level, novel concepts in organic chemistry have the possibility for making an impact on a wide range of fields.

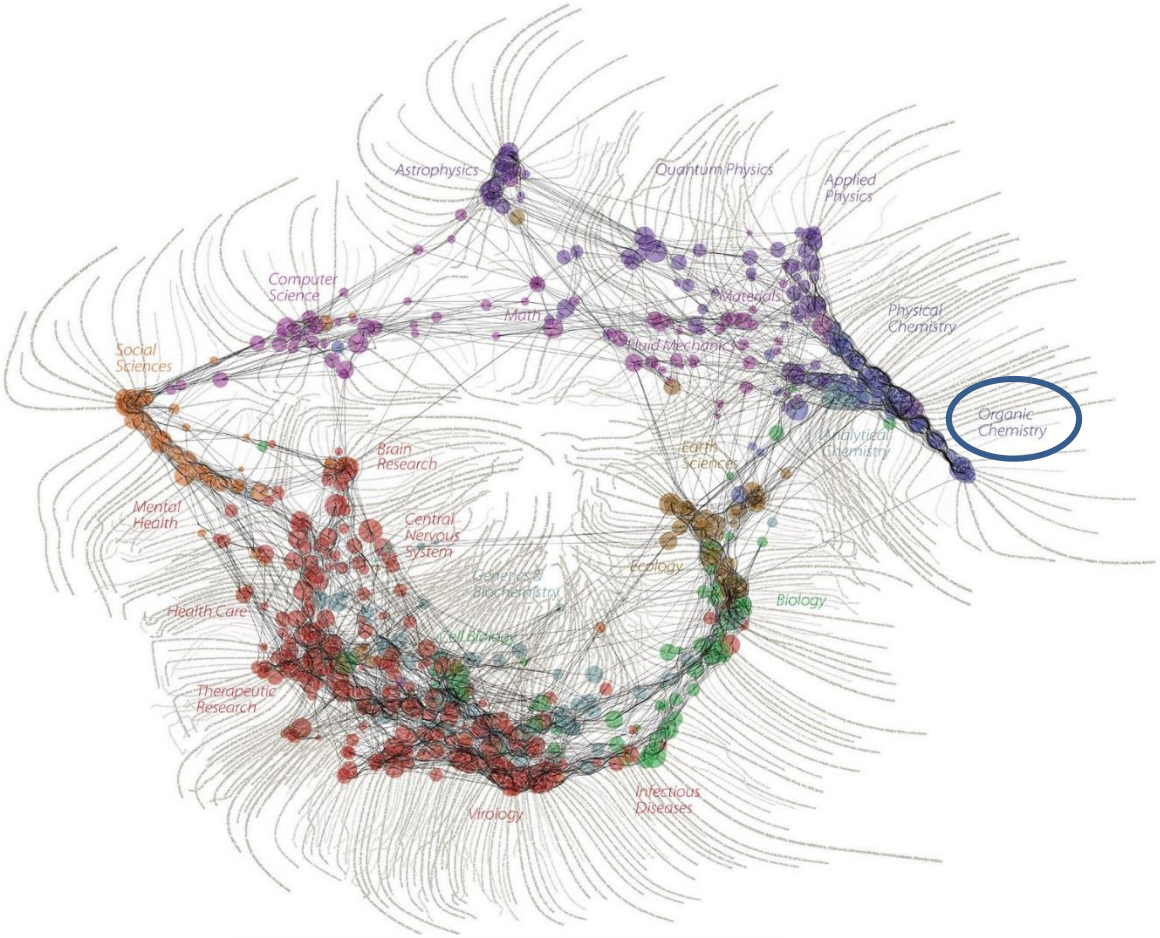

K. Boyack, D. Klavans, W. B. Paley, and K. Börner. *SEED* (2007).

Figure 1 | Relationships among scientific paradigms.

In the field of organic chemistry, asymmetric synthesis and chiral molecular transformation have been extensively developed during the last few decades. Beginning with the discovery of a proline catalyst (*3*-*8*), asymmetric synthesis has grown into one of the main research areas of modern organic chemistry. Catalytic asymmetric transformations have contributed to wide range of fields including medicinal chemistry and biochemistry because majority of organic compounds associated with living organisms are chiral.

Various kinds of chiralities are shown in Figure 2 (*9*-*20*). Asymmetric construction of conventional chiralities such as central chirality, axial chirality (*21*-*25*), planar chirality (*21*), and helical chirality (*26*-*30*) have already been actively studied. With the current state of chemical science, asymmetric synthesis of these fixed chiralities over covalent bonds is reaching a level of mature science.

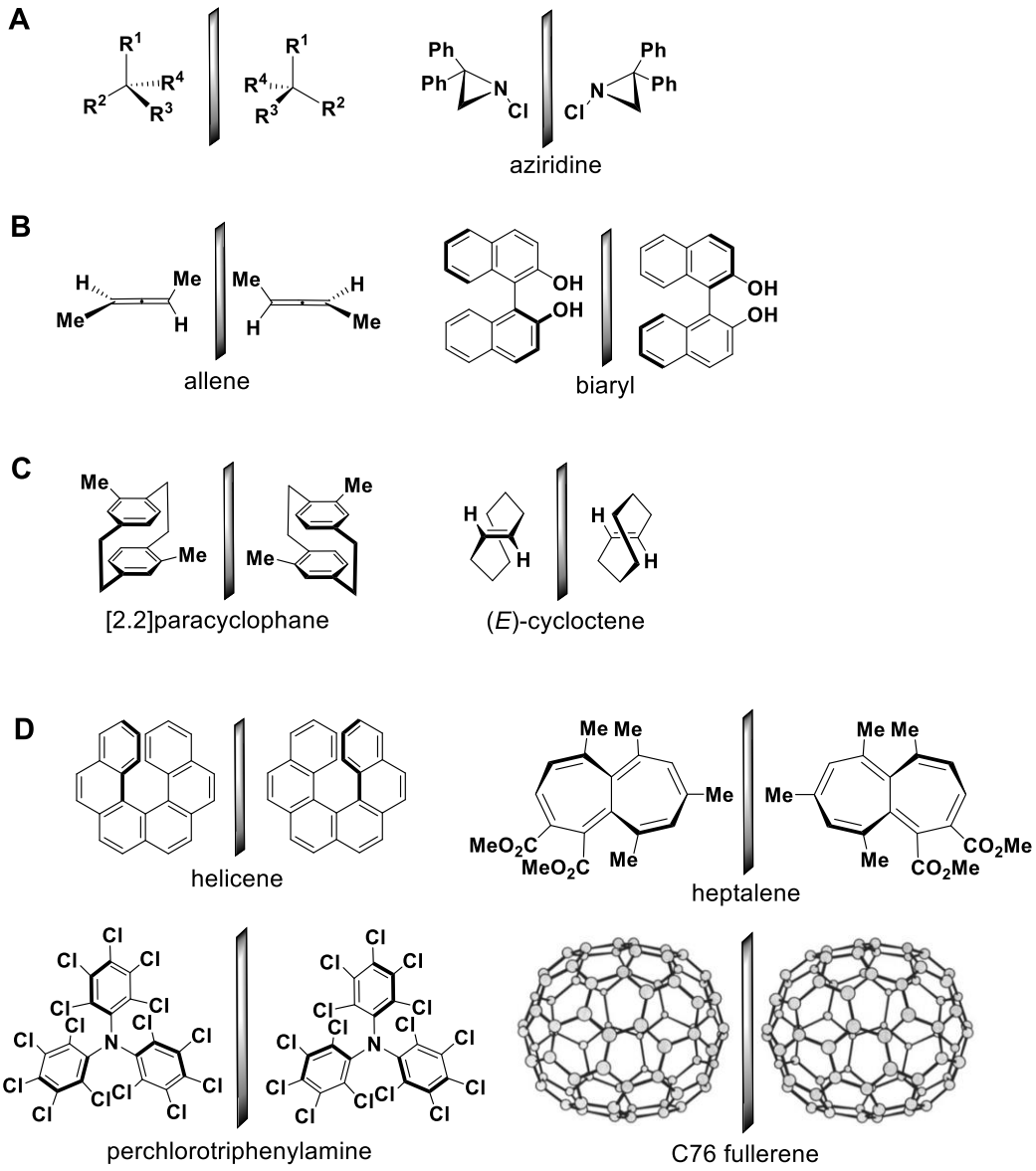

Figure 2 | Various kinds of chiralities. Conventional fixed chiralities over covalent bonds. (**A**) Central chirality. (**B**) Axial chirality. (**C**) Planar chirality. (**D**) Helical chirality.

On these fields approaching mature science, however, asymmetric synthesis of supramolecules still stands as an unsolved problem. Supramolecules such as rotaxanes and catenanes, consisting of more than two components linked non-covalent system, are known to possess unique supramolecular chirality as shown in Figure 3. Even though each component has no chirality, their combination brings topologically linked chirality, when each of the component has structural dissymmetry. Such chirality generated from the orientation of the components is called topological chirality (*31-33*).

The difference between topological chirality of supramolecules and other chiralities is the mobility of the topological chirality itself. Since two components can move freely from each other, the topological chirality, generated from the combination of these two phases, has mobility in the chiral environment itself. A molecule possessing topological chirality continuously changes its chiral environment with kinetically

lability. Thus, topological chirality of rotaxanes and catenanes can be called *mobile supramolecular chirality*. This mobile nature of topological chirality makes asymmetric construction of topologically chiral molecules much more difficult than the compounds with conventional chiralities. In fact, traditional molecular transformation does not work efficiently for the construction of the molecule with mobile supramolecular system. The most successful and pioneering example of asymmetric synthesis of topologically chiral supramoelcules so far achieved gave the rotaxane in up to only 4% ee (*34*). Thus, novel concept and method for the molecular transformation are required in organic chemistry, for achieving asymmetric synthesis of supramolecules.

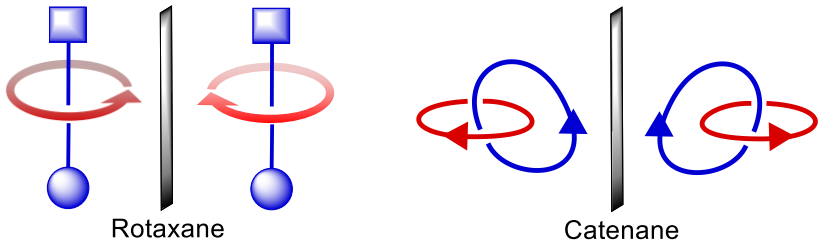

Figure 3 | Mobile supramolecular chirality. Topological chirality consisting of more than two components linked non-covalent system.

Toward discrimination of mobile supramolecular chirality, I first investigated the fundamental nature of catalytic acylation. In our laboratory, various acylative molecular transformations have been developed by using chiral 4-pyrrolidinopyridine (PPY) catalysts bearing substrate-recognition sites consisting of amino acid side chains (*35*-*39*). Among them, I focused on the most simple and fundamental molecular transformation (*35*), and elucidated the molecular recognition process promoted by the chiral PPY catalyst (Chapter 2). Then, I challenged asymmetric synthesis of supramolecules by using the chiral PPY catalyst. I achieved the first example of highly selective asymmetric discrimination of mobile supramolecular chirality (Chapter 4). In this thesis, I propose the concept of dynamic molecular recognition by catalysts for discrimination of mobile supramolecular chirality. The concept enables asymmetric synthetic chemistry to set foot into the fields of mobile supramolecular chemistry linked non-covalent system, beyond the conventional fixed covalent system. Furthermore, considering the high interest in applications of supramolecules in areas as diverse as molecular machine (*40, 41*), material science (*42, 43*), medicinal chemistry (*44, 45*), and synthetic chemistry (*46*-*48*), I expect that attractive chiral architectures of topologically chiral supramolecules will bring completely novel concepts into these fields, as well as the field of organic chemistry, as distinct new chiral sources. The concept of dynamic molecular recognition discussed in this thesis will establish new relationships among scientific paradigms in Figure 1.

Chapter 1: Overview

1.1 Mechanistic study for organocatalytic chemoselective monoacylation of 1,5-pentanediol

Various molecular transformations concerning site-selective acylation of polyol compounds have been developed by using PPY catalysts bearing substrate-recognition sites consisting of amino acid side chains. Among them, I focused on the organocatalytic chemoselective monoacylation of 1,5-penetanediol (**4**) (*35*) for elucidation of the molecular recognition process promoted by the catalyst. Although 1,5-pentanediol (**4**) has only hydroxy groups as recognition sites, the mechanistic aspect seems not so simple. Indolyl NH group in the amide side chains of the catalyst was found to be critically important for chemoselective monoacylation of **4**.

To elucidate the origin of the high selectivity for monoacylation, I investigated the monoacylation of 1,5-pentanediol (**4**) in the presence of C_2-symmetric catalysts **1**-**3** (Figure 4). The amide carbonyl group of the catalysts was suggested to play a main role for the selective monoacylation of **4**, and the indolyl NH group seems to also contribute to increasing the chemoselectivity and reactivity. The effect of the NH groups were found to be significant only when the catalyst has C_2-symmetric structure by comparison with the experimental results employing the corresponding C_1-symmetric catalysts.

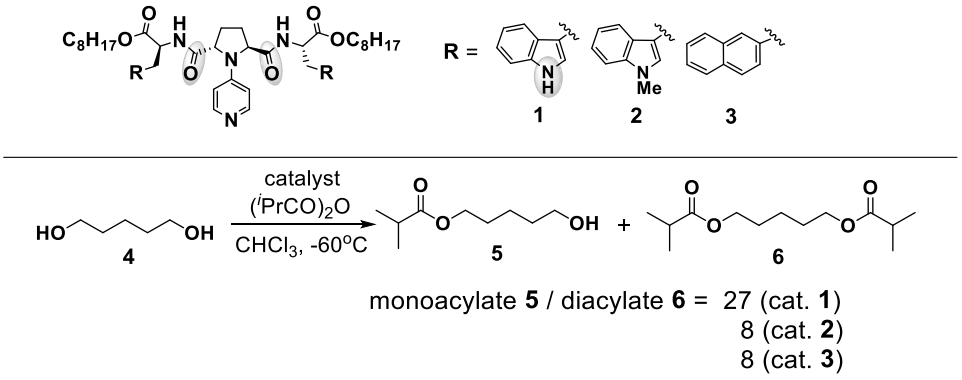

Figure 4 | Chemoselective monoacylation of 1,5-pentanediol (4).

Catalyst **1** has also been reported to promote substrate-selective acylation of **4** in the presence of other linear diols with different chain lengths. To elucidate the molecular recognition process, competitive acylations between **4** and 1,2-ethanediol (**7**) were carried out in the presence of catalysts **1**-**3** (Figure 5). Among catalysts **1**-**3**, only catalyst **1** was found to effectively accelerate the acylation of **4** in the presence of 1,2-ethylenediol (**7**) (Chemoselectivity = relative rate of acylation between **4** and **7** = $k_{\text{(acylation of 4)}} / k_{\text{(acylation of 7)}} = 4.5$).

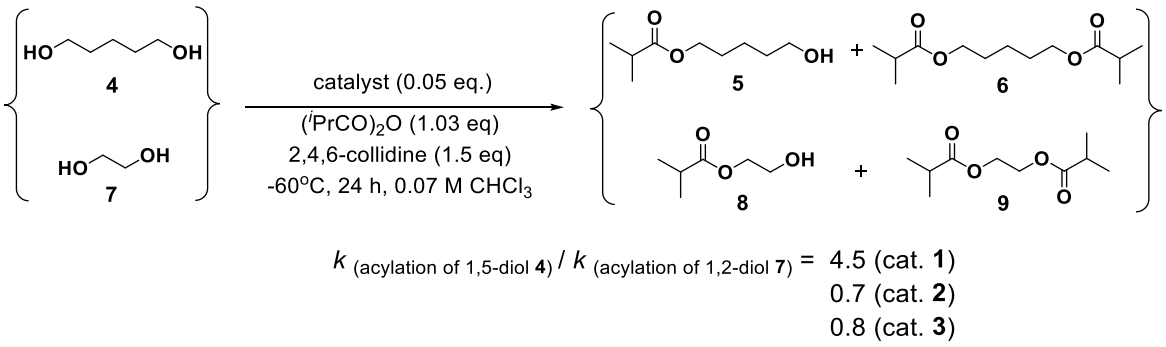

Figure 5 | Substrate-selective acylation of 1,5-pentanediol (4).

Theoretical study to elucidate the mechanism of the catalyst-controlled chemoselective acylation was well consistent with the experimental results. The computational results also indicated the importance of indolyl NH groups arranged in a C_2-symmetric fashion for chemoselective monoacylation of 1,5-diol **4** (Figure 6). C_2-Symmetric chiral PPY catalyst **1** flexibly changes its molecular recognition mode depending on the substrate structures.

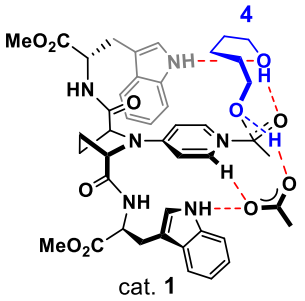

Figure 6 | Transition state of monoacylation of 1,5-pentanediol (4).

1.2 DMAP-catalyzed efficient synthesis of rotaxanes

Since supramolecules such as rotaxanes and catenanes possess attractive architectures, syntheses of these supramolecules have been one of the foci of current organic synthesis. Acylative end-cappings of the hydroxy group of pseudorotaxanes by DMAP catalyst have been known to produce rotaxanes, however, it afforded rotaxanes in low yields in the most cases. Under these circumstances, I developed DMAP-catalyzed efficient sysnthesis of rotaxanes. A pseudorotaxane, which is expected to be formed by mixing the axis component **10** and the ring component **11**, was treated with acyl chloride as an acyl donor, ^{t}BuCO$_2$H as a carboxylate ion source, and $AgPF_6$ in the presence of DMAP. Desired rotaxane **12** was successfully obtained in 94% yield (Figure 7).

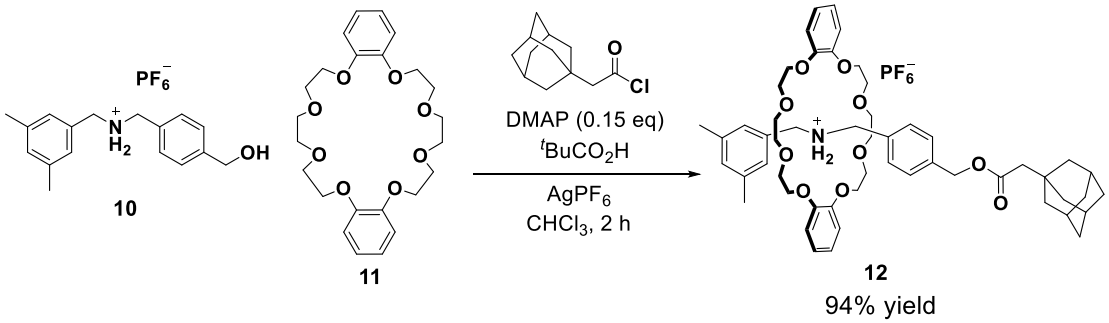

Figure 7 | DMAP-catalyzed synthesis of a rotaxane.

1.3 Discrimination of mobile supramolecular chirality: Kinetic resolution of topologically chiral racemic rotaxanes by organocatalysis

Among the fields of asymmetric synthesis approaching the mature science, asymmetric discrimination and catalytic synthesis of chiral supramolecules still stand as unsolved problems. Supramolecules such as rotaxanes and catenanes are known to possess topological chirality when each of the axis and/or ring components has dissymmetry. The extreme difficulty in asymmetric synthesis of such supramolecules may be resulting from conformational diversity and movability of topologically chiral supramolecules.

I have achieved the first example of highly enantioselective synthesis of topologically chiral rotaxanes by acylative kinetic resolution of the racemate. In the presence of **3**, an acylative kinetic resolution of a racemic rotaxane **13** afforded a topologically chiral rotaxane **13** with perfect enantiopurity (>99% ee) in excellent selectivity (*s* >16) along with acylate **14** (Figure 8). This kinetic resolution likely proceeded via the mechanism in which two molecules of catalysts **3** are involved. The concept of dynamic molecular recognition enabled asymmetric synthesis of mobile supramolecules constructed by non-covalent interaction.

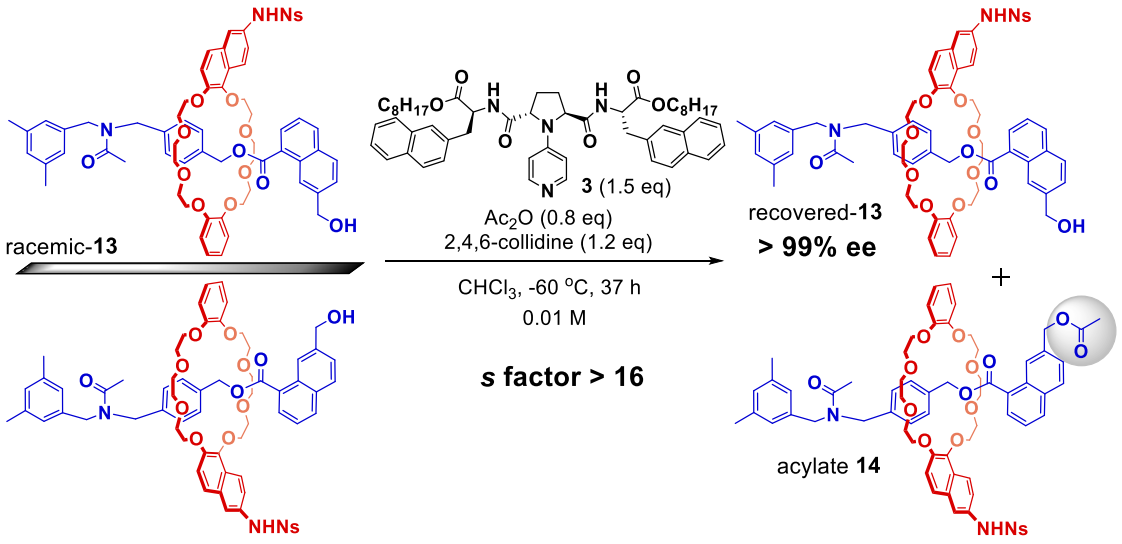

Figure 8 | Kinetic resolution of a topologically chiral racemic rotaxane.

Chapter 2: Mechanistic study of organocatalytic chemoselective monoacylation of 1,5-pentanediol

2.1 Backgrounds

2.1.1 Backgrounds of acylative molecular transformation

Fine molecular transformation is one of the fundamental challenges in organic synthesis. Kawabata and co-workers have developed numerous acylative molecular transformations of polyol compounds by using C_2-symmetric chiral 4-pyrrolidinopyridine (PPY) catalysts bearing substrate-recognition sites consisting of amino acid side chains (Figure 9, 10). For example, in the presence of chiral PPY catalyst **3** consisting of L-2-naphthylalanine side chains, geometry-selective acylation of NsHN-substituted α,α'-alkenediols have been achieved in >99% *E*-selectivity (Figure 9A) (*38*). Asymmetric desymmetrization of NsHN-substituted 1,7-diol was also accomplished with catalyst **3** to deliver the acylate in 97% ee (90% yield) (Figure 9B) (*39*).

Mechanistic insights into these selective acylation catalyzed by **3** have been proposed (Figure 9) (*49*). In both cases, multiple hydrogen-bonding interactions between catalyst **3** and the substrates depending on the substrate structures play important roles in the molecular recognition. The fundamental hydrogen bond between the amide carbonyl group of catalyst **3** and the acidic hydrogen of NHNs group in the substrate mainly contributes to the selective acylation, and simultaneously the other amide side chain of the catalyst acts cooperatively to further stabilize transition state of the selective acylation. Namely, catalyst **3** possesses the dual function of the two amide groups at C(2) and C(5) of the pyrrolidine ring in a C_2-symmetric fashion.

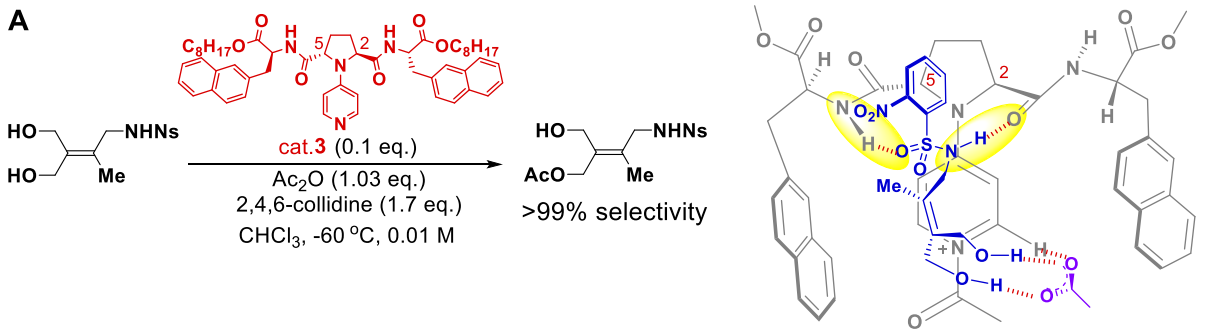

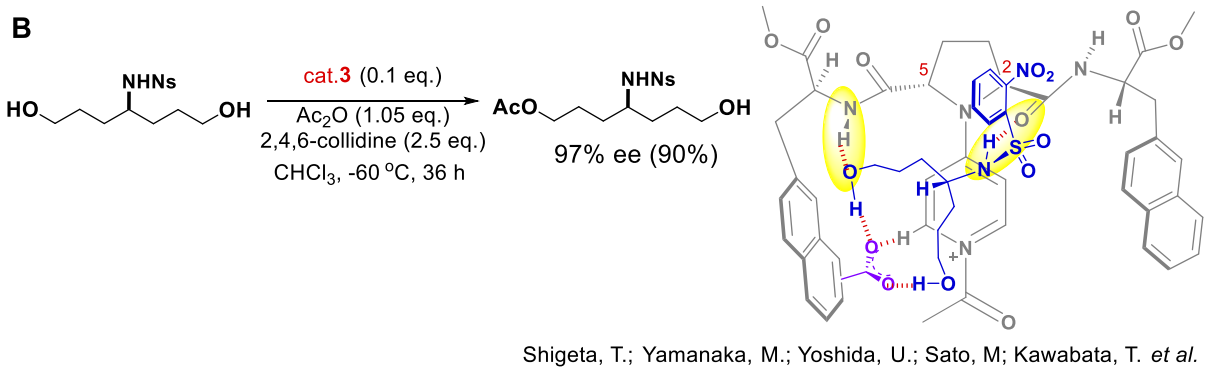

Figure 9 | Molecular transformations by chiral PPY catalyst 3. (**A**) Geometry-selective acylation of NsHN-substituted α,α'-alkenediols and the transition state model. (**B**) Asymmetric dissymmetrization of NsHN-substituted 1,7-diol and the transition state model.

Chiral PPY catalyst **1**, bearing L-tryptophan side chains, has been also known to achieve various selective molecular transformation. The chemoselective monoacylation of 1,5-pentanediol (**4**) proceeded to give the monoacylate **5** and the diacylate **6** in 92% and 3% yield, respectively (**5**/**6** = 31). Catalyst **1** also promoted substrate-selective monoacylation of 1,*n*-linear diols. 1,5-Pentanediol (**4**) was preferentially acylated 5.2 times faster than a one-carbon-longer diol (1,6-hexnaediol), in the competitive acylation between them (Figure 10A). The observed phenomena obviously indicate that the molecular recognition process between catalyst **1** and the substrate diols would be involved. Catalyst **1** recognize the overall molecular structures of substrates to give selectively acylated products.

With chiral PPY catalyst **1**, the chemo- and regioselective acylation of glycopyranoses have also been developed (*37*). Acylation of the secondary hydroxy group at C(4) of octyl β-D-glucopyranoside proceeded with >99% selectivity in the presence of a primary hydroxy group and two other secondary hydroxy groups (Figure 10B). The site-selective acylation took place preferentially even in the presence of a primary alcohol (2-phenyletanol), which was supposed to be achieved by the precise molecular recognition promoted by catalyst (Figure 10B).

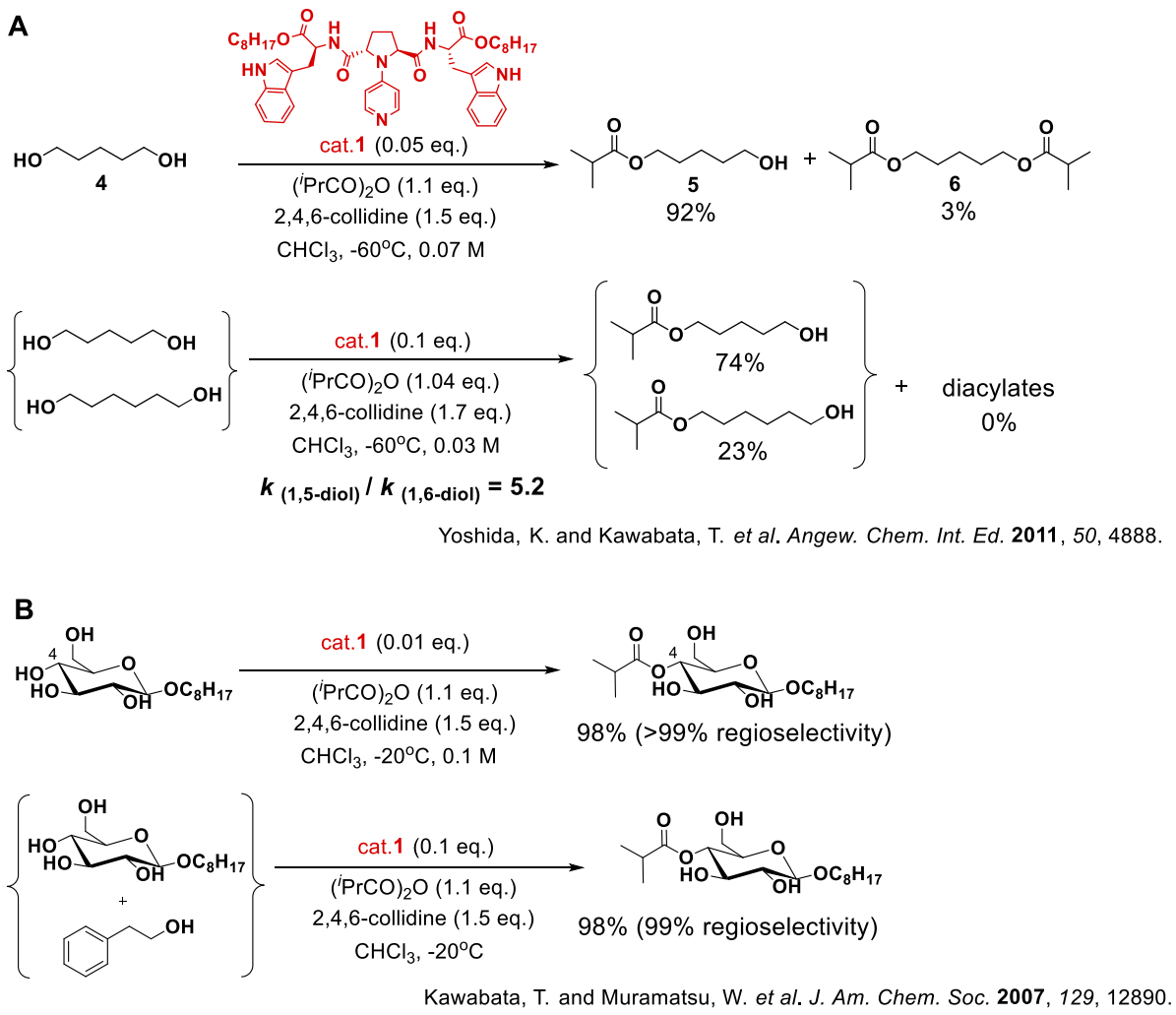

Figure 10 | Molecular transformations by chiral PPY catalyst 1. (**A**) Chemoselective acylation of linear diols and competitive acylation between diols having different chain length. (**B**) Chemo- and regioselective acylation of glycopyranose and competitive acylation between glycopyranose and primary alcohol.

Whereas intriguing results suggesting mechanistic aspects of the molecular transformation catalyzed by **3** have been obtained, mechanistic insights of selective acylation catalyzed by **1** remain unexplained. Since the selective monoacylation of 1,5-diol **4** (Figure 10A) seems to be one of the most simple system because 1,5-diol **4** has only hydroxy groups as recognition sites, its mechanistic analysis is expected to lead fundamental understanding of these chemo- and site-selective molecular transformation. With these views in mind, I elucidated the origin of the high chemoselectivity on monoacylation of 1,5-diol **4** catalyzed by **1**.

2.1.2 Backgrounds of chemoselective monoacylation of 1,*n*-diol

Selective monoacylation of 1,*n*-linear diols seems to be a simple molecular transformation, however, it has been one of the difficult subject in organic synthesis because overacylation affording the diacylate is usually unavoidable, especially in the acylation of long-chain linear diols. For example, acylation of 1,5-pentanediol (**4**) with typical acylation catalyst, 4-dimethylaminopyridine (DMAP), generated significant amount of diacylate **6** as well as monoacylate **5** (**5**/**6**= 45%/26%), even under the carefully controlled conditions at –60 °C (Figure 11, entry 1) (*35*). The relative rate ($k_{1\ (\text{acylation of } \mathbf{4})}$ / $k_{2\ (\text{acylation of } \mathbf{5})}$) for acylation between 1,5-diol **4** and monoacylate **5** with DMAP catalyst was experimentally estimated to be 1.0 (*35*). This result indicates that the intrinsic reactivity of 1,5-diol **4** was assumed to be equal to that of monoacylate **5**.

To avoid the overacylation (*50*), excess amounts of the diol substrates were often used (*51-53*). For example, acylation of 3.0-6.0 equivalents of **4** with a carboxylic acid in the presence of *N,N'*-dicyclohexylcarbodiimide (DCC) gave the monoacylate **5** and the diacylate **6** in a 3.5 : 1 ratio (entry 2) (*53*). Selective acylation of **4** has been reported by the use of an enzyme (*54*, *55*), however, overacylation is again unavoidable (mono/diacylate = 9.0, entry 3) (*55*). Under these backgrounds, Kawabata and co-workers have achieved highly selective monoacylation of 1,*n*-linear diols by using chiral PPY catalyst **1** (entry 4) (*35*). In the presence of catalyst **1**, acylation of 1,5-diol **4** gave the monoacylate **5** in a highly chemoselective manner (mono/diacylate = 31).

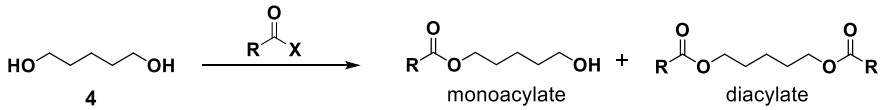

entry	conditions	R	monoacylate (%)	diacylate (%)	mono-/diacylate
1*	DMAP (0.05 eq.), (^{i}PrCO)$_2$O, $CHCl_3$, -60 ^{o}C	^{i}Pr	45	26	1.7
2‡	DCC, $ArSO_2CH_2CO_2H$, THF	$ArSO_2CH_2$	70	20	3.5
3#	Novozyme 871, $AcOCH=CH_2$, toluene	Me	81	9	9.0
4*	**1** (0.05 eq.), (^{i}PrCO)$_2$O (1.1 eq.), $CHCl_3$, -60 ^{o}C	^{i}Pr	92	3	31

* Yoshida, K. and Kawabata, T. *et al*. *Angew. Chem. Int. Ed.* **2011**, *50*, 4888.
‡ P. R. Blakemore *et al. Synlett* **2010**, 374.
# P. Clapés *et al. Tetrahedron Lett.* **2004**, *45*, 5031.

Figure 11 | Acylation of 1,5-pentanediol (4). Ar = benzothiazole-2-yl.

For such highly selective monoacylation catalyzed by **1**, the step for monoacylation must be much faster than the step for diacylation ($k_{1\ (\text{monoacylation})} >> k_{2\ (\text{diacylation})}$). A high relative rate ($k_{1\ (\text{monoacylation})}$ / $k_{2\ (\text{diacylation})}$) is supposed to be essential for selective monoacylation. In fact, the relative rate ($k_{1\ (\text{monoacylation})}$ / $k_{2\ (\text{diacylation})}$) for acylation between 1,5-diol **4** and monoacylate **5** with catalyst **1** was experimentally estimated to be 113 (Figure 12) (*35*). The strong preference for acylation of **4** over that of **5** in the presence of **1** indicates the precise molecular recognition of the substrate structure by catalyst **1** on the selective monoacylation.

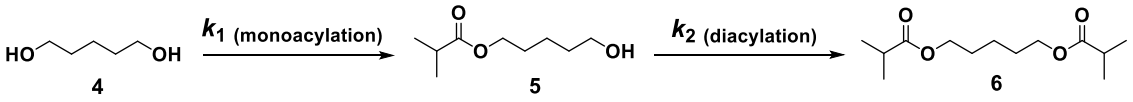

$k_{1\ (\text{monoacylation})}$ / $k_{2\ (\text{diacylation})}$ ~ 1.0 (DMAP)
~ 113 (cat. **1**)

Yoshida, K. and Kawabata, T. *et al*. *Angew. Chem. Int. Ed.* **2011**, *50*, 4888.

Figure 12 | Relative rate for acylation ($k_{1\ (\text{monoacylation})}$ / $k_{2\ (\text{diacylation})}$) between diol 4 and monool 5. Chemoselectivity was determined on the competitive acylation between **4** and **5**. Conditions: Treatment of a 1:1 mixture of **4** and **5** with isobutyric anhydride (0.70 equivalents of the total amount of the alcohols) and 2,4,6-collidine (1.7 equivalents) in the presence of catalyst **1** (0.1 equivalents) in 0.03 M $CHCl_3$ at -60 °C for 48 hours.

The preferential acylation of 1,5-diol **4** over other linear diols with different chain length has been also achieved in the presence of **1** (*35*). The relative rates ($k_{\text{(acylation of 1,}n\text{-diol)}}$ / $k_{\text{(acylation of 1,5-diol 4)}}$) of acylation between 1,*n*-diol (*n* = 4, 6 or 7) and 1,5-diol **4** are shown in Figure 13. The acylation of 1,5-diol **4** proceeded 2.0, 5.6, and 6.6 times faster than that of 1,4-butanediol, 1,6-hexanediol, and 1,7-heptanediol, respectively (Figure 13A). On the other hand, negligible substrate-selectivity was observed in DMAP-catalyzed acylation of these diols (Figure 13B). Thus, catalyst **1** was found to promote substrate-selective monoacylation of linear diols by discriminating the just one-carbon difference in their chain length.

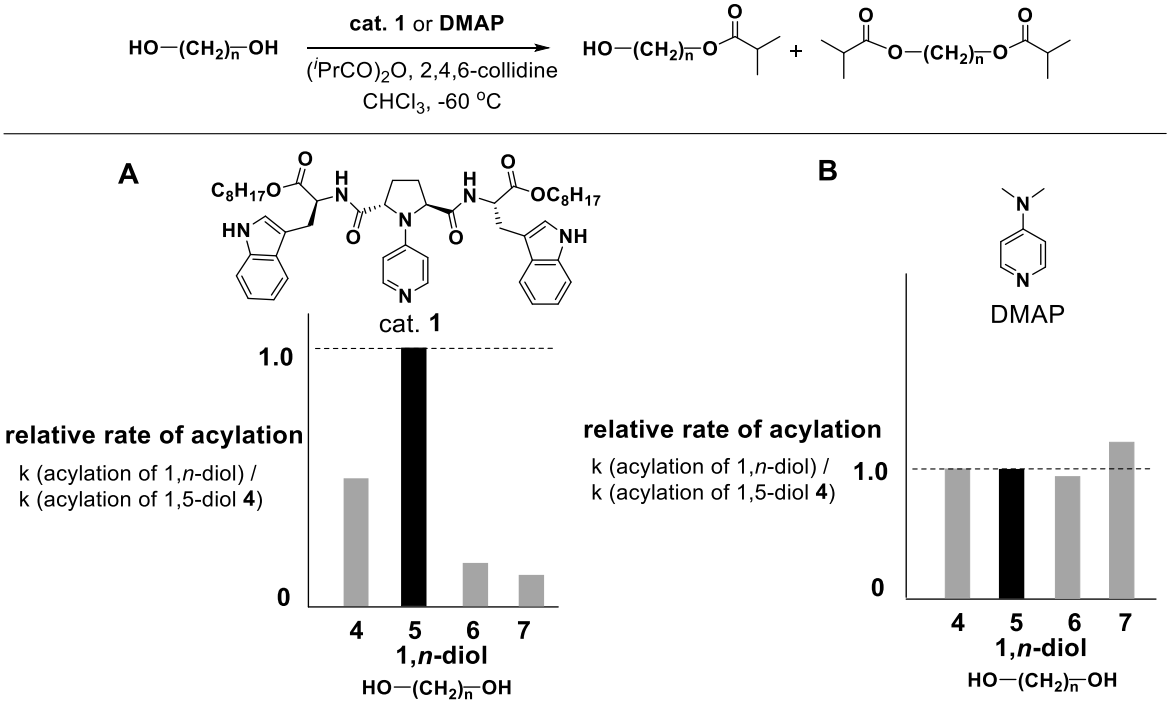

Yoshida, K. and Kawabata, T. *et al*. *Angew. Chem. Int. Ed.* **2011**, *50*, 4888.

Figure 13 | Relative rate of acylation ($k_{\text{(acylation of 1,}n\text{-diol)}}$ / $k_{\text{(acylation of 1,5-diol 4)}}$). (**A**) Catalyzed by **1**. (**B**) Catalyzed by DMAP.

The hypothetical transition state model for monoacylation of **4** catalyzed by **1** (Figure 14) has been proposed on the basis of some experimental results in the previous studies (Figure 15) (*35*). Hydrogen-bonding between catalyst **1** and the primary hydroxy group of 1,5-diol **4** is assumed to be essential for selective monoacylation from the experimentally observed solvent and temperature effects (Figure 15B, 15C). Two amide carbonyl groups seem to be important for the chemoselective acylation because selective monoacylation took place throughout the reactions with catalysts **1**, **15** and **16**, each possessing two amide carbonyl groups as common functionalities, regardless of the steric bulkiness of the side chains (Figure 15A). The model shown in Figure 14 may account for the preferential acylation of 1,5-diol **4** over the corresponding monoacylate **5** and substrate-specific acylation of 1,5-diol **4**. However, the actual mechanism seems to be not so simple. Since structures of catalyst side chains affect the degree of selectivity (Figure 15A), the catalyst side chains seem to play important roles for the chemoselectivity. These backgrounds prompted me to further elucidate the mechanistic aspects of the organocatalytic chemoselective acylation based on experimental and computational studies.

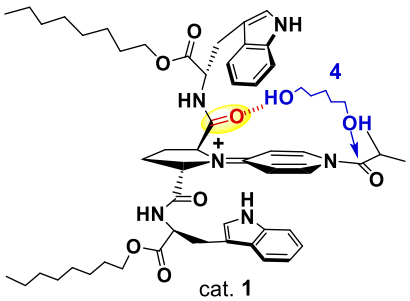

Yoshida, K. and Kawabata, T. *et al*. *Angew. Chem. Int. Ed.* **2011**, *50*, 4888.

Figure 14 | Hypothetical explanation.

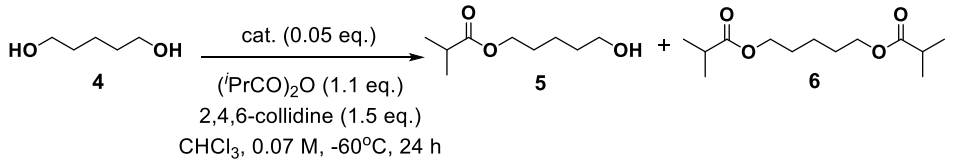

A

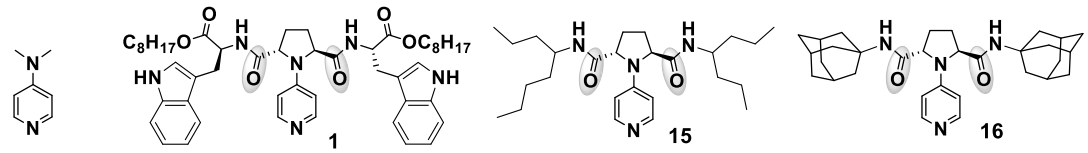

5/6	1.7	31	15	15

B

temp. (°C)	**5/6**
-60	27
-20	9
20	6

C

solvent	**5/6**
$CHCl_3$	>71
toluene	8
DMF	2

Yoshida, K. and Kawabata, T. *et al*. *Angew. Chem. Int. Ed.* **2011**, *50*, 4888.

Figure 15 | Various effects on selective monoacylation of 1,5-diol 4. (**A**) Effects of steric bulk of catalyst side chain. (**B**) Effects of temperature. (**C**) Effects of solvents.

2.2 Experimental studies for elucidation of mechanistic aspects of chemoselective monoacylation of 1,5-pentanediol

2.2.1 Effects of side chain structures of catalysts

I first investigated the effects of the side chain structures of catalysts on chemoselective monoacylation of **4** (Figure 16). I performed the acylation of 1,5-diol **4** with 1.03 equivalents of isobutyric anhydride in the presence of C_2-symmetric chiral PPY catalysts **1**-**3**, each having two identical side chains consisting of L-tryptophan, 1-mehyl-L-tryptophan and L-2-naphthylalanine moiety, respectively. Among these catalysts, the distinct high selectivity for monoacylation was observed with catalyst **1** (**5**/**6** = 27, entry 1) (*56*). With catalyst **2** or **3**, monoacylate was still predominant, but with decreased chemoselectivity (**5**/**6** = 8) and reactivity (57-63% conversion, entries 2, 3), when compared with the acylation promoted by catalyst **1** (**5**/**6** = 27, 84% conversion, entry 1). These results indicate the critical importance of the indolyl NH groups in catalyst **1** for the chemoselective acylation.

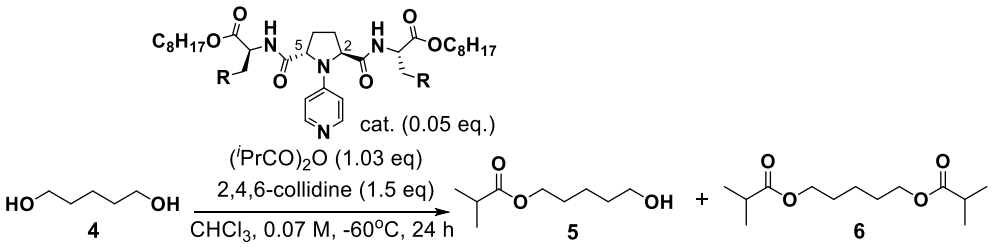

entry	R		**5** : **6** (%) (%)	**5**/**6**	Recovery of **4** (%)
1		cat. **1**	**80** : **3**	**27**	16
2		cat. **2**	56 : 7	8	37
3	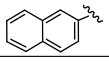	cat. **3**	51 : 6	8	43

Figure 16 | Effects of side chains of catalysts on chemoselective monoacylation of 1,5-diol.

2.2.2 Effects of C_2-symmetric structure in the catalysts

The effects of the C_2-symmetric structure of catalysts were next examined by employing the corresponding C_1-symmetric catalysts, **17**-**19**. Almost no differences in chemoselectivity and reactivity were found among reactions catalyzed by C_1-symmetric **17**-**19** (**5**/**6** = 10-13, 32% conversion, Figure 17), regardless of whether the indolyl NH group was involved in catalyst structures **17**-**19** or not. It is worthy to note that *the indolyl NH group is responsible for further increasing the selectivity and reactivity in the monoacylation of 1,5-diol **4** only when the PPY-catalyst has C_2-symmeric structure.*

In the absence of indolyl NH group in the catalyst structure, C_1-symmetric catalysts **18** and **19** showed similar selectivity and diminished reactivity compared to C_2-symmetric catalysts **2** and **3**. This result indicates the importance of the amide carbonyl groups for the chemoselectivity, and the amide groups seem to contribute to acceleration of reactions. Since C_2-symmetric catalysts **2** and **3** have two amide groups, the reactivity was improved compared to the corresponding C_1-symmetric catalysts **18** and **19**, without affecting the chemoselectivity.

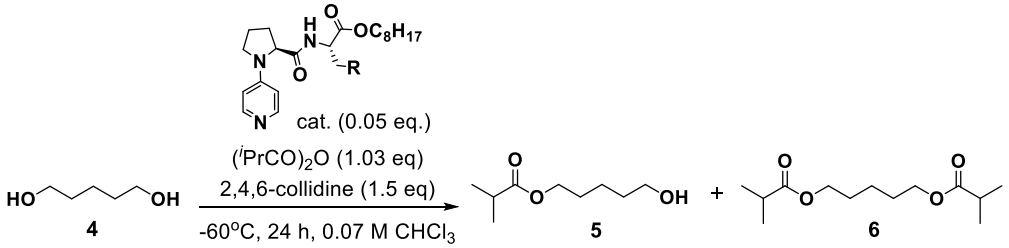

entry	R		**5** : **6** (%) (%)	**5**/**6**	Recovery of **4** (%)
1		cat. **17**	31 : 3	12	68
2		cat. **18**	29 : 3	10	68
3	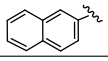	cat. **19**	30 : 2	13	68

Figure 17 | Selective monocylation of 1,5-diol 4 with C_1-symmetric catalysts.

2.3 Experimental studies for elucidation of the mechanistic aspects in substrate-selective acylation of 1,5-pentanediol

2.3.1 Effects of catalyst structures on monoacylation of 1,2-ethanediol

To elucidate the mechanistic aspects of substrate-selective acylation of 1,5-pentanediol (**4**), I next examined catalytic properties of **1**-**3** and **17**-**19** in acylation of 1,2-ethanediol (**7**) (Figure 18). C_2-symmetric PPY catalysts **1**-**3** promoted chemoselective monoacylation of **7** in high selectivities (**8**/**9** = 23-35, Figure 18A), regardless of whether the indolyl NH groups are involved in the catalyst structure or not. Indolyl NH groups of catalyst **1** did not affect the chemoselectivity on monoacylation of 1,2-diol **7**, even though catalyst **1** has C_2-symmetric structure (**8**/**9** = 69%/3%-70%/2%, Figure 18A). Thus, on acylation of 1,2-diol **7**, the indolyl NH groups have almost no impact on chemoselectivity. This result is a contrast to monoacylatio of 1,5-diol **4**, where indolyl NH groups of C_2-symmetric catalyst **1** played an important role for selective monoacylation (Figure 16).

Chemoselective monoacylation of 1,2-diol **7** with C_1-symmetric catalysts **17**-**19** proceeded in slightly less but similar selectivity and reactivity (**8**/**9** = 62%/5%-64%/4%, 64-68% conversion, Figure 18B), when compared with the acylation promoted by C_2-symmetric catalyst structure. Thus, on acylation of 1,2-diol **7**, the amide carbonyl group at C(2) and/or C(5) of the pyrrolidine ring of the catalyst, as well as the indolyl NH group, has almost no impact on chemoselectivity and reactivity.

The acylation of 1,2-diol **7** showed relatively high chemoselectivity and reactivity throughout the reactions promoted by both C_1- and C_2-symmetric PPY-catalysts. This could be ascribed mainly to the less intrinsic reactivity of monool **8** than 1,2-diol **9**. Bulkiness of the acyl group of monoacylate **8** effectively decelerate the second acylation, especially in the cases of such short-chain diol, by using steric interaction to prevent the diacylation. 1,2-Diol **7** is expected to have an intrinsically high reactivity for monoacylation because of its intramolecular hydrogen bonding.

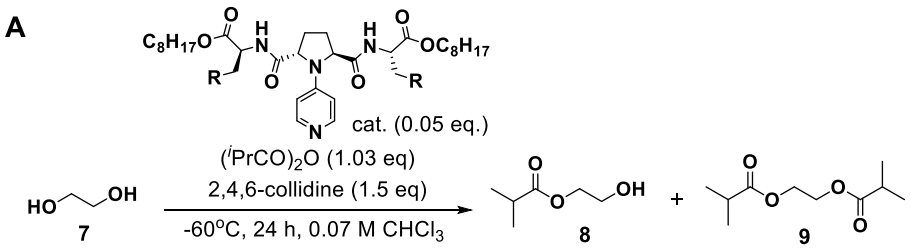

entry	R		8 : 9 (%) (%)	8/9	Recovery of 7 (%)
1		cat. **1**	70 : 2	35	27
2		cat. **2**	69 : 3	23	27
3	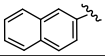	cat. **3**	69 : 2	31	28

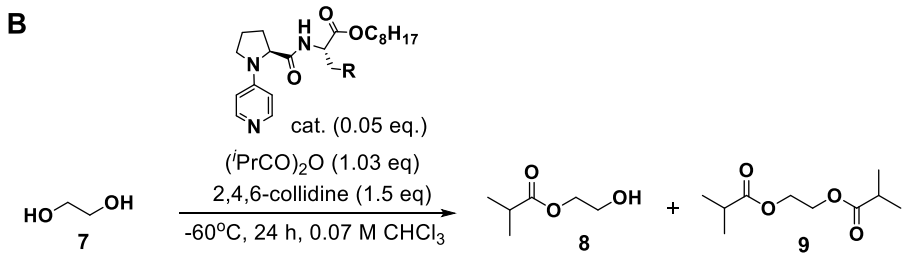

entry	R		8 : 9 (%) (%)	8/9	Recovery of 7 (%)
1		cat. **17**	64 : 4	15	32
2		cat. **18**	60 : 4	14	36
3	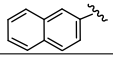	cat. **19**	62 : 5	13	33

Figure 18 | **Acylation of 1,2-ethanediol (7) by chiral PPY catalysts.** (**A**) Catalyzed by C_2-symmetric **1**-**3**. (**B**) Catalyzed by C_1-symmetric **17**-**19**.

2.3.2 Effects of catalyst structures on substrate-selective acylation of 1,5-pentanediol

To elucidate the mechanistic aspects of substrate-selective acylation of 1,5-pentanediol (**4**), relative rates of acylation ($k_{\text{(acylation of 4)}} / k_{\text{(acylation of 7)}}$) between 1,5-diol **4** and 1,2-diol **7** were determined by the competitive acylation between them in the presence of C_2-symmetric catalysts **1**-**3** (Figure 19). Catalyst **1** with the indolyl NH groups promoted the acylation of 1,5-diol **4** 4.5 times faster than that of 1,2-diol **7** (entry 1). In contrast, in the presence of catalysts **2** or **3** without the indolyl NH group, 1,2-diol **7** was acylated relatively faster than 1,5-diol **4** ($k_{\text{(acylation of 4)}} / k_{\text{(acylation of 7)}}$ = 0.7-0.8, entries 2, 3). The marked difference in the catalytic properties between catalysts **1**-**3** depending on the presence or the absence of the indolyl NH group indicates that two indolyl NH groups arranged in a C_2-symmetric fashion are essential for transition state stabilization, resulting in accelerative monoacylation of 1,5-diol **4**. The critical stabilization of transition state by indolyl NH groups enables 1,5-diol **4** to be preferentially acylated over the other linear diols.

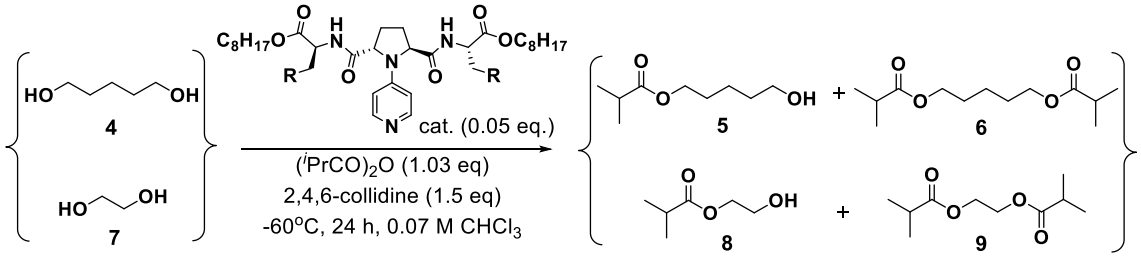

entry	R		5+6 : 8+9 (%) (%)	Chemoselectivity $k_{\text{(acylation of 1,5-diol 4)}} / k_{\text{(acylation of 1,2-diol 7)}}$
1		cat. **1**	36 : 12	**4.5**
2		cat. **2**	11 : 16	**0.7**
3	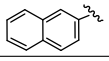	cat. **3**	14 : 18	**0.8**

Figure 19 | Competitive acylation between 1,5-diol 4 and 1,2-diol 7 with catalysts 1-3.

2.4 Computational study

Based on the experimental studies, theoretical study was performed by Professor Masahiro Yamanaka and Dr. Makoto Sato (Rikkyo University). DFT calculations (B3LYP/6-31G*, Gaussian 09 package) were carried out using C_1- and C_2-symmetric catalyst models (**cat1** and **cat2**, Figure 20).

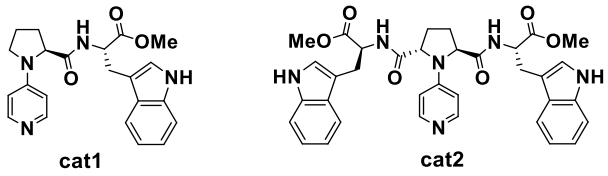

Figure 20 | Chemical models of catalysts **17** and **1**.

To gain deep insights of the high chemoselectivity through transition state (TS) stabilization, the nucleophilic attack process in monoacylation of 1,5-diol **4** was investigated. The relative Gibbs free energy difference between TSs of monoacylation and diacylation was compared in each C_1-symmetric **cat1** and C_2-symmetric **cat2** systems (Figure 21). Monoacylation is energetically favored than diacylation in both systems. Although the diacylation TSs are located at almost the same energy level, the significant stabilization of the monoacylation TS was observed in the **cat2** system (**TS-iii**). These computational results are well consistent with the experimental results.

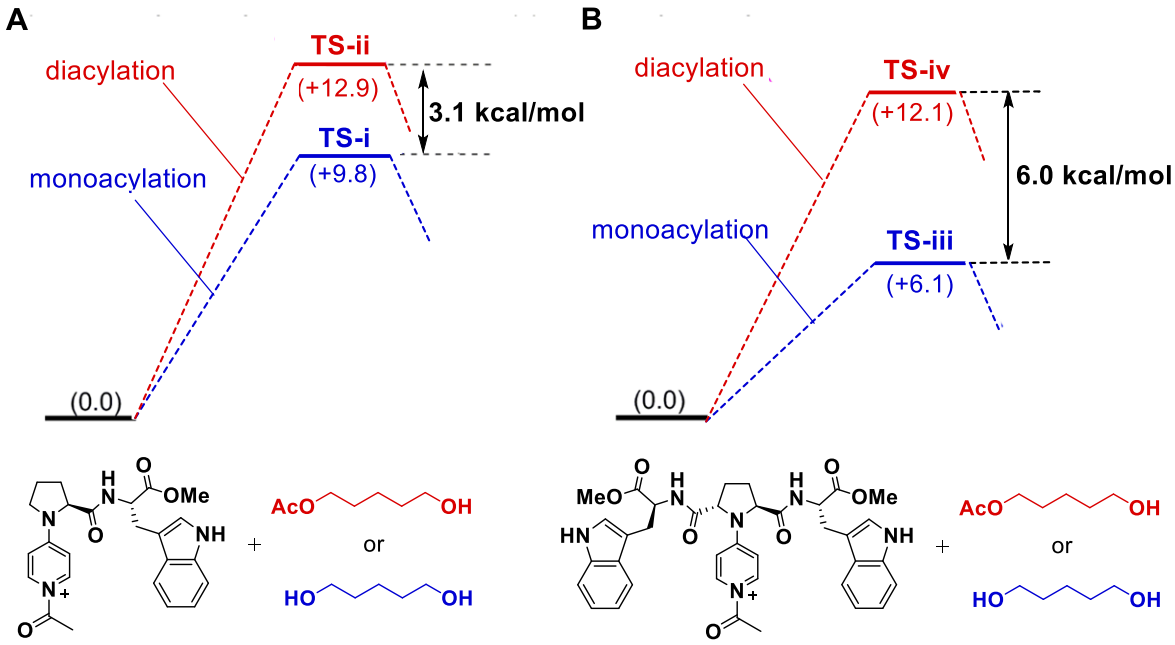

Figure 21 | Relative Gibbs free energy differences (kcal/mol) between transition states of monoacylation (blue) and diacylation (red). (**A**) **cat1** system. (**B**) **cat2** system. Calculated by Professor Masahiro Yamanaka and Dr. Makoto Sato (Rikkyo University) at B3LYP/6-31G* level.

Figure 22 shows the most stable TSs in the **cat1**-catalyzed monoacylation (**TS-i**) and diacylation (**TS-ii**). In both reactions, the nucleophilic addition of the hydroxy group on the *N*-acylpyridinium carbonyl group proceeded through the proton abstraction from the nucleophilic hydroxy group with the acetate anion (*54*, *55*). The acetate anion ($CO_{acetate}$) strongly coordinates with the indolyl NH group (NH_{indole}).

Since the $NH_{indole}/CO_{acetate}$ hydrogen bond participates in both reactions, the energy difference between **TS-i** and **TS-ii** should be derived from other factors. The energetically favored **TS-i** has the significantly strong hydrogen bond between the amide carbonyl group of **cat1** (CO_{amide}) and the remaining hydroxy group of 1,5-diol **4** (OH_{diol}). In contrast, **TS-ii** does not have such additional strong hydrogen bond. Thus, **TS-ii** is located at the higher energy level compared to **TS-i**. The indicated importance of the CO_{amide}/OH_{diol} hydrogen bond for stabilizarion of the monoacylation TS (**TS-i**) is well consistent with the experimental results shown in Figure 17.

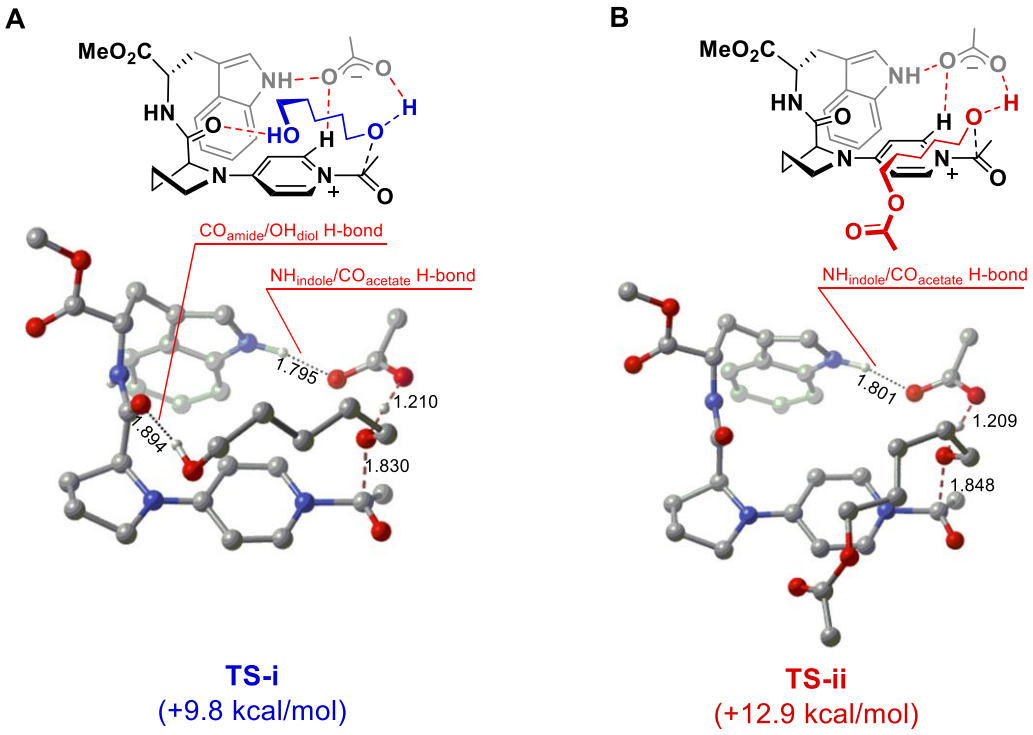

Figure 22 | Transition states in C_1-symmetric cat1 system. (**A**) TS of monoacylation. (**B**) TS of diacylation. Calculated by Professor Masahiro Yamanaka and Dr. Makoto Sato (Rikkyo University) at B3LYP/6-31G* level.

Then, TSs of monoacylation (**TS-iii**) and diacylation (**TS-iv**) in the **cat2** system were explored (Figure 23). In a similar manner to the **cat1** system, the relatively stable TSs of both reactions have the strong $NH_{indole}/CO_{acetate}$ hydrogen bond. On the other hand, the second indolyl NH group causes a significant change in the hydrogen bonding network in **TS-iii** (Figure 23A). The remaining hydroxy group works as a general acid catalyst by coordinating with the negatively charged *N*-acylpyridinium carbonyl oxygen. The increased Lewis basicity of the oxygen atom of OH_{diol} forms the strong NH_{indole}/OH_{diol} hydrogen bond. The multiple hydrogen bonding network through two indolyl groups, the acetate anion, and 1,5-diol **4** construct the most

stable TS structure (**TS-iii**). **TS-v** (Figure 24), having a similar coordination mode with **TS-i**, is no longer the most stable TS because the second indolyl group does not contribute to the hydrogen bonding network in **TS-v**. These results indicate that catalyst **1** (e.g., **cat2**) achieves the precise molecular recognition for 1,5-diol **4** by dramatically changing its coordination mode from catalyst **17** (e.g., **cat1**).

In the diacylation TS (**TS-iv**) (Figure 23B), NH_{indole} residue directly coordinates with the *N*-acylpyridinium carbonyl oxygen to form the relatively weak hydrogen bond. The acetyl group of the substrate does not coordinate with NH_{indole} residue but the amide NH residue. Two indolyl NH groups rarely contribute to the molecular recognition process of the diacylation.

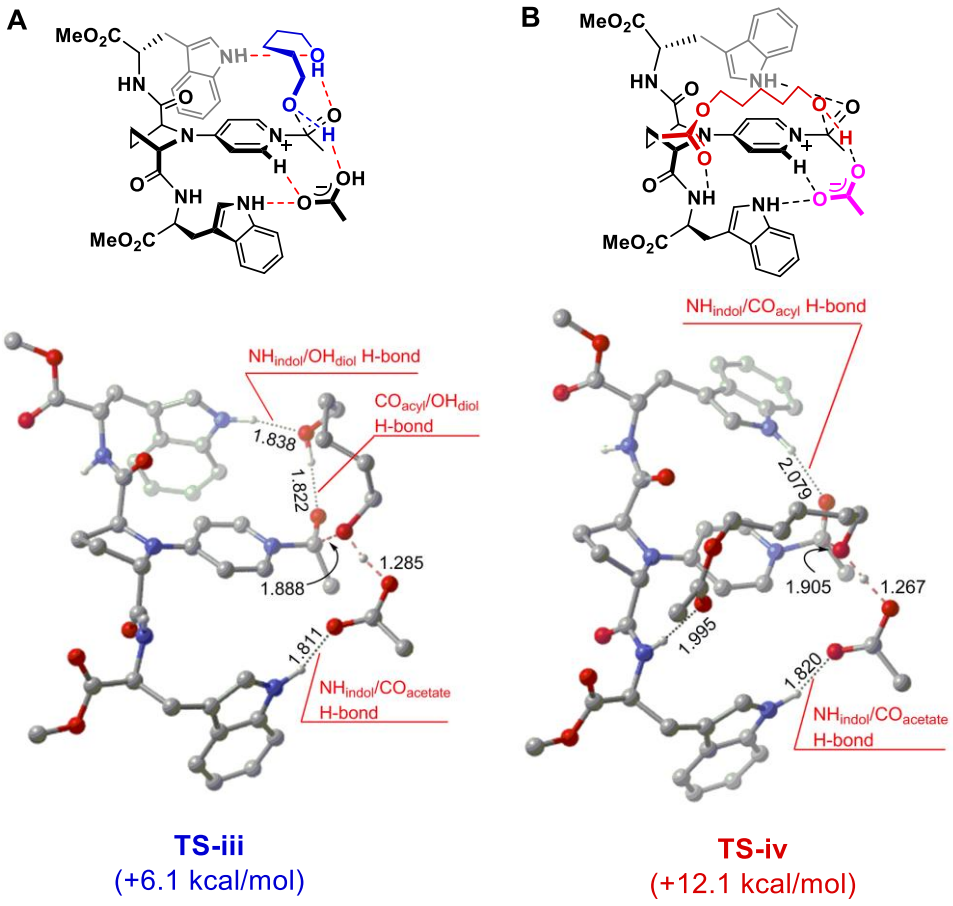

Figure 23 | Transition states in C_2-symmetric cat2 system. (**A**) TS of monoacylation. (**B**) TS of diacylation. Calculated by Professor Masahiro Yamanaka and Dr. Makoto Sato (Rikkyo University) at B3LYP/6-31G* level.

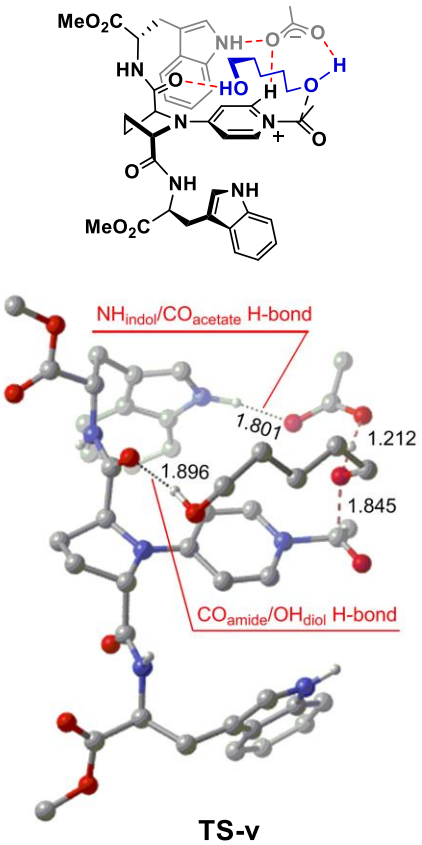

TS-v
(+9.1 kcal/mol)

Figure 24 | **Transition state in C_2-symmetric cat2 system without involving the second indolyl group.** Calculated by Professor Masahiro Yamanaka and Dr. Makoto Sato (Rikkyo University) at B3LYP/6-31G* level.

2.5 Conclusion

Mechanistic aspects of chemoselective monoacylation of 1,5-pentanediol (**4**) has been experimentally and computationally investigated by employing various C_1- and C_2-symmetric PPY catalysts. Although 1,5-diol **4** has a simple structure possessing only hydroxy groups as recognition sites by the catalyst, the multiple hydrogen bonds between the C_2-symmetric catalyst **1** and 1,5-diol **4** significantly stabilized the monoacylation transition state of 1,5-diol **4**. The indolyl NH groups arranged in a C_2-symmetric fashion were found to be critically important for both chemoselective monoacylation and the substrate-specific acylation of 1,5-diol **4**. C_2-symmetric catalyst **1** performed the precise molecular recognition for 1,5-diol **4** through the quite different coordination mode from that by C_1-symmetric catalyst **17**. In the reaction mode, catalyst **1** possesses the dual function of the two indolyl NH groups in the L-tryptophan side chains. This recognition mode is quite different from that proposed for other molecular transformations as shown in Figure 9. Thus, these chiral PPY catalysts seem to adapt themselves to various transformations by flexibly changing their molecular recognition mode depending on the substrate structures. These results prompted me to apply such molecular transformation by chiral PPY catalysts to more complex system. The topic for unprecedented asymmetric molecular transformation will be discussed in Chapter 4.

Chapter 3: DMAP-catalyzed efficient synthesis of rotaxanes

3.1 Backgrounds

Since supramolecules such as rotaxanes and catenanes possess attractive architectures, syntheses of these supramolecules have been one of the foci of current organic synthesis. Acylative end-capping of the hydroxy group of the pseudorotaxane is one of the most reliable methods to synthesize rotaxanes (*59*-*62*). A pseudorotaxane (Figure 25B), which is expected to be formed by mixing the axis component and the ring component, affords the corresponding rotaxane by acylative end-capping of the hydroxy group at the terminus of the axis component. In the presence of tributylphosphine, acylations of the pseudorotaxanes have been reported to afford corresponding rotaxanes in a high yield (90%, Figure 25A, entry 1) (*59*, *62*).

Although DMAP is a highly efficient catalyst for a wide variety of acylation reactions, DMAP-catalyzed acylative end-cappings of pseudorotaxanes often produce rotaxanes in low yields. For example, in the presence of 10 mol% of DMAP catalyst, only 3% of the rotaxane was reported to be obtained (entry 2). Increasing the amount of catalyst (50 mol%) slightly increased the yield of the rotaxane, but the yield was still low (13%, entry 3). Triethylamine is supposed to deprotonate the ammonium salt of the axis component and prevent the formation of the pseudorotaxane which is essential for the rotaxane synthesis. Thus, the basic reaction conditions must be avoided to prevent neutralization of the ammonium salt.

When acyl chloride was used as an end-capping agent instead of acid anhydride, tributylphosphine-catalyzed synthesis, as well as DMAP-catalyzed synthesis, have been known to give the rotaxane in a low yield (entries 4, 6) (*62*). The hydrogen-bonding interaction between chloride ion and ammonium group seems to prevent the formation of pseudorotaxane (Figure 25B). To remove the chloride ion, without using a base such as trimethylamine, silver hexafluorophosphate was added to the system (Figure 25A, entry 5). The rotaxane was obtained in moderate yield (50%), however, a large amount of catalyst (10 equivalents) was required.

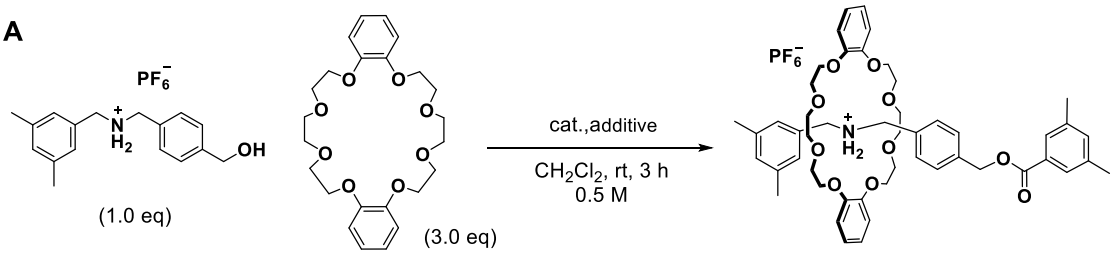

entry	acylating reagent	catalyst	additive	yield (%)
1	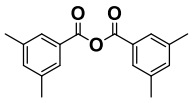	PBu_3 (0.1 eq)	none	90
2		DMAP (0.1 eq)	none	3
3		DMAP (0.5 eq)	Et_3N (1.5 eq)	13
4	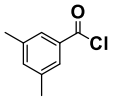	PBu_3 (0.1 eq)	none	10
5		PBu_3 (**10 eq**)	$AgPF_6$ (1.5 eq)	50
6		DMAP (0.5 eq)	Et_3N (1.5 eq)	7

Toshikazu Takata *et al. J. Org. Chem.* **2006**, *71*, 5093.

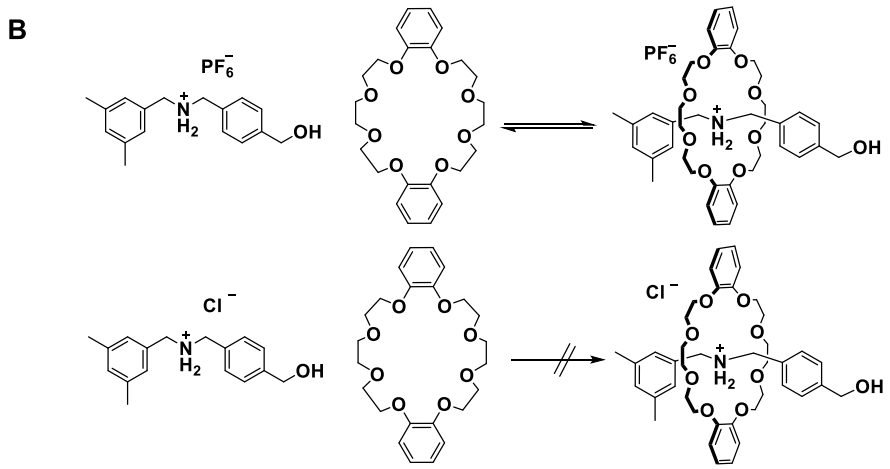

Figure 25 | DMAP-catalyzed synthesis of rotaxanes. (**A**) Reported synthesis of a rotaxane by DMAP catalysis or tributylphosphine catalysis. (**B**) Effects of the counter anion of the ammonium salts on the formation of pseudorotaxanes.

Under these backgrounds, I investigated DMAP-catalyzed synthesis of rotaxanes. Removing the chloride ion from the reaction system and the improvement of catalytic performance seem to be important. On DMAP or PPY-catalyzed acylation of alcohols, the active catalytic species are acylpyridinium intermediates (Figure 26). To improve the catalytic performance of DMAP and to get fundamental insights in DMAP-catalyzed acylation, I first elucidated the formation of acylpyridinium ion pair generated from various acylating agents.

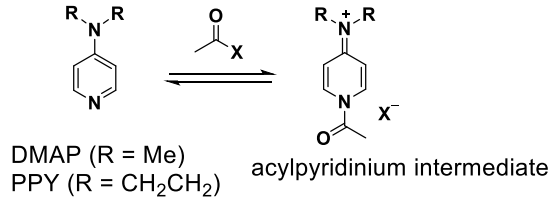

Figure 26 | Acylpyridinium intermediate.

3.2 Formation of acylpyridinium ion pairs

Toward the development of efficient method for DMAP-catalyzed synthesis of rotaxanes, I first investigated the fundamental nature of the PPY-catalyzed acylation. The amount of acylpyridinium on pairs generated from PPY and various acylating agents including acetic anhydride (Ac_2O), benzoic anhydride (Bz_2O), acyl chloride (AcCl), and benzoyl chloride (BzCl), was estimated by NMR study.

First, I performed variable-temperature NMR experiment to investigate the formation of acylpyridinium ion pair **20** generated from PPY and acetic anhydride. A $CDCl_3$ solution containing acetic anhydride and PPY was monitored by NMR in the temperature range between -30 ~ -65 ℃, and the position of equilibrium (*K*) was directly determined from the integration ratio of PPY to **20** at each temperature (Figure 28). The ΔH and ΔS were calculated to estimate the formation of **20** on various conditions. I found that ΔH and ΔS were -7.53 kcal/mol and -33.8 eu, respectively, and that only small amount of acylpyridinium ion **20** was formed in the system. The ratio of formation of **20** in a solution of acetic anhydride (0.005 M) and PPY (0.015 M) at -60 ℃ was calculated to be only 1.05% based on the amount of PPY (Figure 27A) (*63*).

Formation of acylpyridinium ion pair **21** generated from benzoic anhydride and PPY was also investigated in a similar way to investigation of formation of acylpyridinium ion pair **20** by variable-temperature NMR experiment in the temperature range between -45 ~ -70 ℃ (Figure 29). In the case of benzoic anhydride, formation of further less amount of acylpyridinium ion **21** was observed by the NMR spectrum. ΔH and ΔS were determined to be -8.90 kcal/mol and -45.4 eu, respectively, and only 0.08% of **21** was suggested to be formed in a solution of benzoic anhydride (0.005 M) and PPY (0.015 M) at -60 ℃ (Figure 27A).

Then, I investigated the formation of acylpyridinium ion pairs **22** and **23** generated from PPY and the corresponding acyl chlorides by measuring NMR at 20 ℃ (Figure 30, 31). In the both cases of acetyl chloride and benzoyl chloride, quantitative formation of acylpyridinium ion pairs **22** and **23** were observed (Figure 27B).

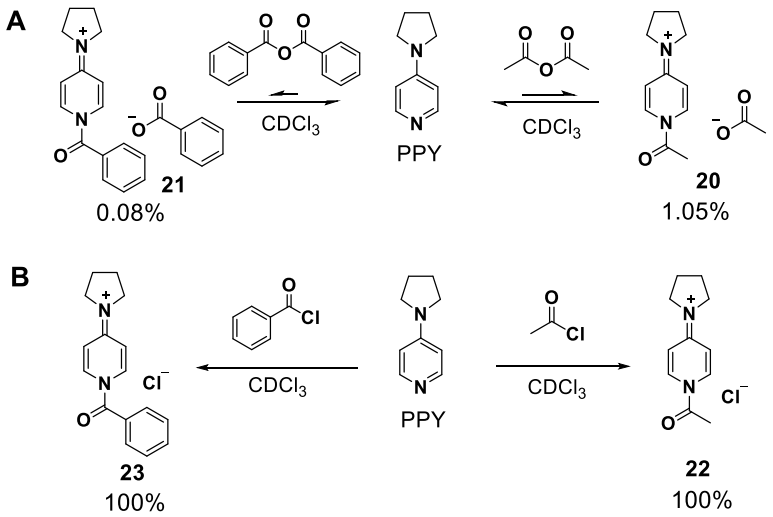

Figure 27 | Formation of acylpyridinium ion pairs. (**A**) Formation of acylpyridinium ion pairs from acid anhydride. Conditions: PPY (0.015 M), acid anhydride (0.005 M), -60 °C. (**B**) Formation of acylpyridinium ion pairs from acyl chloride. Conditions: PPY (0.07 M), acyl chloride (0.07 M), 20 °C.

The efficiency in the formation of the acylpyridinium ion pair changed significantly depending on the leaving group of the acylating agent. Quantitative formation of the acylpyridinium ion pair was observed when acyl chloride was used as an acyl donor, whereas only small amount of the acylpyridinium ion pair was formed when acid anhydride was used as an acyl donor. These results prompted me to use acyl chloride for DMAP-catalyzed synthesis. Acyl chloride was expected to improve the catalytic performance in DMAP-catalyzed synthesis of rotaxanes if the chloride ion can be removed from the reaction system. With these views in mind, I focused on the development of the efficient method for DMAP-catalyzed synthesis of rotaxanes.

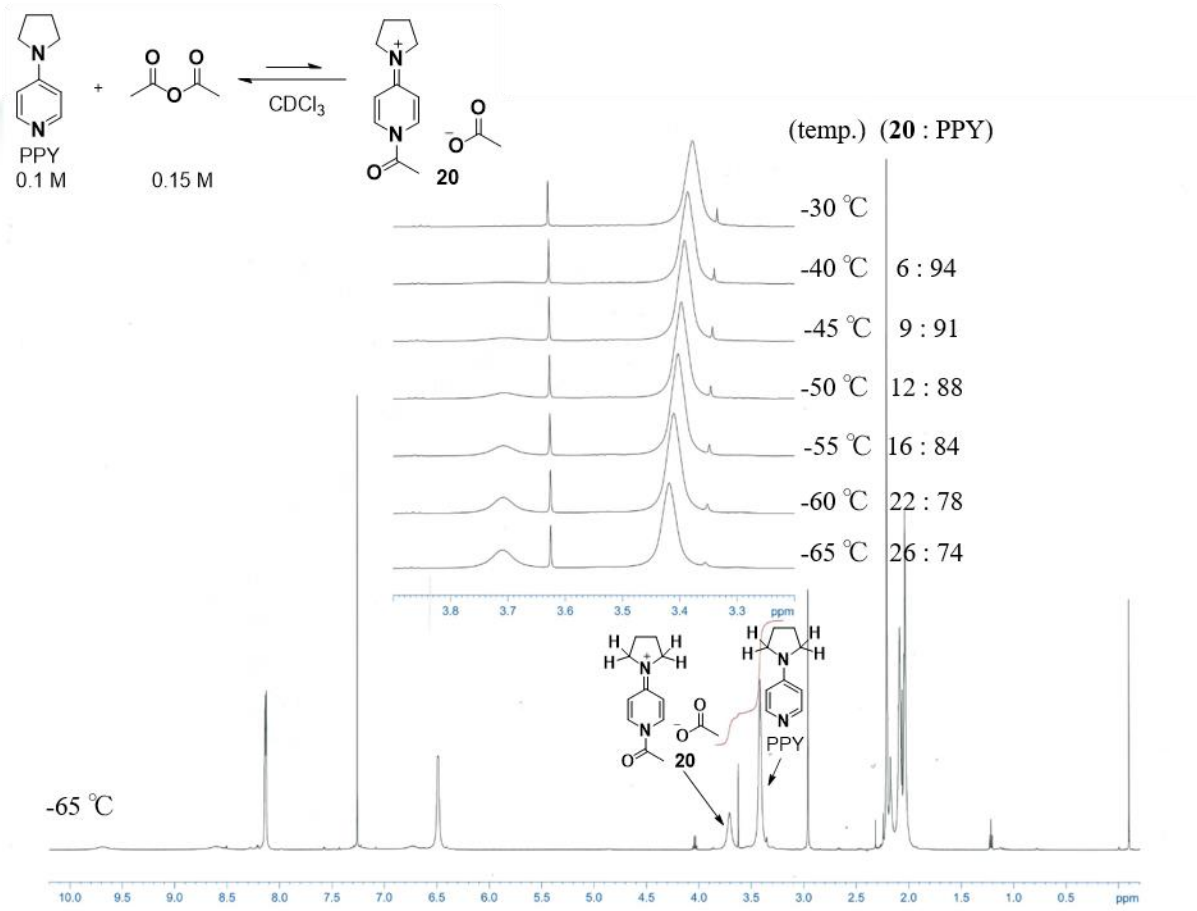

temp (°C)	formation of **20** (%)	K (mol^{-1})	ΔG (kcal/mol)
-40	6.3	0.48	0.34
-45	8.8	0.70	0.16
-50	11.8	1.02	-0.07
-55	16.0	1.52	-0.18
-60	21.8	2.37	-0.37
-65	26.5	3.26	-0.49

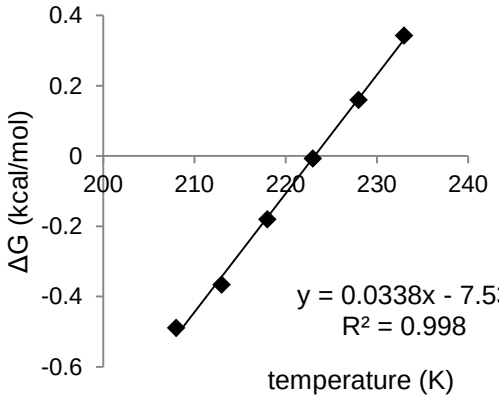

ΔH = -7.53 kcal/mol
ΔS = -33.8 eu

Figure 28 | Formation of acylpyridinium ion pair 20 from acetic anhydride.

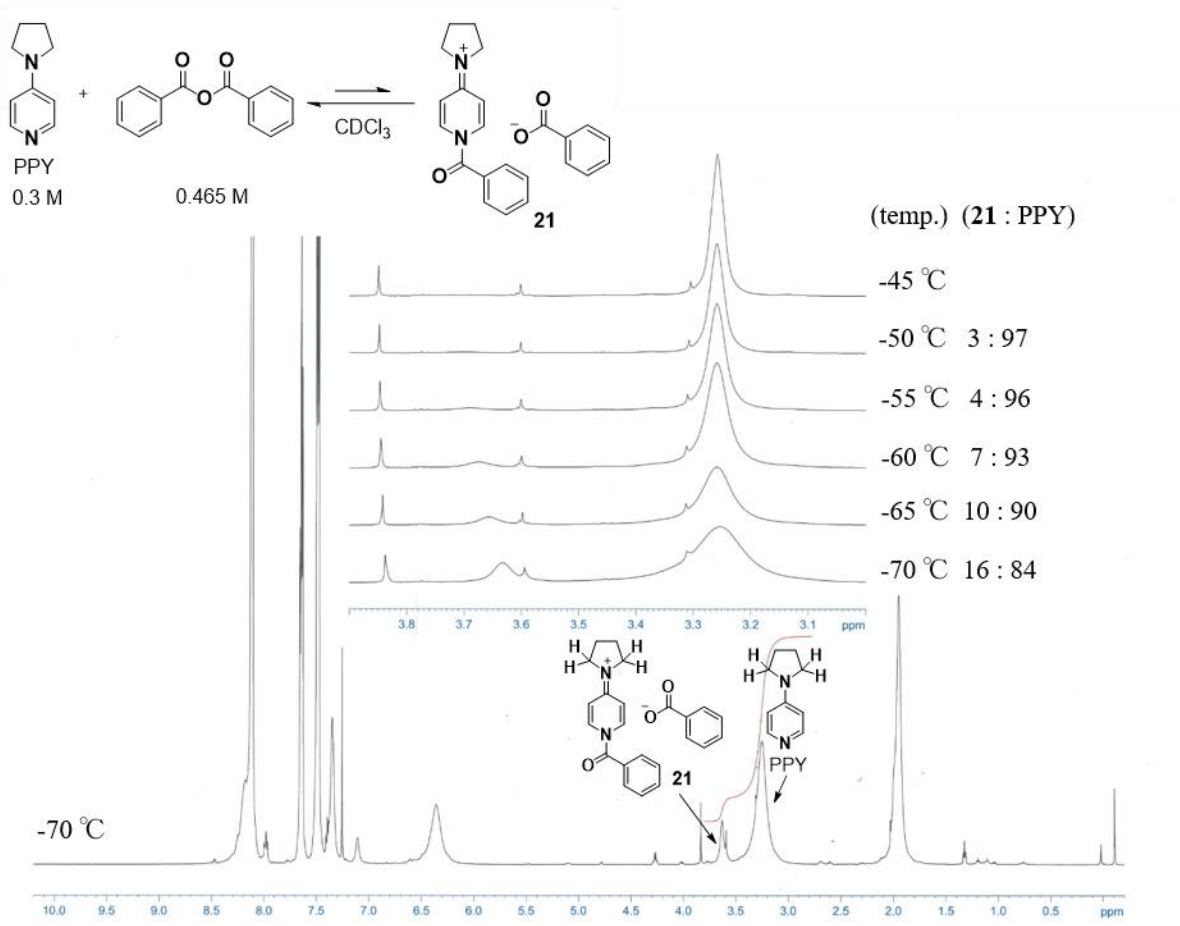

temp (°C)	formation of **21** (%)	K (mol^{-1})	ΔG (kcal/mol)
-50	2.8	0.064	1.22
-55	4.3	0.10	1.00
-60	6.6	0.16	0.77
-65	9.7	0.25	0.57
-70	15.8	0.48	0.30

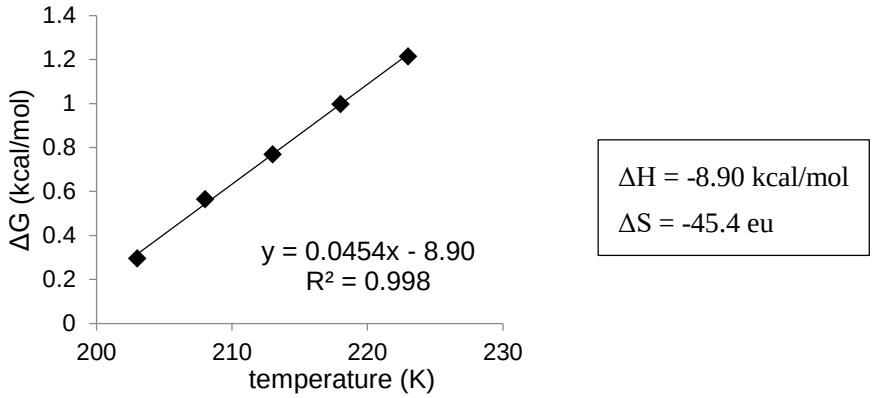

Figure 29 | Formation of acylpyridinium ion pair 21 from benzoic anhydride.

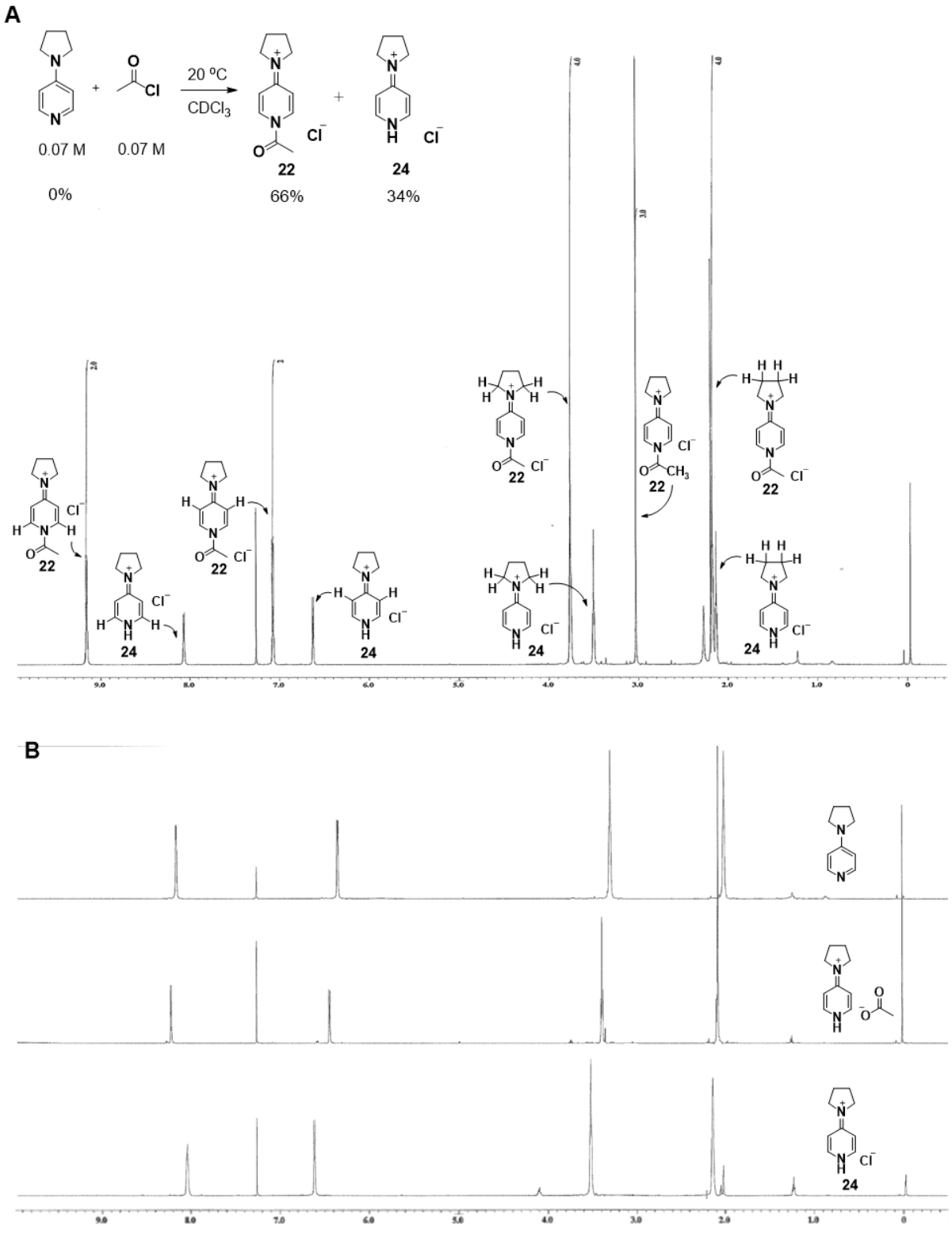

Figure 30 | **Formation of acylpyridinium ion pair 22 from acetyl chloride.** (**A**) Formation of **22**. (**B**) Standard spectra.

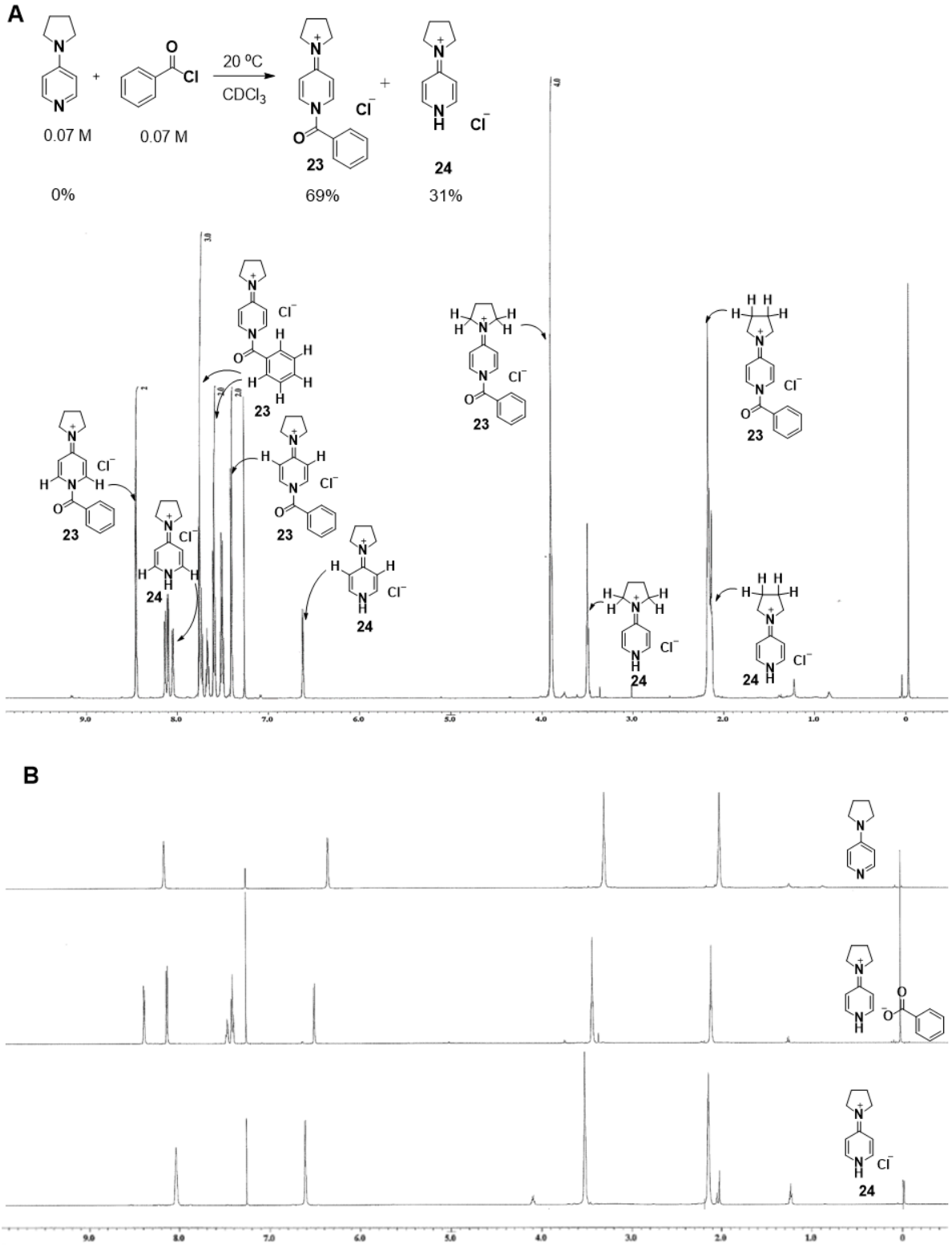

Figure 31 | Formation of acylpyridinium ion pair 23 from benzoyl chloride. (**A**) Formation of **23**. (**B**) Standard spectra.

3.3 DMAP-catalyzed synthesis of a rotaxane

A pseudorotaxane, which is expected to be formed by mixing the axis component **10** and the ring component **11**, was treated with acyl chloride and $AgPF_6$ in the presence of DMAP (Figure 32, entry 1). Pivalic acid ($^tBuCO_2H$) was added to the system to improve the catalytic performance. Since the carboxylate ion acts as an effective general base on acylation of alcohols, addition of the carboxylic acid to the acyl chloride system have been suggested to be effective in overall performance of the catalytic acylation process by *in situ* exchange of the chloride counter ion to the carboxylate (*64*). Under the conditions, desired rotaxane **12** was successfully obtained in 94% yield. The use of corresponding acid anhydride instead of acyl chloride was ineffective under these reaction conditions (entry 2). In the absence of $AgPF_6$, the yield of rotaxane **12** decreased to 14% (entry 3). The use of amine base instead of $AgPF_6$ dramatically decreased the efficiency (entries 4, 5).

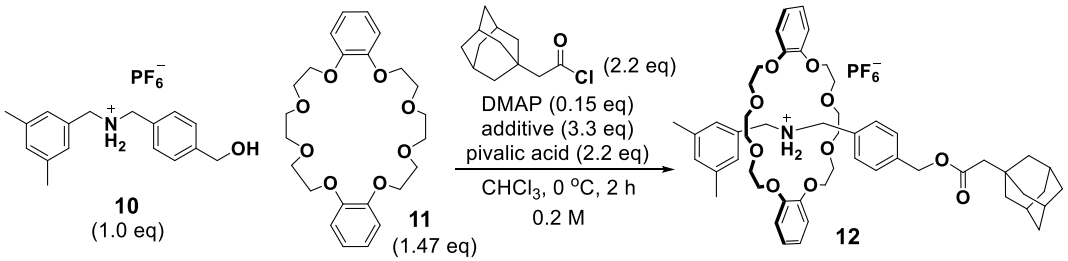

entry	additive	results (%)
1	$AgPF_6$	**94**
2	$AgPF_6$	not detected[#]
3	none	14*
4	$^iPr_2NEt$	not detected
5	2,4,6-collidine	trace

Figure 32 | DMAP-catalyzed synthesis of a rotaxane. [#] Acid anhydride was used instead of acyl chloride. Run for 2 days. * DMAP (1.5 equivalents) was used.

3.4 Conclusion

DMAP-catalyzed efficient synthesis of a rotaxane was developed. Acylation of a pseudorotaxane with acyl chloride and $AgPF_6$ in the presence of DMAP catalyst afforded the desired rotaxane in a high yield. This method is expected to be further explored toward asymmetric rotaxane synthesis with chiral DMAP analogues.

Chapter 4: Discrimination of Mobile Supramolecular Chirality

4.1 Backgrounds

Asymmetric synthesis has extensively developed during the last few decades for the construction of ubiquitous chiral molecules involving conventional chiral elements such as central, axial or planer chirality. With the current state of chemical science, asymmetric synthesis of such fixed chirality over covalent bond is reaching a level of mature science.

On the other hand, mechanically interlocked supramolecules such as rotaxanes and catenanes are known to possess unique supramolecular chirality consisting based on non-covalent binding (Figure 33A). Even though each of the ring and/or axis components has no chiral elements in itself, their combination brings supramolecular chirality linked non-covalent system when each of the components has dissymmetry. Such attractive chiral architectures of supramlecules have captured the attention of synthesis chemists for over five decades. In 1960, catenanes consisting of two dissymmetric ring components were mensioned that they could exist as pairs of enantiomers (*31*). In 1997, these topologically chiral racemic rotaxanes and catenanes were shown to be separable on chiral HPLC (Figure 33B) (*65*, *66*). However, even by virtue of current high achievement in the field of asymmetric synthesis, asymmetric discrimination and catalytic synthesis of chiral supramolecules stand as unsolved problems.

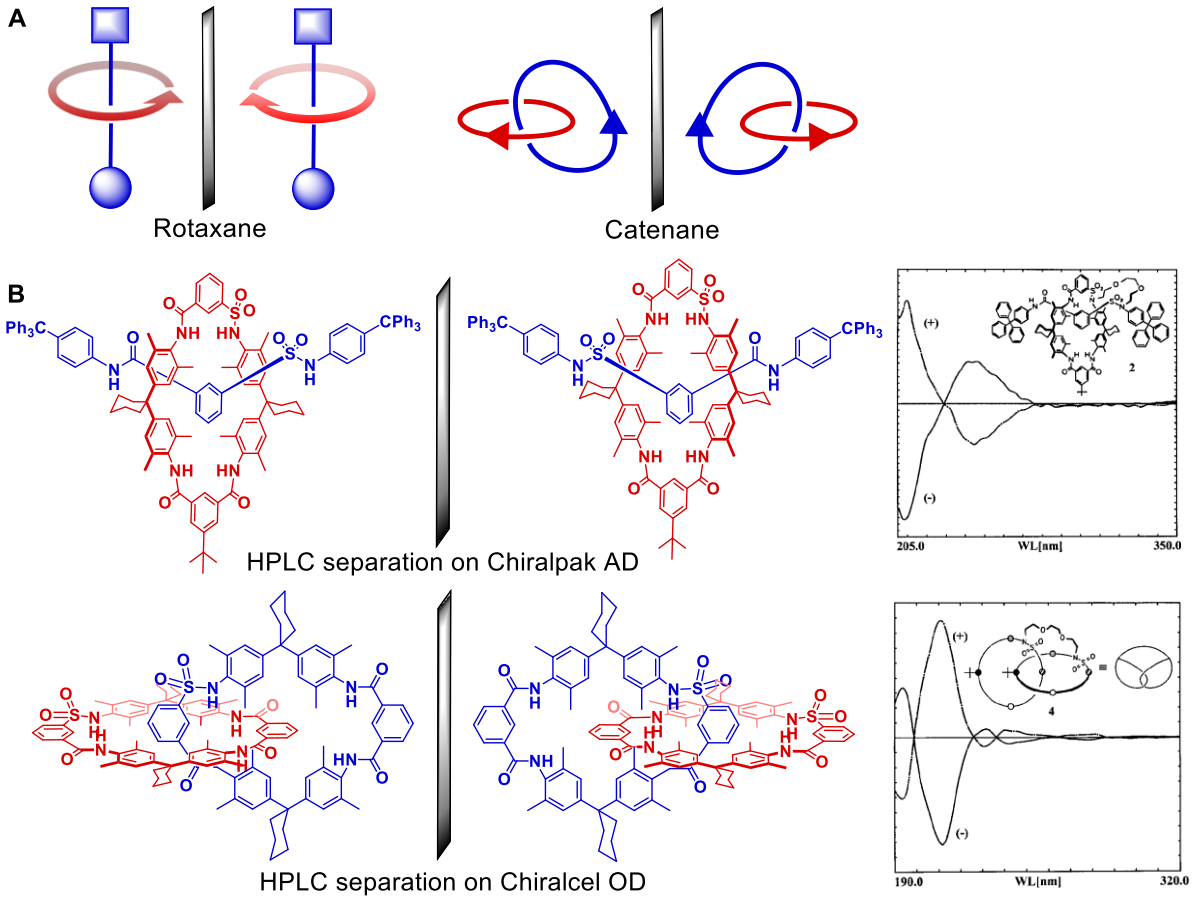

Y. Okamoto, F. Vogtle *et al. J. Am. Chem. Soc.* **1997**, *119*, 10547-10548.

Figure 33 | Topological chirality of supramolecules. (**A**) Topologically chiral rotaxanes and catenanes. (**B**) Separation of topologically chiral enantiomers by chiral HPLC.

For the preparation of chiral supramolecules, incorporation of an additional conventional chiral element such as central, axial, or planer chirality has been indispensable in most cases (*67*). Chiral supramolecules with additional chiral elements such as central (*68*, *69*), axial (*70*, *71*) or planer (*72*) chirality on their ring or axis component, have already been actively synthesized (Figure 34).

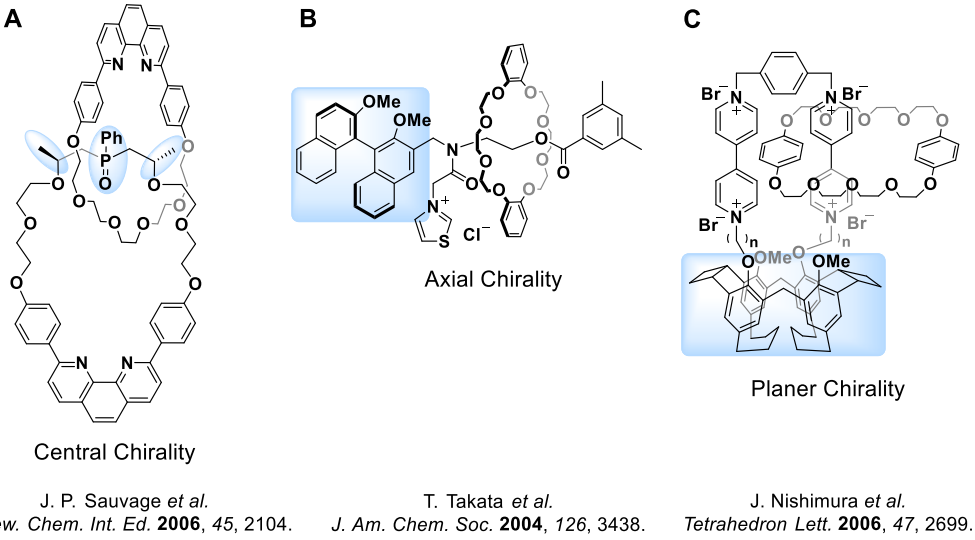

Figure 34 | Chiral supramolecules with additional chiral elements. (**A**) Catenane with central chirality. (**B**) Rotaxane with axial chirality. (**C**) Catenane with planar chirality.

Diastereomeric rotaxanes with an additional chiral element as well as a topological chirality have also been synthesized. Lacour and co-workers have reported a diastereoselective synthesis of pseudorotaxanes consisting of an additional helical chirality and an inherent topological chirality, however the diastereoselectivity was only 8% de (Figure 35A) (*73*). Quite recently, separation of diastereomers of a rotaxane was reported to be effective for the preparation of enantiopure topologically chiral rotaxanes. Goldup and co-workers synthesized a rotaxane as a mixture of diastereomers (2% de) consisting of a topological chirality and an additional central chirality in the chiral ester group. These mixtures of diastereomers were separated by column chromatography, then the ester group with the central chirality was removed and replaced by an achiral amide group, to give the topologically chiral enantiomers (Figure 35B) (*74*).

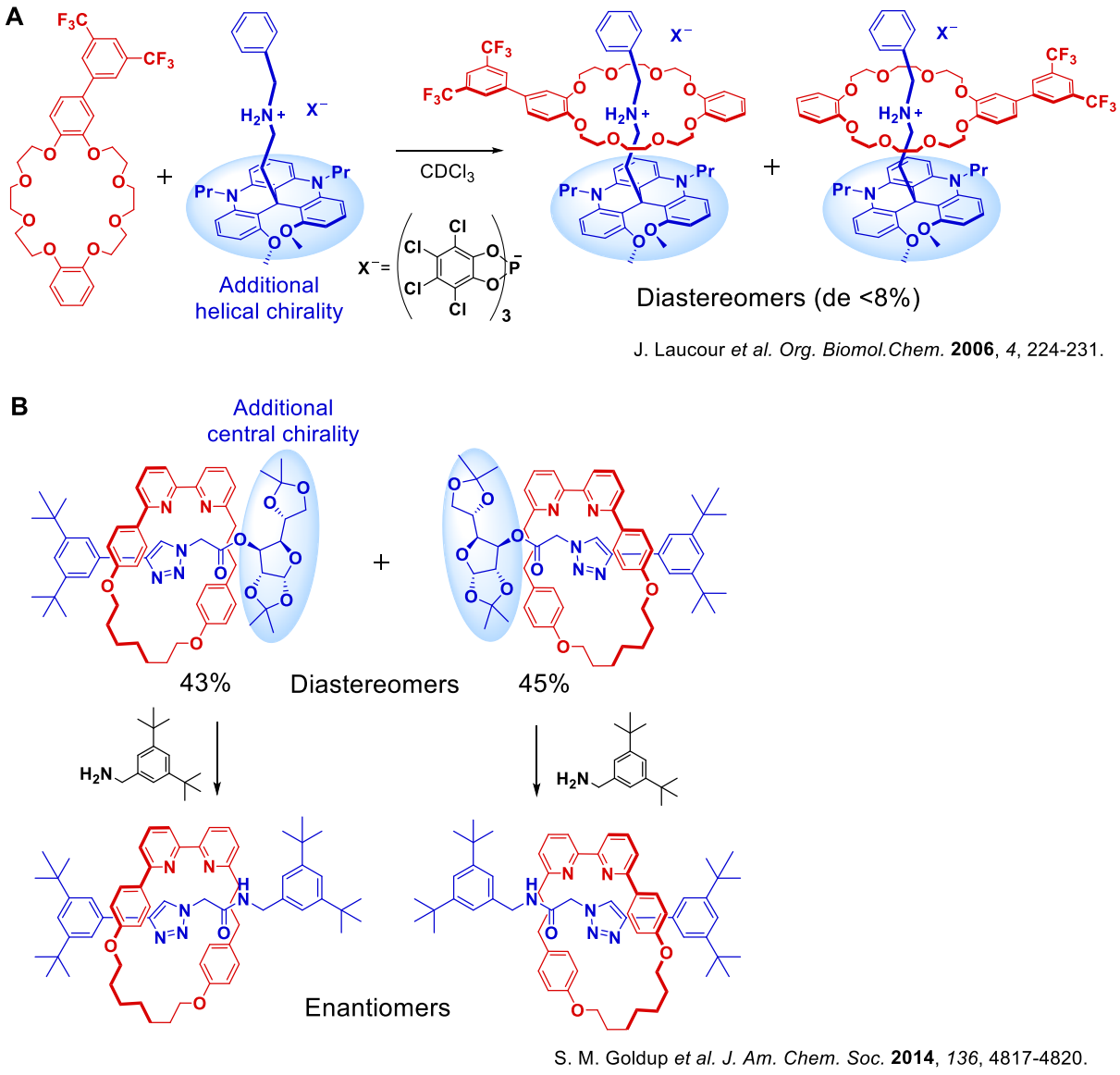

Figure 35 | Diastereomeric rotaxanes with a topological chirality and an additional chirality. (**A**) Attempts to diasteresoselective synthesis of pseudorotaxanes. (**B**) Separation of diastereomers for preparation of topologically chiral rotaxanes. Diastereomers consist of a topological chirality and a central chirality.

However, an efficient asymmetric synthesis of supramolecules possessing only inherent topological chirality still has never been achieved, despite active studies in this direction (*75*, *76*). To the best of our knowledge, only example of enantioselective synthesis of rotaxanes and catenanes has been reported by Takata and co-workers (Figure 36) (*34*). Dynamic kinetic resolution of a racemic pseudorotaxane was performed by catalytic asymmetric acylation of hydroxy group in the axis component. This most successful and pioneering example of discrimination of topological chirality delivered a rotaxane in up to only 4% ee.

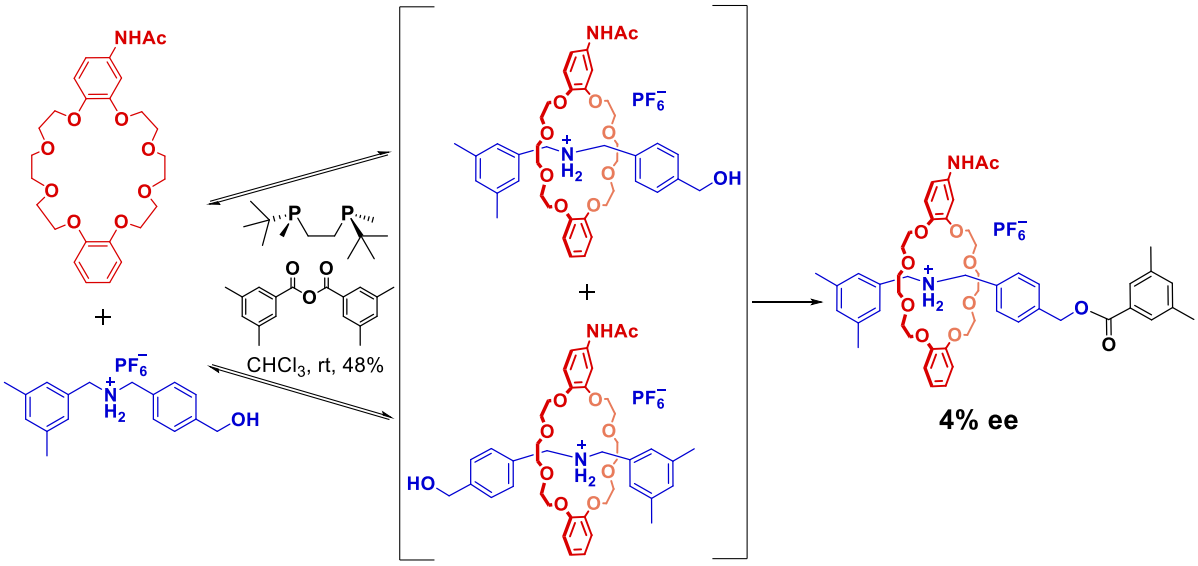

T. Takata *et al. Chem. Lett.* **2007**, *36*, 162-162.

Figure 36 | Most successful asymmetric synthesis of a topologically chiral supramolecule.

Under these backgrounds, I made a challenge toward highly enantioselective synthesis of topologically chiral rotaxanes by organocatalysis.

4.2 Mobile supramolecular chirality

Asymmetric synthesis of topologically chiral supramolecules is a conventionally difficult subject. The extreme difficulty in asymmetric molecular transformation of such supramolecules may be resulting from conformational diversity and movability of topologically chiral supramolecules. Topological chirality is in itself *mobile*, and kinetically labile topologically chiral supramolecules continuously change chiral environments. The expected chiral conformations **A**-**F** of an enantiomeric form of **13** are shown in Figure 37. All of the typical six chiral conformers **A**-**F** belong to just one single enantiomer *ent*-**13a**. Conformers **A**-**F** have different asymmetric microenvironments depending on the location of the ring component. Conformers **A** and **D** are pseudo-enantiomeric to each other from the view point of planer chirality (Figure 37C). Conformer **E** and **F** are in a similar relationship with **B** and **C**, respectively. Thus, a topologically chiral rotaxane has conformational diversity and movability. For the actual asymmetric discrimination of enantiomers with topological chirality, the enantiomers shown in Figure 37B should be distinguished, whereas the conformers **A** (**B**, **C**) and **D** (**E**, **F**) (Figure 37C) should *not* be distinguished because they are the identical enantiomer**.** Thus, it seems to be extremely challenging to discriminate mobile supramolecular chirality.

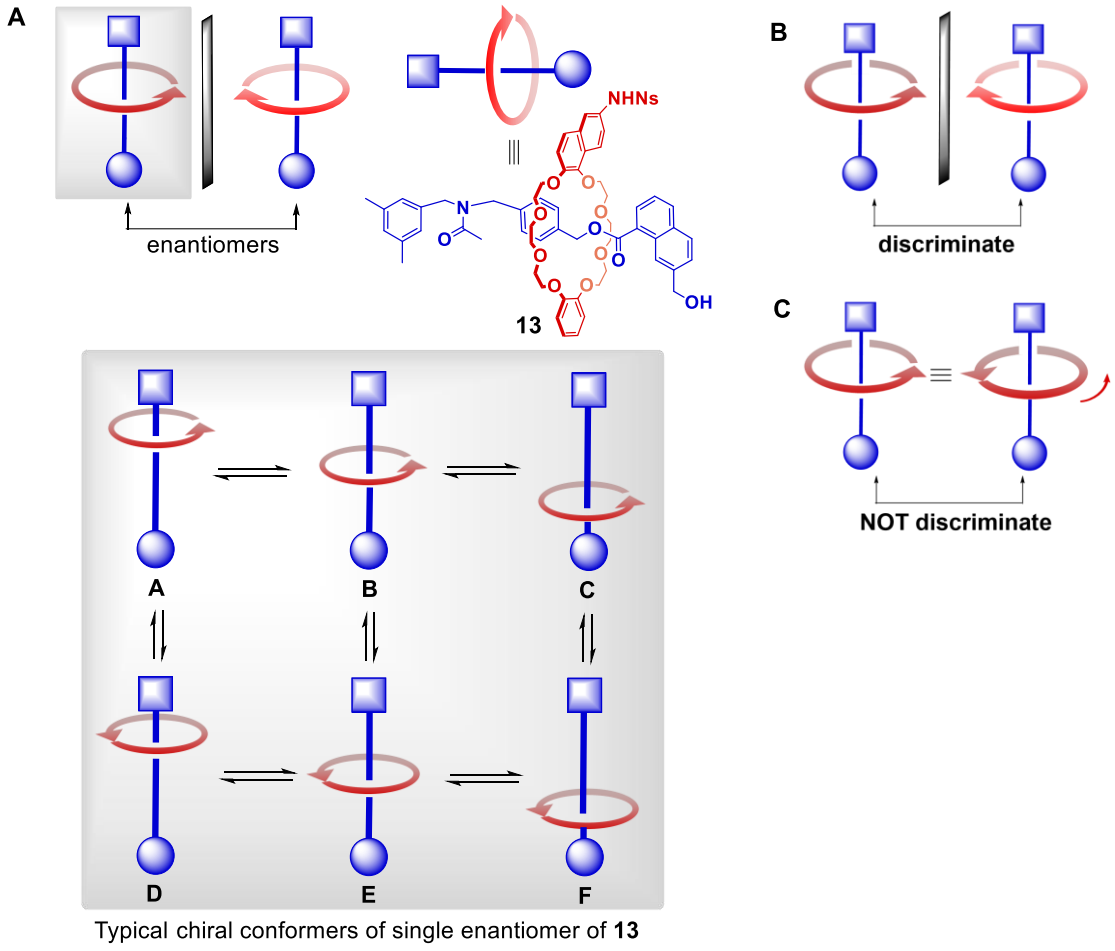

Figure 37 | Mobile supramolecular chirality. (**A**) Typical six chiral conformers of single enantiomer of **13**. (**B**) Pair of enantiomers of rotaxane **13**. (**C**) Chiral conformers (**A** and **D**) of identical enantiomer.

Such mobile nature of topological chirality could be experimentally observed. I measured CD spectra of rotaxane **14** (Figure 38). Figure 38A shows a CD spectrum of a pair of separated enantiomers (+)-**14** and (-)-**14**, which was measured at 20 ℃. A mirror image of the CD spectra clearly showed the enantiomeric relationship of these enantiomers. In Figure 38B, variable-temperature CD spectrum of a separated single enantiomer (+)-**14** is shown, which were measured by heating a MeCN solution of (+)-**14** from -10 ℃ to 60 °C. The CD behavior dramatically changed depending on temperature. Molar CD became smaller by raising temperature, although the rotaxane was existing as consistently a pure enantiomer (99% ee) throughout the experiments. The CD absorption maximum was red-shifted from 245 nm to 250 nm and the shape of the CD spectra changed with increasing temperature. In contrast, (*S*)-(-)-1,1'-bi-2-naphthol, which is known as a typical axially chiral compound, did not show such temperature dependence in a variable-temperature CD spectra (Figure 39). The small decrease of molar CD of (*S*)-(-)-1,1'-bi-2-naphthol seems to be caused by thermal expansion of the volume of the solvent. Thus, the unusual CD behavior of rotaxane **14** suggests mobile nature of supramolecular chirality caused by conformational diversity of topologically chiral rotaxane as schematically shown in Figure 37A. Such temperature-dependent CD behavior of rotaxane **14** was found to be reversible. I measured variable-temperature CD spectra of (+)-**14** by cooling a solution from 60 ℃ to -10 ℃, and the molar CD increased with decreasing the temperature (Figure 38C).

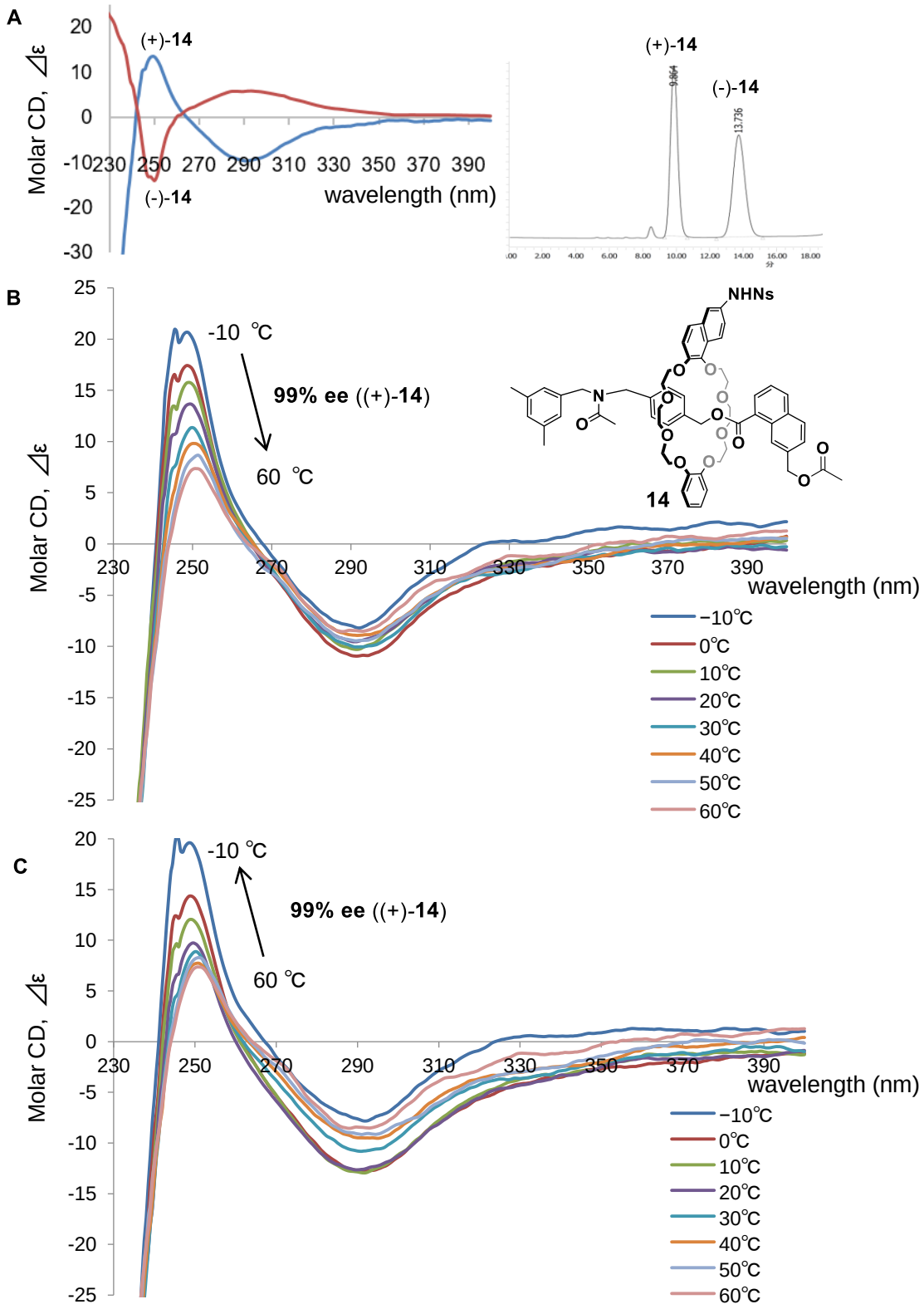

Figure 38 | CD spectra of rotaxane 14. (**A**) CD spectra and chiral HPLC chromatograms of a pair of enantiomers of rotaxane **14**. CD spectra were recorded in 1.38×10^{-5} M MeCN at 20 °C. Conditions for HPLC: CHIRALPAK IC column (4.6×250 mm); eluent 1:60 EtOH/CH_2Cl_2; flow rate 0.7 ml/min; detection 254 nm, temperature 20 °C. (**B**, **C**) Variable-temperature CD spectra of (+)-**14** measured by heating (**B**), or cooling (**C**) a solution. Recorded in 1.38×10^{-5} M MeCN.

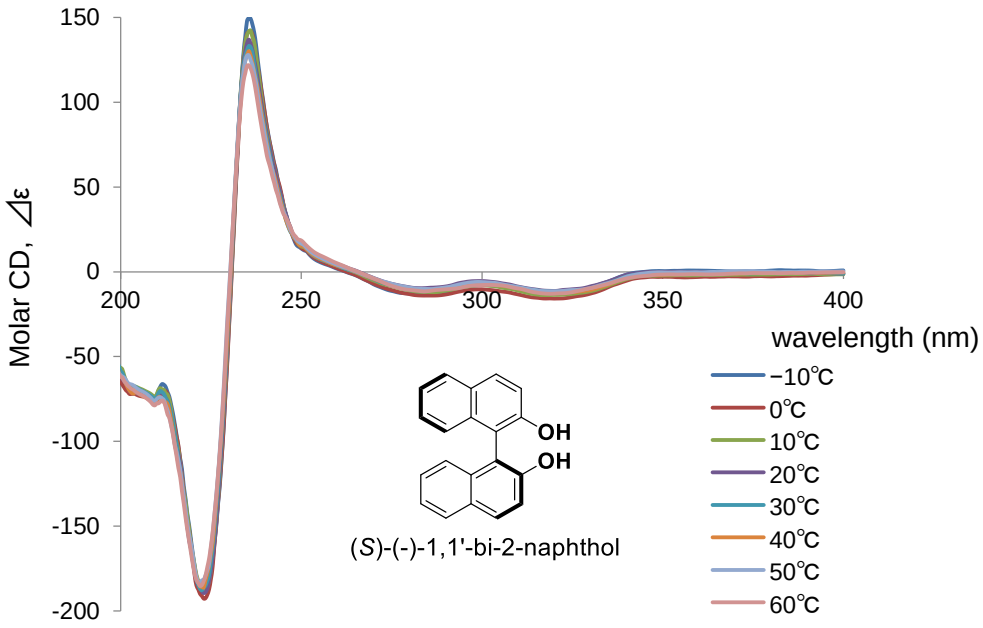

Figure 39 | **Variable-temperature CD spectra of (*S*)-(-)-1,1'-bi-2-naphthol.** Conditions: Recorded by heating 0.5×10^{-5} M MeCN solution of (*S*)-(-)-1,1'-bi-2-naphthol from -10 to 60 °C.

Based on these observation of CD spectra, I measured a variable-temperature NMR of rotaxane **14** in acetonitrile-d_3 in the temperature range from -40 °C to 60 °C (Figure 40). The assignments of the ^{1}H NMR spectra of rotaxane **14** were made using COSY, HMQC, HMBC and DEPT 135 methods at 20 °C. The NMR spectra of **14** showed strong temperature dependency. Upon heating, many pairs of signals coalesced or broadened. Notably, these chemical shifts at the coalescence temperature were not the average chemical shifts of the corresponding individual two signals observed at the low temperature. For example, benzylic proton signals Hb (Figure 40), which were observed at ca. 6.24 and 5.92 ppm at -40 °C, appeared at 6.21 and 6.18 ppm at 60 °C. The average chemical shift (6.08 ppm) at -40 °C was shifted downfield and observed at 6.20 ppm by elevating the temperature at 60 °C. Methylene proton signals of crown ether appeared in the range of 4.6-2.6 ppm at -40 °C drastically changed the resonance in the range of 4.3-3.3 ppm at 60 °C. These observation suggest the change of the ratio of chiral conformers depending on temperature. The observed NMR spectra of rotaxane **14** indicates the diversity and mobility of chiral environment of rotaxanes.

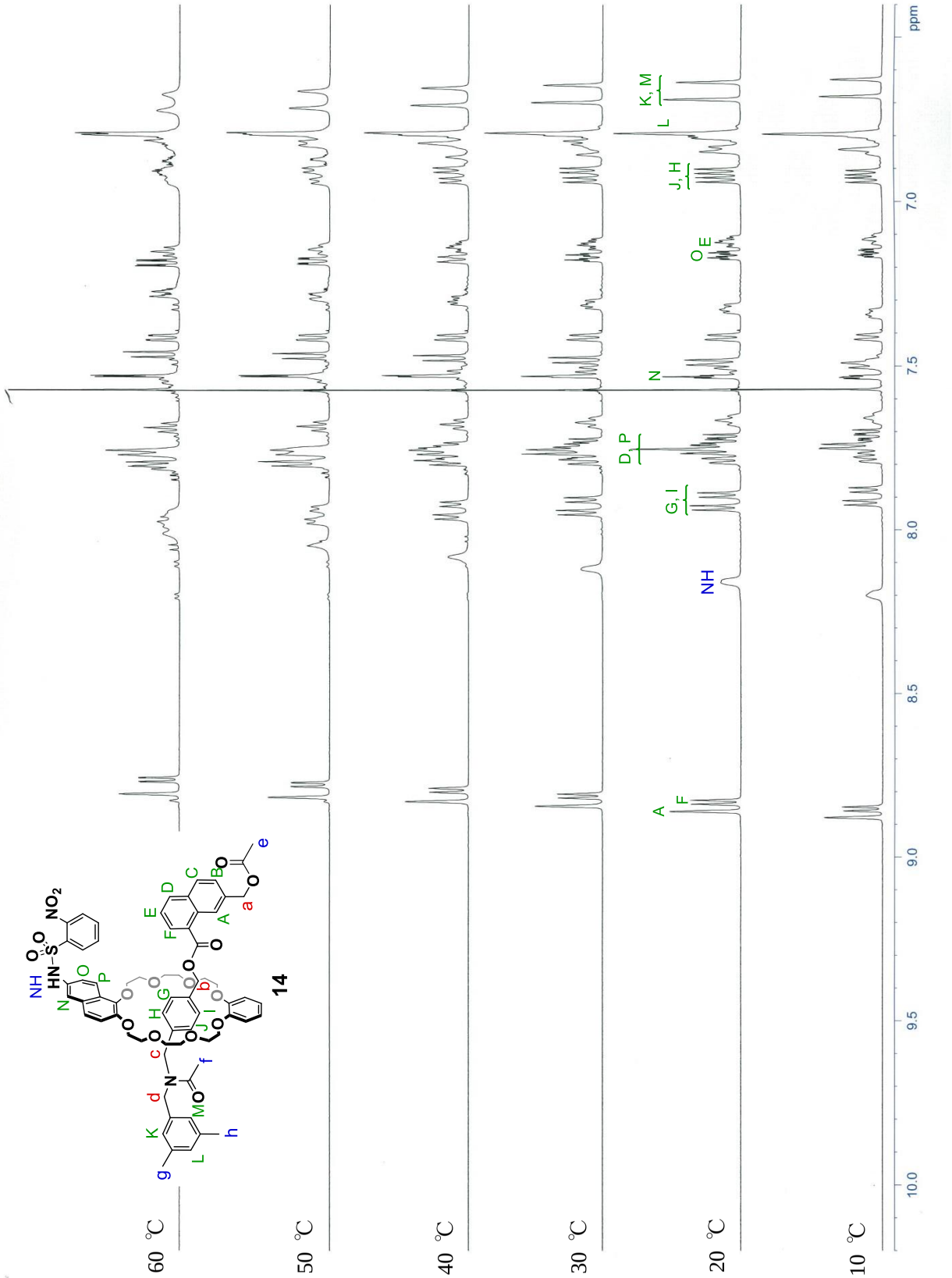

Figure 40 | **Variable-temperature NMR spectra of rotaxane 14.** Conditions: Heating a CD_3CN solution of rotaxane **14** from -40 °C to 60 °C.

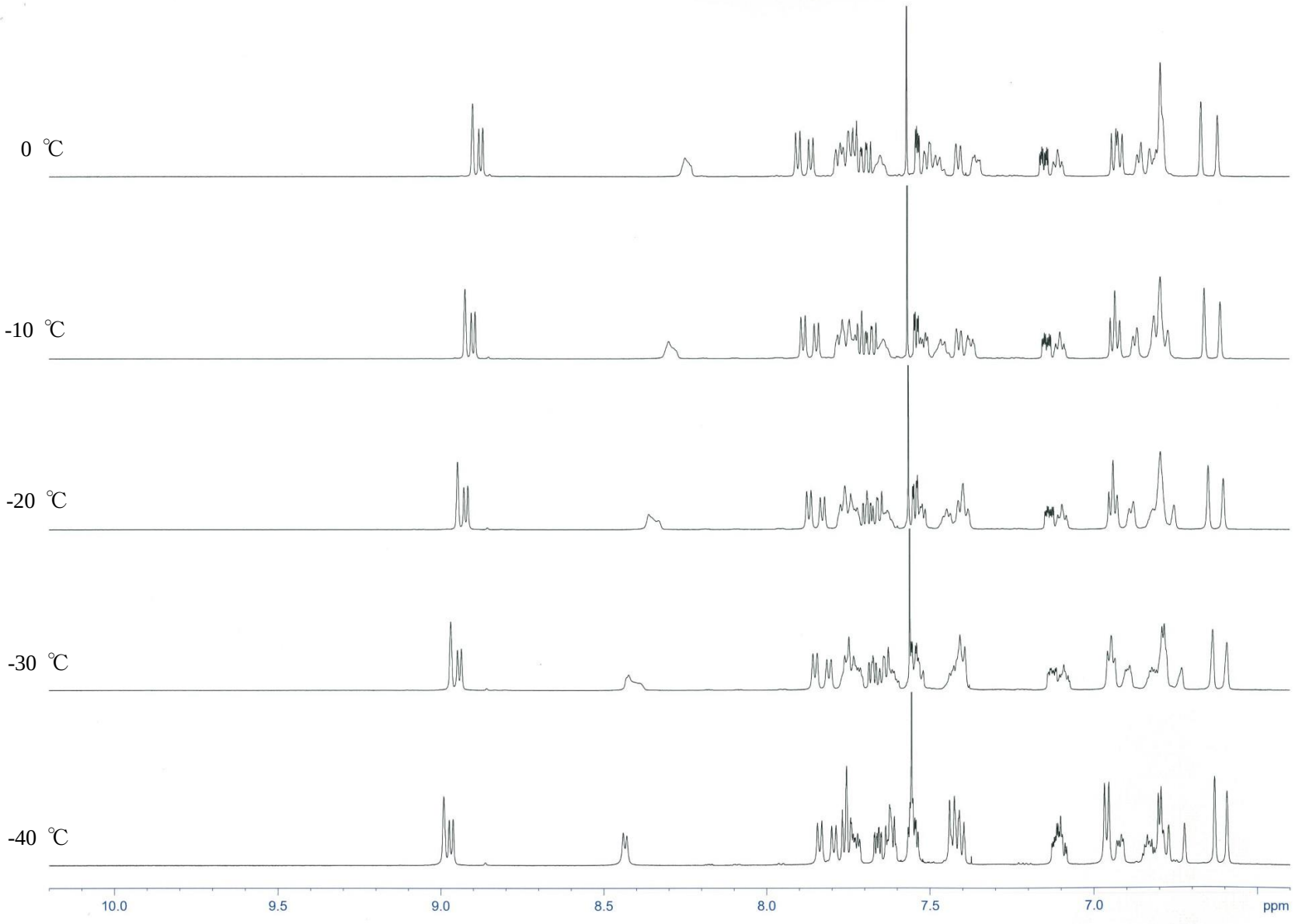
0 ℃
-10 ℃
-20 ℃
-30 ℃
-40 ℃
10.0
9.5
9.0
8.5
8.0
7.5
7.0
ppm

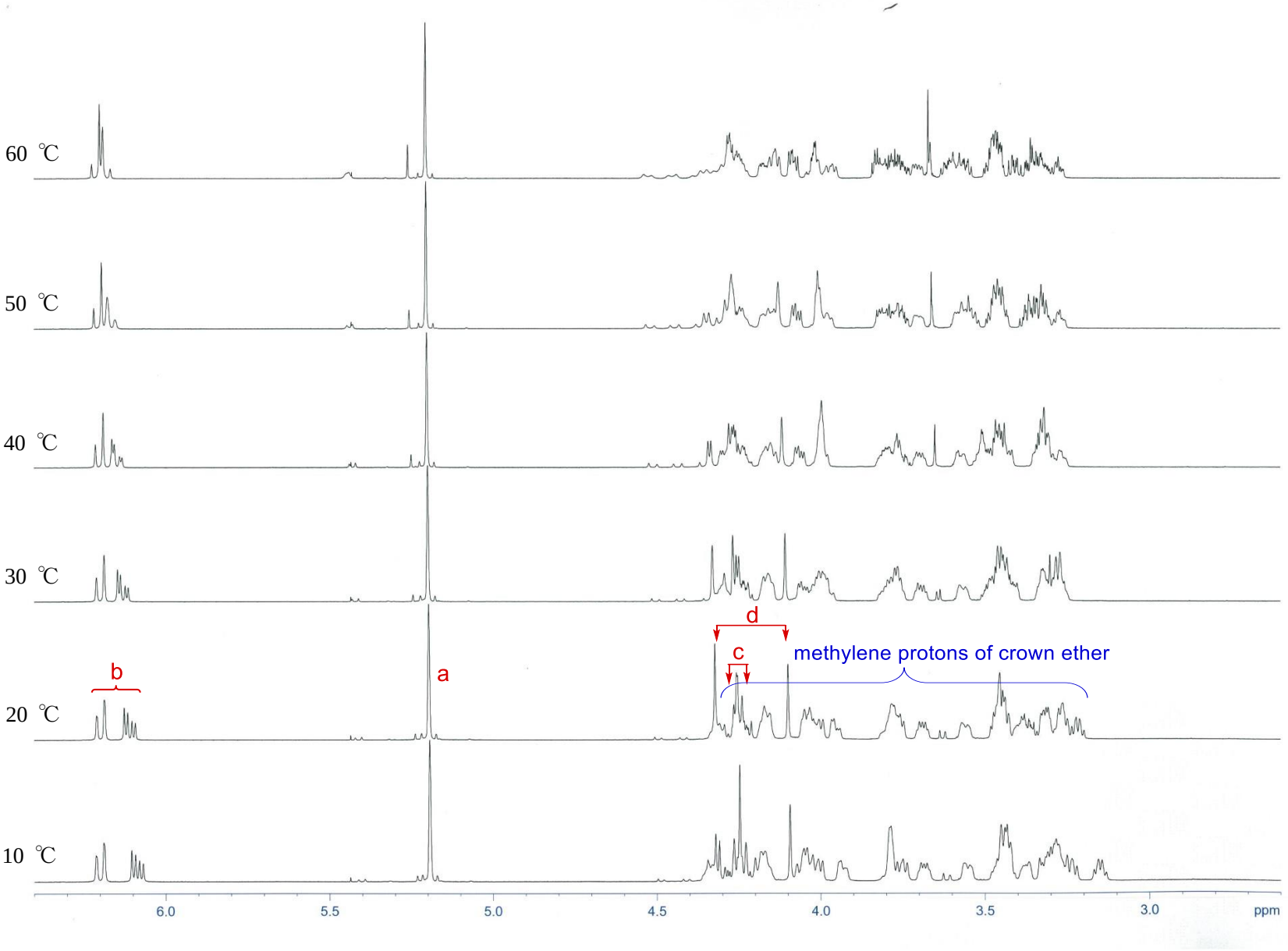
60 ℃
50 ℃
40 ℃
30 ℃
20 ℃
10 ℃
b
a
d
c
methylene protons of crown ether
6.0
5.5
5.0
4.5
4.0
3.5
3.0
ppm

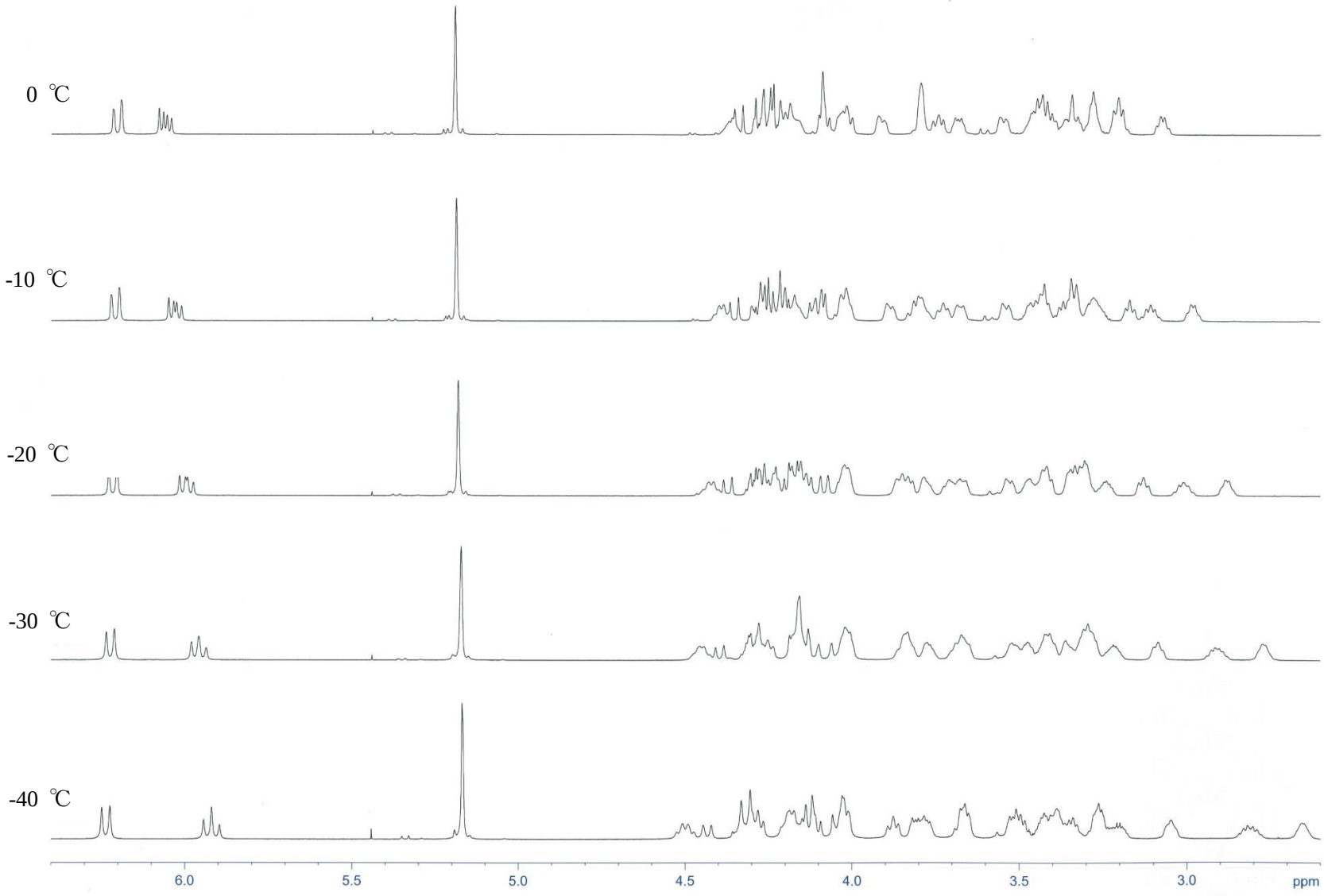
0 ℃
-10 ℃
-20 ℃
-30 ℃
-40 ℃
6.0
5.5
5.0
4.5
4.0
3.5
3.0
ppm

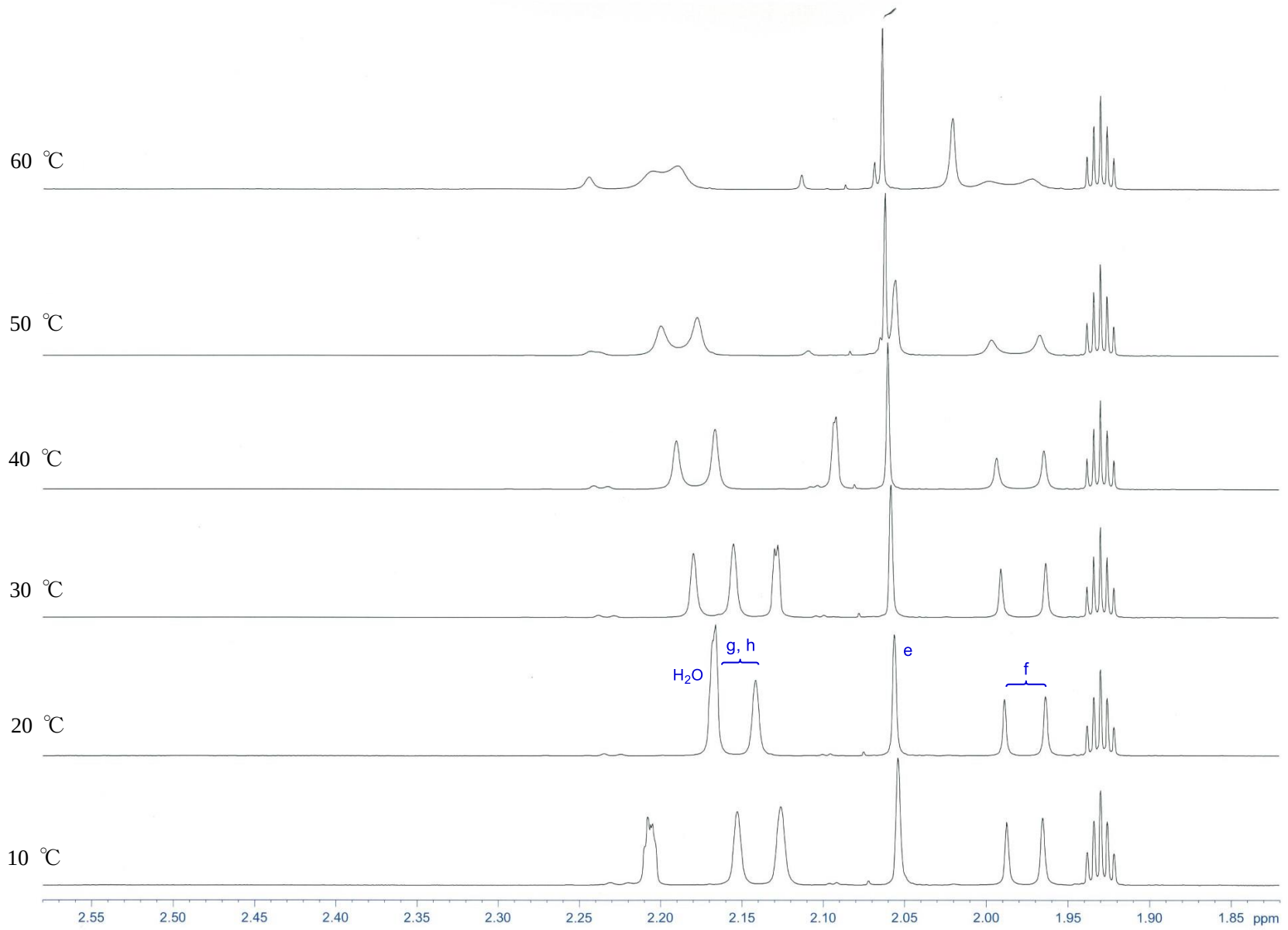
60 ℃
50 ℃
40 ℃
30 ℃
20 ℃
10 ℃
H2O
g, h
e
f
2.55
2.50
2.45
2.40
2.35
2.30
2.25
2.20
2.15
2.10
2.05
2.00
1.95
1.90
1.85 ppm

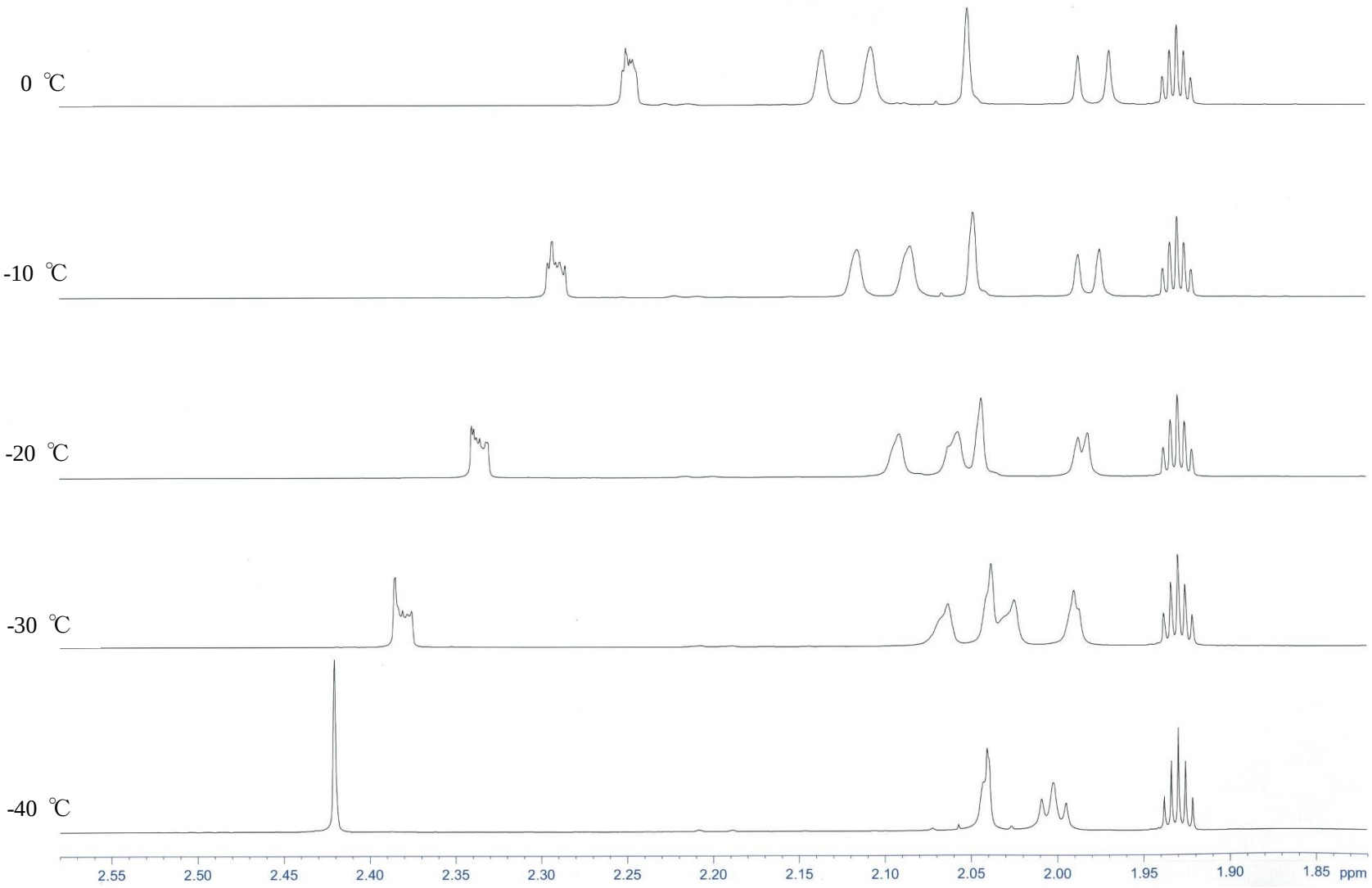
0 ℃
-10 ℃
-20 ℃
-30 ℃
-40 ℃
2.55
2.50
2.45
2.40
2.35
2.30
2.25
2.20
2.15
2.10
2.05
2.00
1.95
1.90
1.85
ppm

4.3 Designed Strategy

Herein I show the first highly enantioselective synthesis of topologically chiral rotaxanes. The designed strategy belongs to an acylative kinetic resolution of topologically chiral racemic rotaxanes by organocatalysis (Figure 41A). This strategy is based on the concept of dynamic molecular recognition of organocatalysts. As the substrate, I chose rotaxane alcohols bearing a NHNs group and a hydroxy group on their ring components and axis components, respectively (Figure 41B) (*36*, *37*, *48*).

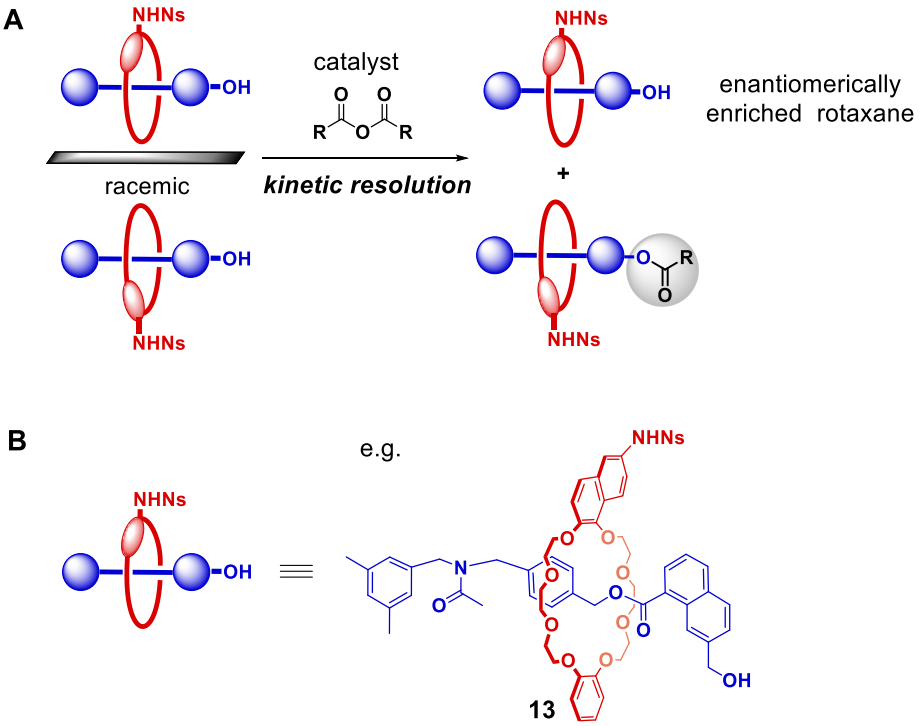

Figure 41 | Designed strategy. (**A**) Kinetic resolution of a topologically chiral racemic rotaxane by organocatalysis. (**B**) Example of rotaxane substrates for kinetic resolution.

As the backgrounds, our laboratory previously achieved asymmetric acylation of prochiral linear diols with conformational flexibility which have a NHNs group and a hydroxy group (Figure 42A). In the presence of catalyst **3**, asymmetric acylations of diols having various distance between these functionallities were investigated. Among them, the diol **27** having 5 Å distance between functionallities afforded its acylate with the highest enantioselectivity, although diols having shorter (**25** and **26**) or longer (**28**) inter-functionality distance than 5 Å showed reduced enantioselectivity. Thus, catalyst **3** likely discrimininates chiral environment most effectively when the distance between these functionalities is around 5 Å.

This hypothesis of discrimination of distance was applied to discrimination of supramolecular chirality (Figure 42B). Rotaxanes have mobile supramolecular chirality, thus, the relative topology between the NHNs group and the hydroxy group continuously changes. However, at the moment when these functionalities reached the distance of 5 Å, the catalyst would be able to discriminate the chiral environment of the rotaxane. Based on this concept of dynamic molecular recognition, I envisaged a kinetic resolution of topologically chiral racemic rotaxane by organocatalysis.

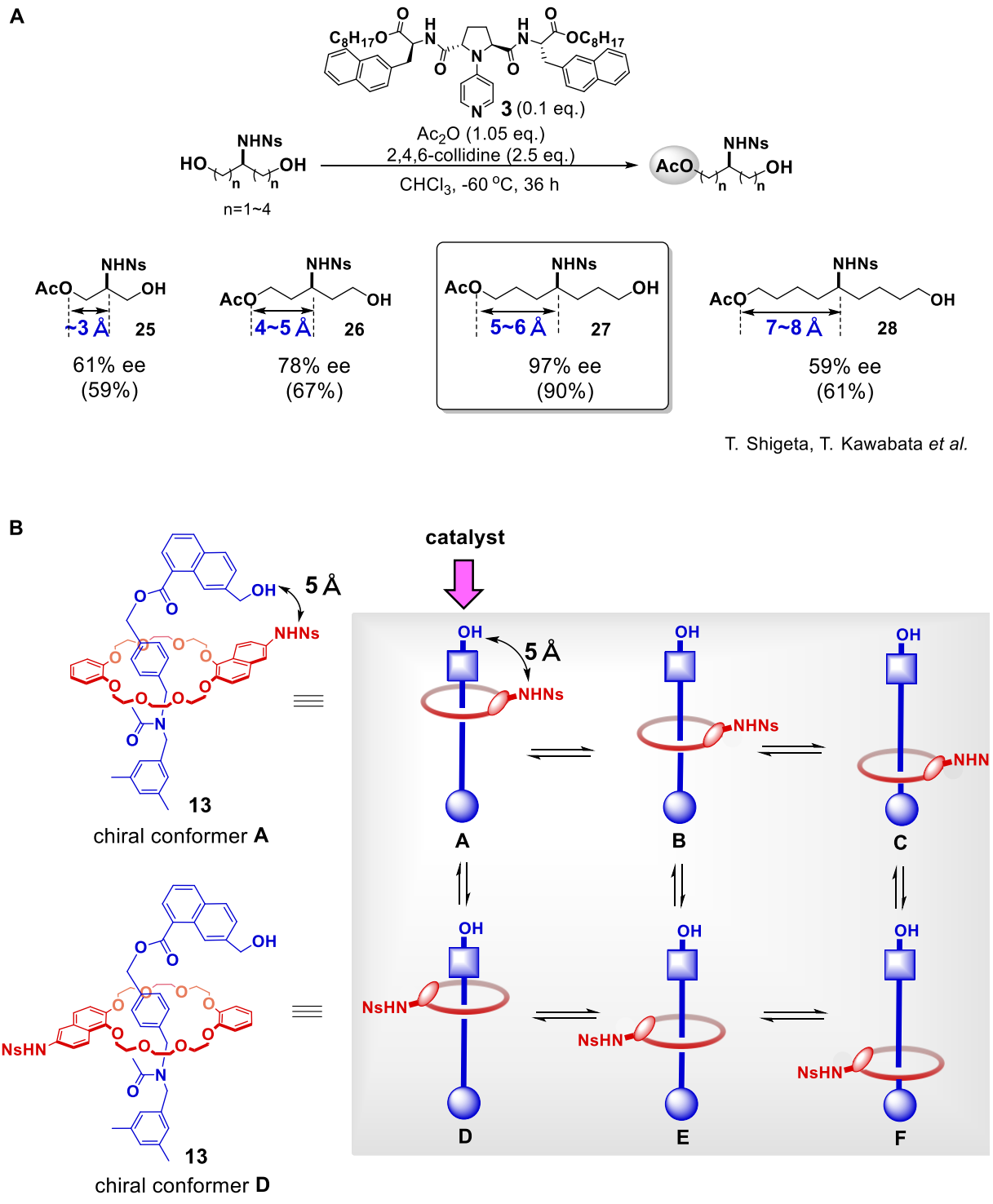

Figure 42 | Concept of dynamic molecular recognition by catalyst. (**A**) Discrimination of distance between functionalities by catalyst **3**. (**B**) Designed strategy for discrimination of mobile supramolecular chirality of rotaxane **13** by dynamic molecular recognition.

4.4 Synthesis of substrates

First of all, I synthesized rotaxaene substrates bearing a hydroxy group on their axis component and a NHNs group on its ring component. Rotaxane **13**, **29** and **30** were synthesized from the corresponding ring components **34**, **35** or **36**, axis component **10**, and endcap **37** (Figure 43).

Synthesis of ring components is shown in Figure 44. Ring components **34**, **35** and **36** were prepared from 6-bromo-2-naphthol. Oxidation of 6-bromo-2-naphthol gave the diketone **38**, which was reduced into naphthalene-1,2-diol **39**. Since naphthalene-1,2-diol **39** was very sensitive to air, **39** was carefully treated under Ar atmosphere. Naphthalene-1,2-diol **39** was converted to stable alcohol **40**. Conversion of alcohol **40** to crown ether **42** was performed by tosylation of hydroxy groups, followed by cesium cation-templated cyclization. The cyclization reaction required at least one week for the completion. Buchwald-Hartwig amination of naphthylbromide **42**, followed by deprotection of the Boc group of **43**, provided amine hydrochloride **44**. Treatment of amine **44** with *o*-NsCl gave desired ring component **34** (9.7 g).

Ring component **36** bearing *N*-methyl substituent was prepared from the ring component **34**.

Ring component **35** was prepared from naphthylbromide **42** in three steps. Rosenmund-von Braun reaction of naphthylbromide **42**, followed by reduction of nitrile **45**, provided naphthylmethylamine **46**. Naphthylmethylamine **46** was converted into desired ring component **35** bearing *o*-Ns substituted naphthylmethylamine.

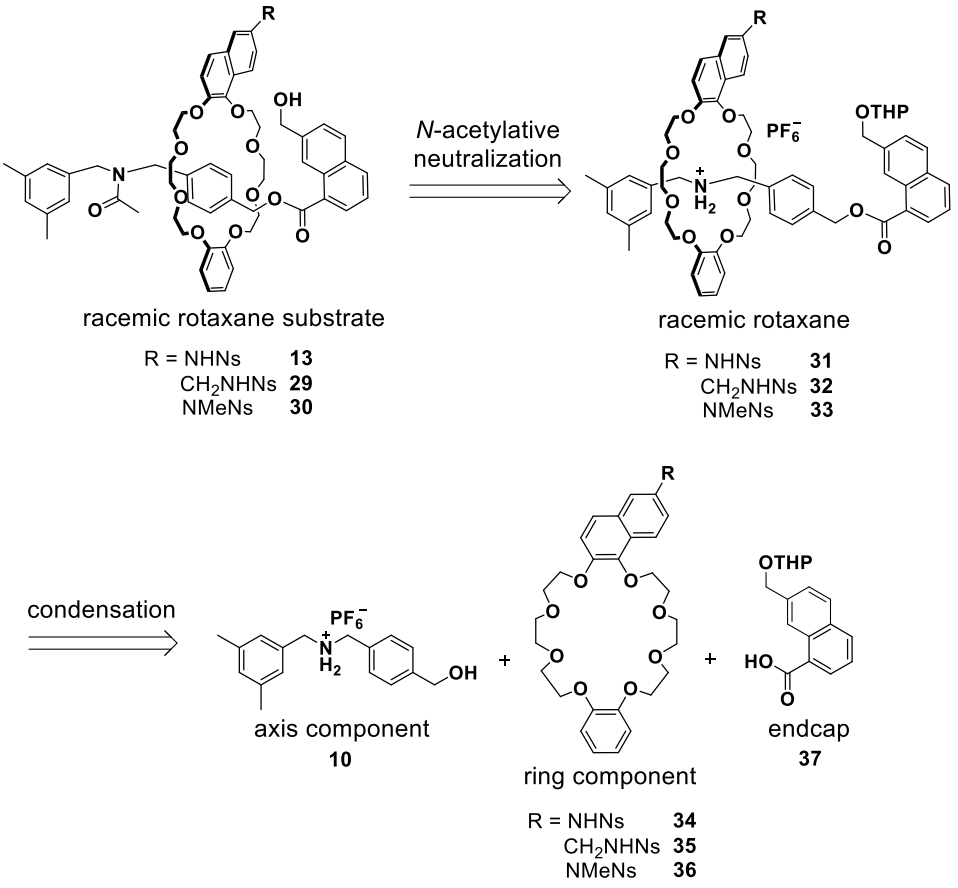

Figure 43 | Retrosynthesis of rotaxane substrates 13, 29 and 30.

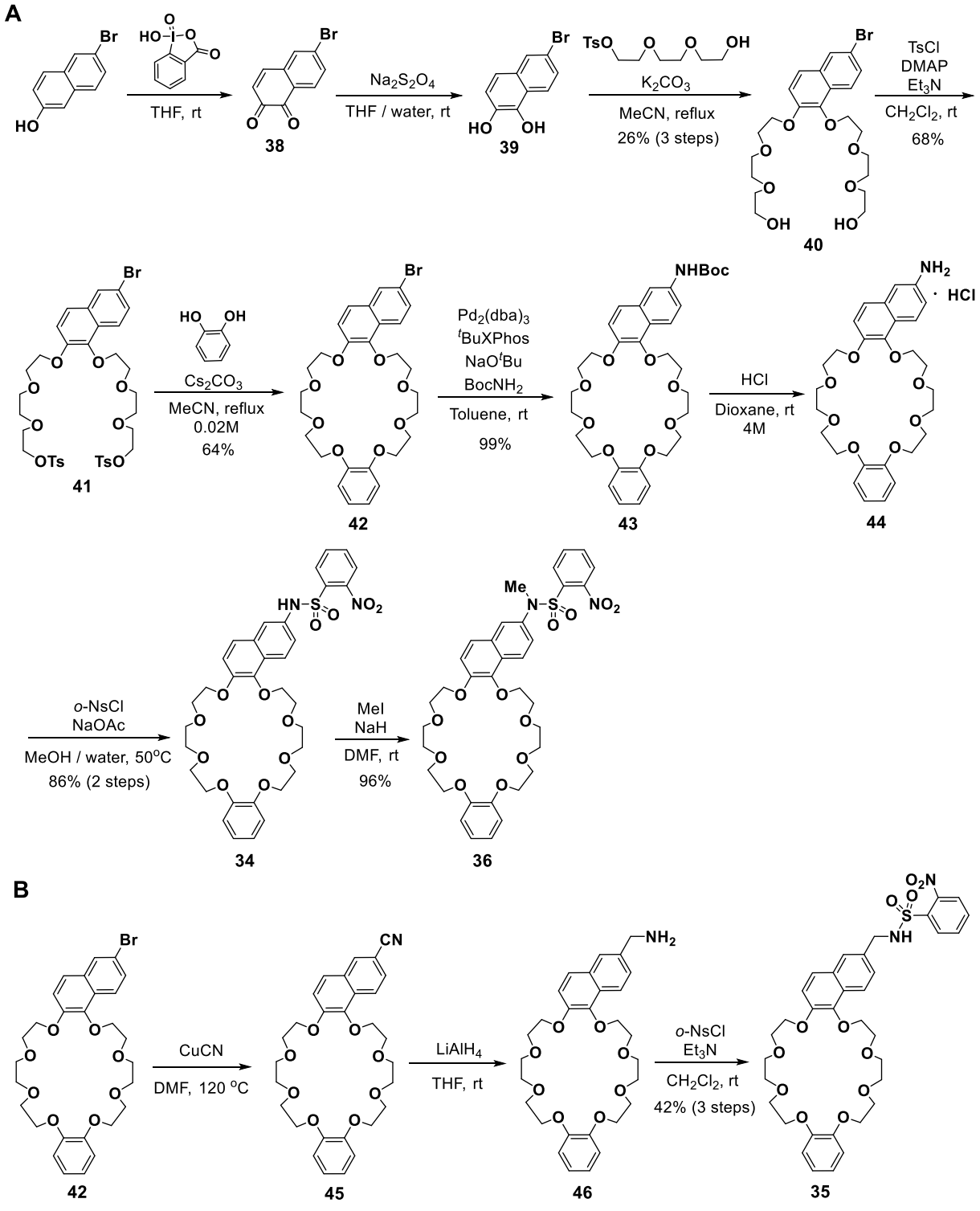

Figure 44 | Synthesis of ring components (**A**) **34**, **36** and (**B**) **35**.

THP-protected endcap **37** was prepared from 1,7-dihydroxynaphthalene (Figure 45). Triflation of 1,7-dihydroxynaphthalene followed by carbonylation gave dimethyl ester **48**. Monosaponification of diester **48** gave desired carbonyl compound **49** after reprecipitation. Reduction to alcohol **50** and THP protection of hydroxy group of **50** preceded the saponification of methyl ester **51**, which led to the desired endcap **37** (5.0 g).

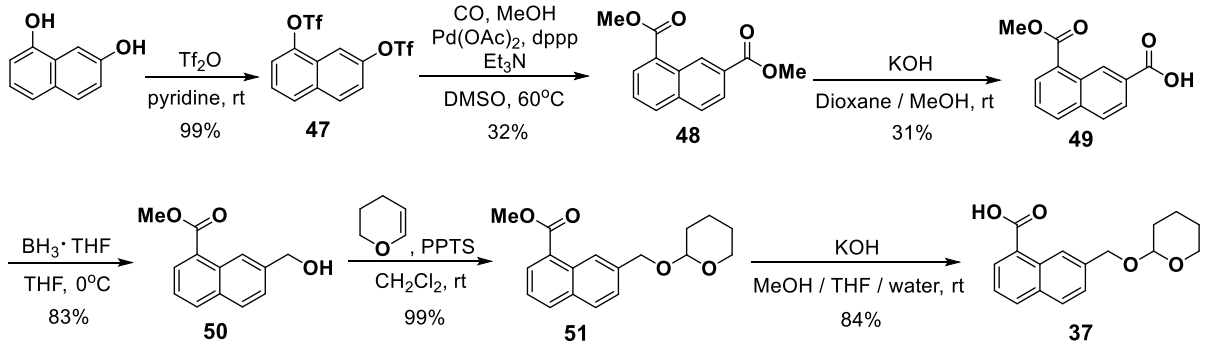

Figure 45 | Synthesis of endcap component 37.

Reported axis component **10** was prepared from 3,5-dimethylbenzoic acid (Figure 46) (*62*). 3,5-Dimethylbenzoic acid was converted to amide **53** followed by reduction to give benzylamine **54**. Conversion of benzylamine **54** to amino alcohol **56** was performed by reductive amination by using lithium aluminum hydride, where the methyl ester of **55** was also reduced to the corresponding alcohol. Amino alcohol **56** was converted into desired axis component **10** via corresponding hydrochloride salt **57**.

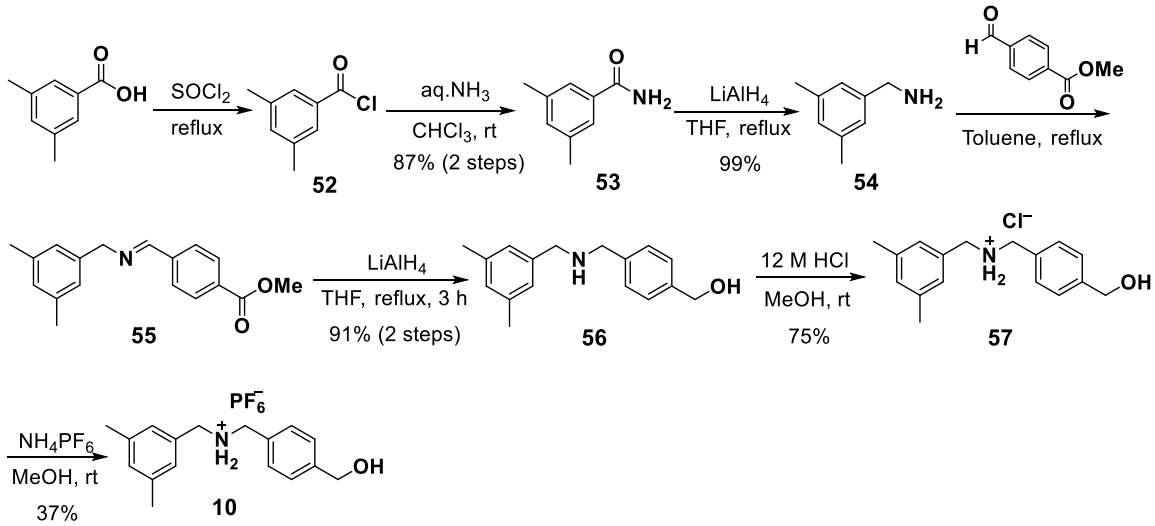

Figure 46 | Synthesis of axis component 10.

Then, racemic rotaxane **13** was synthesized from the corresponding ring component **34**, axis component **10** and endcap **37** (Figure 47). Rotaxane **31** was prepared according to the tributylphosphine-catalyzed acylative end-capping protocol reported by Takata and co-workers (*62*). In this step, rotaxane **31** becomes a racemic mixture because the axis component threads the ring component randomly from both sides of the ring component. Racemic rotaxane **31** was converted to **58** by *N*-acylation of the axis component. Since the amino group on the ring component was also acylated as well as the amino group on the axis component, selective hydrolysis of the amide group on the ring component was performed to give **60**. Finally, deprotection of THP group of **60** provided the desired rotaxane substrate **13** (1.5 g).

Rotaxane substrate **29** (Figure 47A) and **30** (Figure 47B) could be prepared by the similar manner employed for **13**.

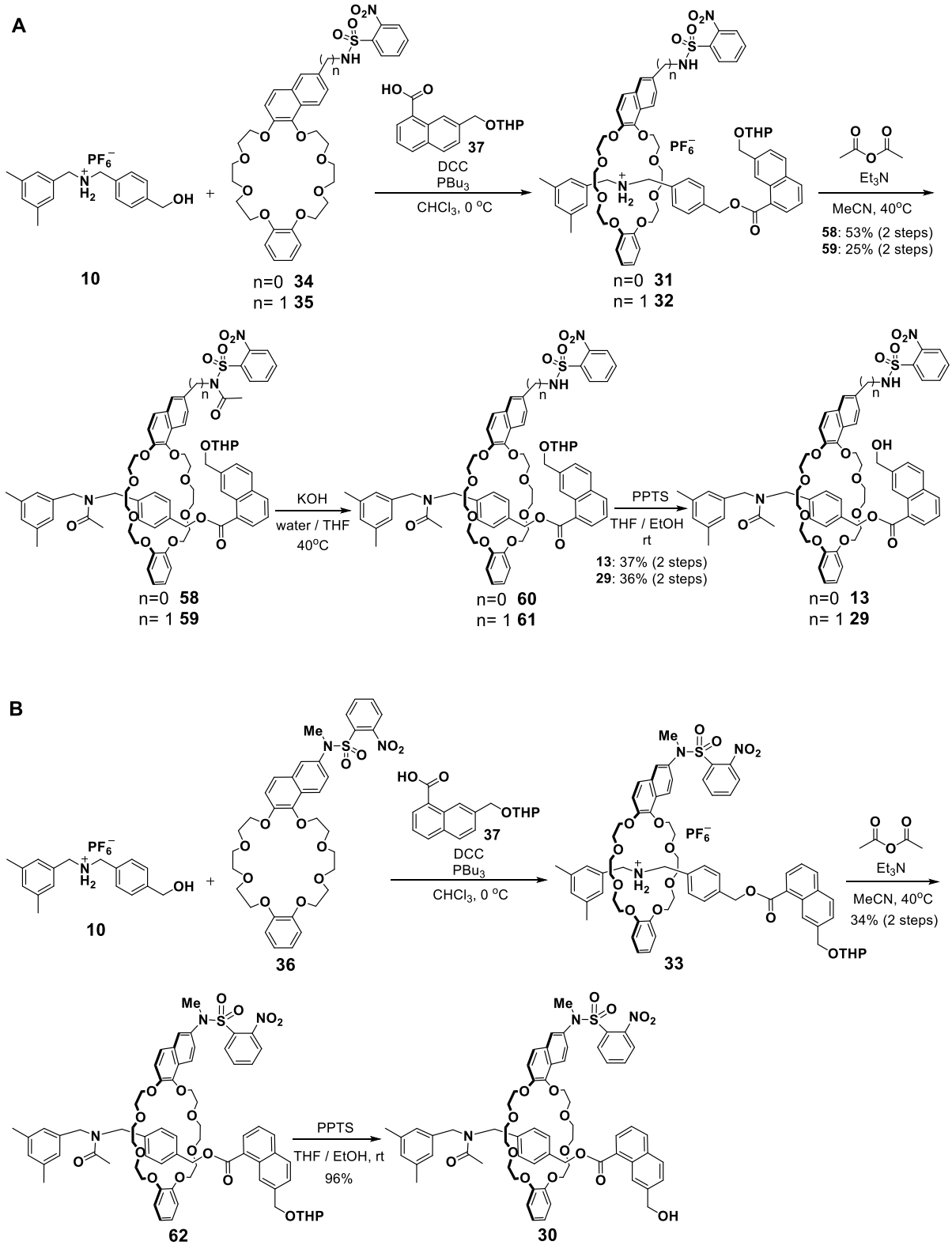

Figure 47 | Synthesis of racemic rotaxanes (**A**) **13**, **29** and (**B**) **30.**

4.5 Optimization of conditions

4.5.1 Screening of substrates

I initially examined various rotaxane alcohols **13**, **64**, **59** and **65** bearing a NHNs group and a hydroxy group for acylative kinetic resolution (Figure 48). In the presence of chiral PPY catalyst **63**, kinetic resolution of topologically chiral racemic rotaxanes were performed in $CHCl_3$ at -60 °C. Catalyst **63** was found to be effective in discrimination of mobile supramolecular chirality. These rotaxanes gave the selectivity factor in the range of 1-2.

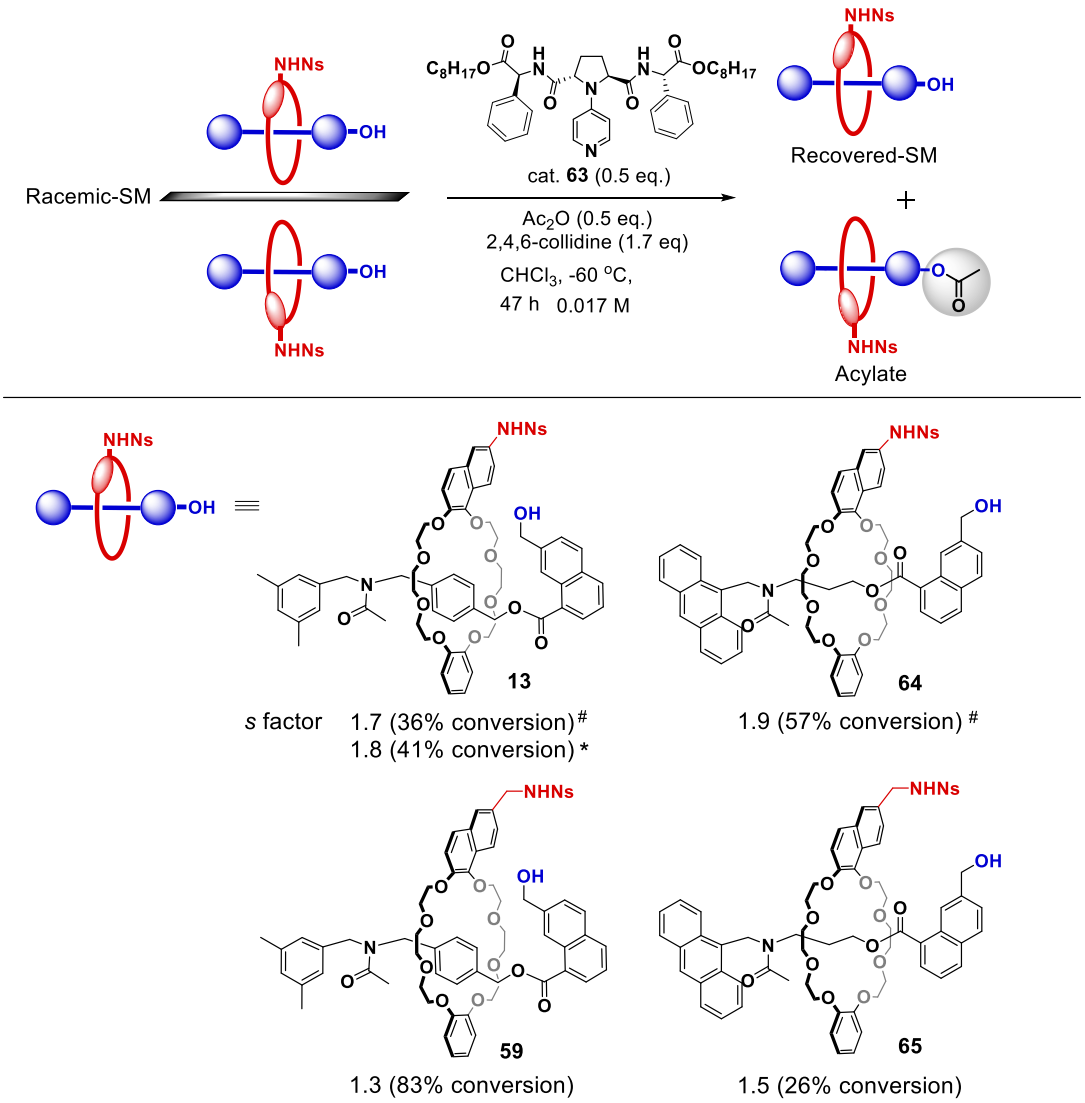

Figure 48 | Initial screening of structure of substrates. #Run in 0.007 M solution. *Reactions performed with 0.1 equivalents of catalyst **3** in 0.07 M solution for 6 days. $(i\text{-PrCO})_2O$ (0.9 equivalents) was used instead of acetic anhydride.

I then examined rotaxane substrates **13**, **66** and **67** possessing an amide group with various degree of steric bulkiness on their axis components (Figure 49). I expected that the bulky amide group on the axis component improves enantioselectivity by pushing the ring component to the edge of the axis component, thereby the NHNs group easily approach the hydroxy group at the distance of 5 Å. However, steric bulkiness of amide groups showed almost no effect on the enantioselectivity.

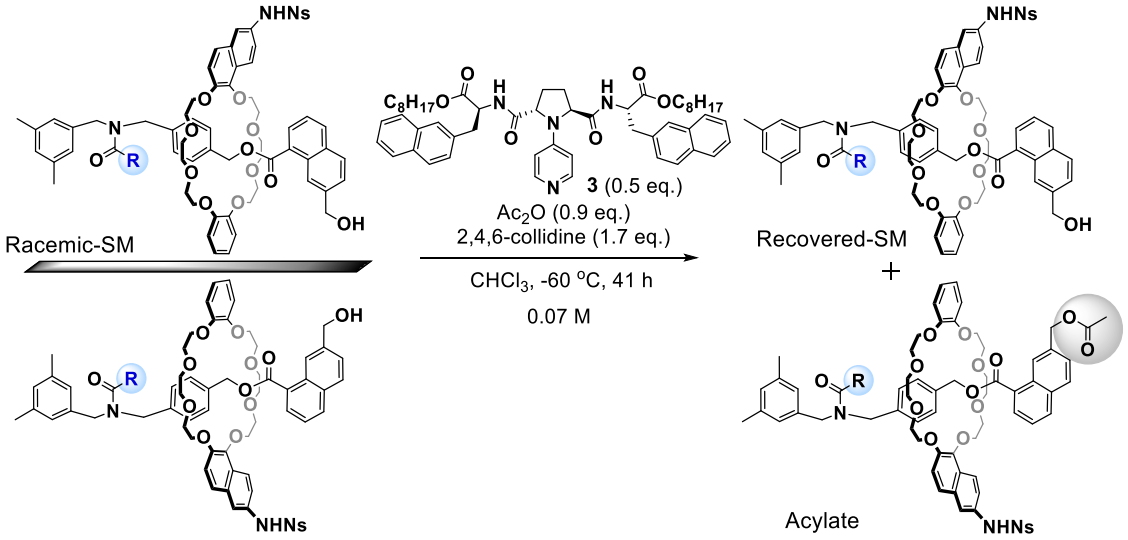

entry	R		ee of acylate (%)	ee of SM (%)	conversion (%)	*s* factor
1	**Me**	**13**	22	15	41	1.8 *
2	**Ph**	**66**	10	43	82	1.7
3		**67**	8	65	89	1.9

Figure 49 | **Effects of steric bulk of amide groups on axis components.** *Reactions performed with 0.1 equivalents of catalyst **3** for 6 days. (*i*-PrCO)$_2$O was used instead of acetic anhydride.

4.5.2 Screening of catalysts

I examined various 4-pyrroridinopyridine (PPY)-based catalysts **3**, **69**, **68**, **70** and **63** for acylative kinetic resolution of topologically chiral racemic rotaxane **13** (Figure 50). Among them, catalyst **3** was found to be the most effective catalyst, which gave acylate **14** and recovered-**13** with 22% ee and 15% ee, respectively, with selectivity factor of 1.8. Catalyst **69**, the diastereomer of catalyst **3**, was found less effective for the kinetic resolution. Catalysts **68**, **70** and **63**, which are replaced the naphthyl side chain of catalyst **3** with other substituents, showed further diminished enantioselectivity.

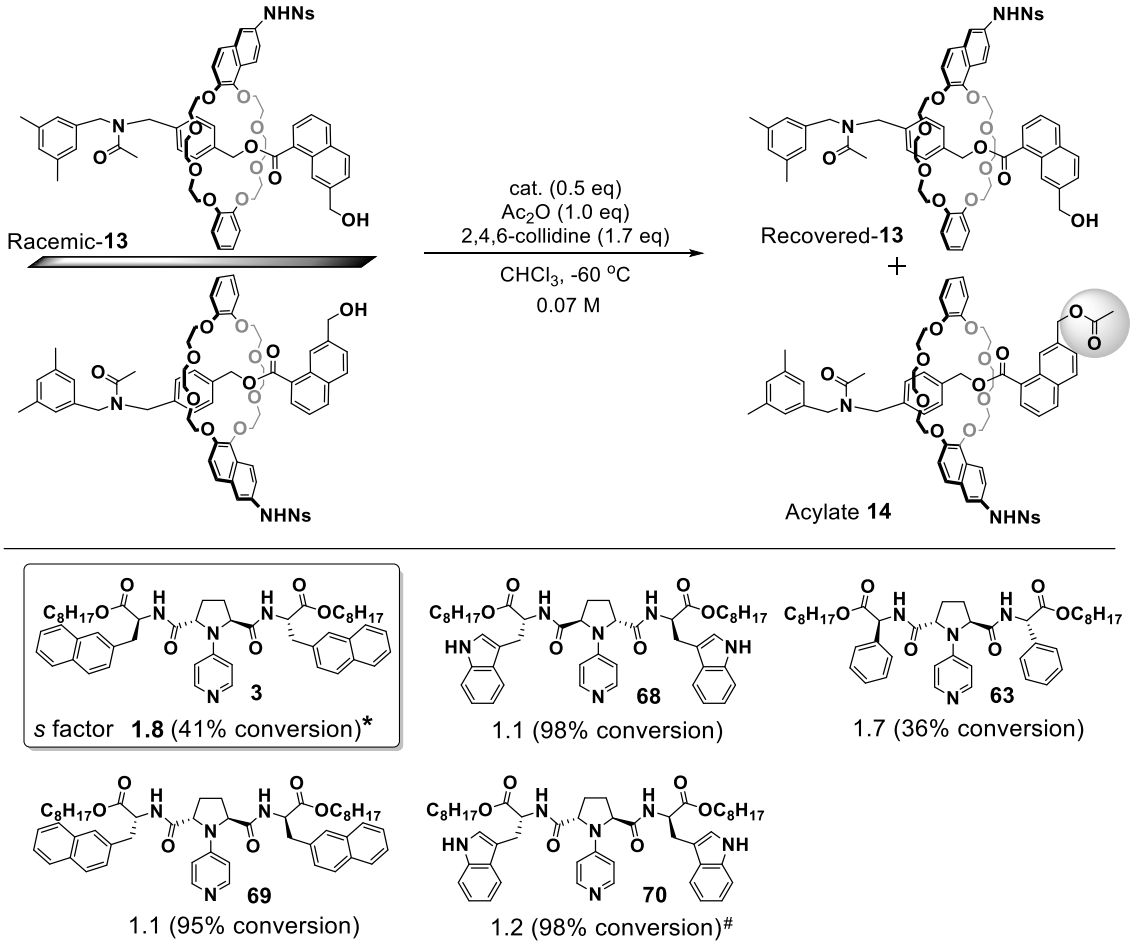

Figure 50 | Screening of catalysts. *Reactions performed with 0.1 equivalents of cat. **3**. (*i*-PrCO)$_2$O (0.9 equivalents) was used instead of acetic anhydride. #Run in 0.007 M solution.

4.5.3 Effects of catalyst/substrate ratio

Having revealed that catalyst **3** is effective in discrimination of mobile supramolecular chirality, I then investigated variation of reaction parameters, including solvent, acylating agent, base, temperature and concentration. The optimum conditions were found to be the treatment of **13** with acetic anhydride and 1.2 equivalents of 2,4,6-collidine in the presence of catalyst **3** in 0.01 M $CHCl_3$ at -60 °C. Under the conditions, kinetic resolution of rotaxane **13** in the presence of 0.05 equivalents of catalyst **3** gave the acylate **14** in 38% ee and recovered **13** in 1% ee with selectivity factor of 2.2 (Figure 51A, entry 2).

In an effort to obtain higher enantioselectivity, a breakthrough in optimization of conditions came with evaluation of catalyst/substrate ratio. I initially conducted the kinetic resolution using 0.05 equivalents of catalyst **3** for 6 hours, which afford selectivity factor of 2.2, but the conversion was very low (2%, entry 2). For the purpose to increase the reaction conversion, the catalyst loading was then increased to 0.2 equivalents. The conversion was increased to 7% as expected, and the selectivity factor was unexpectedly improved to 4.2 (entry 3). In usual kinetic resolutions, selectivity factors do not change depending on amount of catalyst unless reaction proceeds in the absence of catalysts (entry 1), thus this is an unusual tendency (*77, 78*).

Based on this curious observation, I investigated the effects of the catalyst/substrate ratio in detail. Finally, 1.5 equivalents of catalyst **3** was found to be most effective in asymmetric discrimination of topologically chiral rotaxane **13**, which afforded the acylate **14** in 79% ee and recovered **13** in 63% ee at 44% conversion with an outstanding level of selectivity factor of 16.1 (entry 5). I consider that the kinetic resolution likely proceeded by the mechanism in which more than two molecules of catalyst **3** are involved.

In the course of reactions, the degree of conversions did not affect the selectivity factor (Figure 51B). Catalyst **3** kept the high level of selectivity factor of 16 regardless of the conversions. Thus, the enhanced enantioselectivity shown in Figure 51A results from the effects of the catalyst/substrate ratio, not from the degree of conversions.

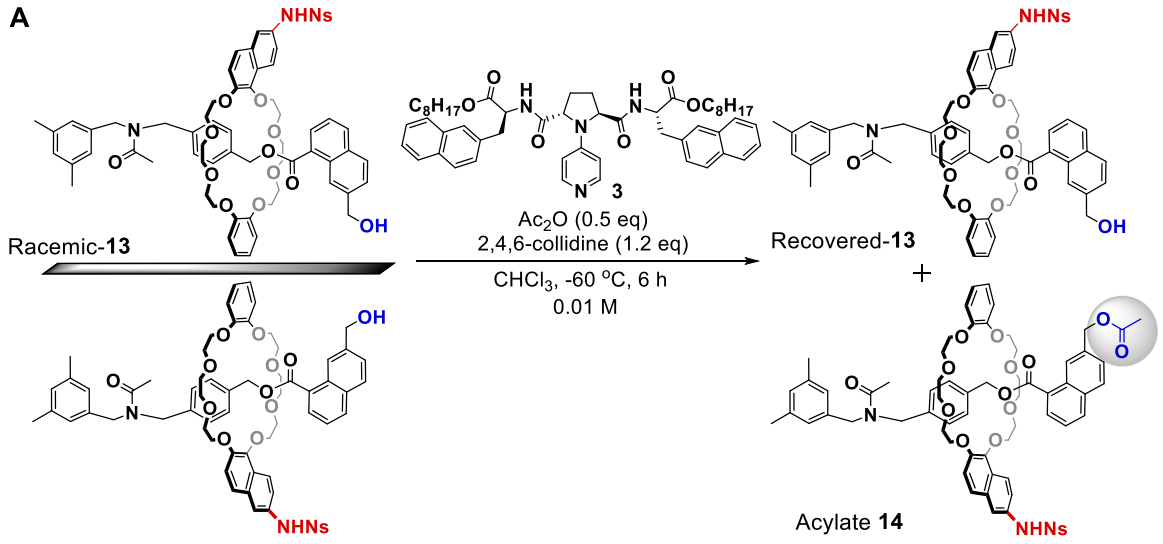

entry	cat.**3** (eq.)	ee of **14** (%)	ee of **13** (%)	conversion (%)	*s* factor
1	none	-	-	< 1	-
2	0.05	38	1	2	2.2
3	0.2	60	5	7	4.2
4	0.5	66	23	26	6.0
5	**1.5**	79	63	44	**16.1**
6	2.0	63	58	48	7.6

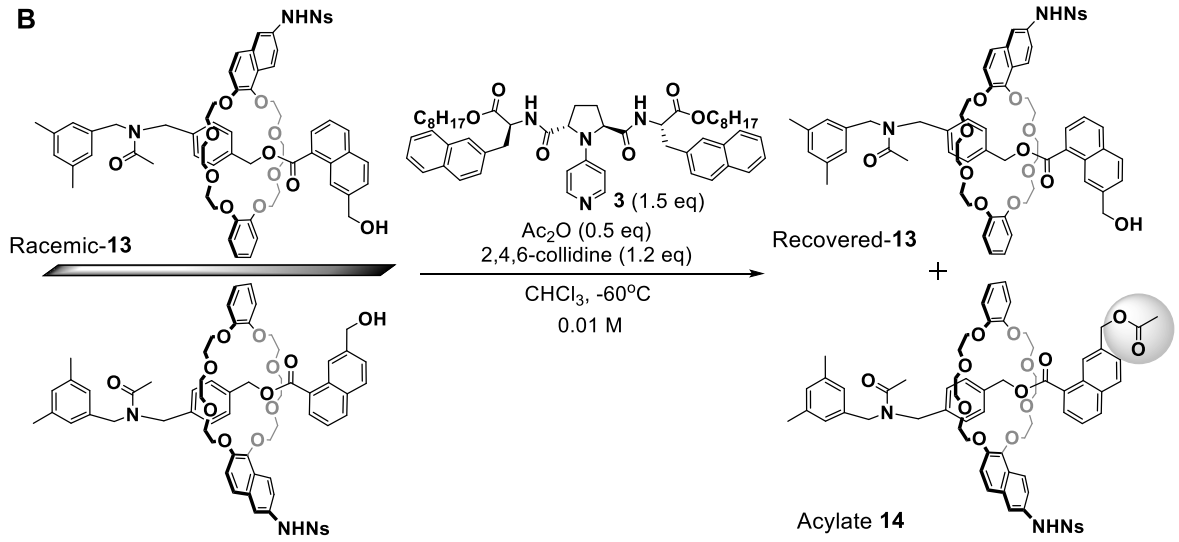

time (h)	ee of **14** (%)	ee of **13** (%)	conversion (%)	*s* factor
2	85	29	**26**	**16.1**
4	83	38	**31**	**15.5**
6	79	63	**44**	**16.1**

Figure 51 | Effects of catalyst/substrate ratio. (**A**) Effects of catalyst/substrate ratio on selectivity factors. Both % conversion (C) and selectivity factor (*s*) were calculated from ee's of the product and the recovered starting material: $C = ee_{recovered\ SM} / (ee_{recovered\ SM} + ee_{product})$, $s = \ln[(1-C)(1-ee_{recovered\ SM})]/\ln[(1-C)\ (1+ee_{recovered\ SM})] = \ln[1-C(1+ee_{product})]/\ln[1-C(1-ee_{product})]$. (**B**) Effects of conversion on selectivity factors.

4.5.4 Effects of concentration

The catalyst/substrate ratio is an important factor in highly selective acylation, and concentration of the reaction mixture also significantly affected the enantioselectivity (Figure 52).

The optimum substrate concentration of the reactioin was 0.01 M (entry 2), where the catalyst/substrate ratio greatly affected the selectivity factors (Figure 51A). However, kinetic resolution at lower concentration (0.001 M) resulted in the reduced enantioselectivity (s = 4.4) regardless of the catalyst/substrate ratio of 1.5 (Figure 52, entry 1). I suspect that the loss in enantioselectivity is due to the predominance of the uni-molecular catalytic process rather than bi-molecular catalytic process at the lower concentration. Kinetic resolution at higher concentration (0.1 M) also provided a reduced enantioselectivity (s = 2.3-2.6) regardless of the same catalyst/substrate ratio (entries 3, 4). The loss in the enantioselectivity is probably because of the negligible contribution of the dimeric association of the substrate at the high concentration, which may not be suitable for proper substrate-catalyst interaction. Thus, the catalyst/substrate ratio was found to be critical only at the optimized concentration (0.01 M).

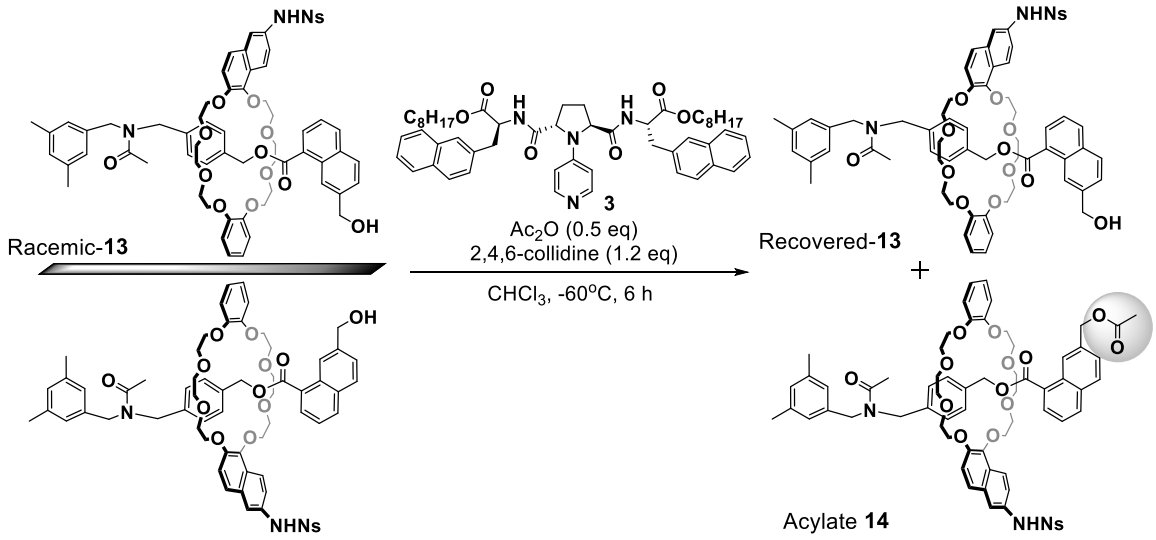

entry	**13** (M)	cat. **3** (M)	**3**/**13**	ee of **14** (%)	ee of **13** (%)	conversion (%)	*s* factor
1	0.001	0.0015	1.5	62	0.3	5	4.4
2	**0.01**	**0.015**	1.5	79	63	44	**16.1**
3	0.1	0.15	1.5	34	25	43	2.6
4	0.1	0.015	0.15	32	18	36	2.3

Figure 52 | Effects of concentration of rotaxane substrate 13 and catalyst 3.

4.6 Preparative scale production of an enantiopure rotaxane

With such a high selectivity in the kinetic resolution of the rotaxane with mobile supramolecular chirality in hand, it is now possible to obtain topologically chiral rotaxane **13** in excellent ee with good yield. To demonstrate the utility of the present method, I performed the reaction on preparative-scale (Figure 53A). The kinetic resolution of topologically chiral racemic rotaxane **13** on 50 mg scale was performed with 1.5 equivalents of **3** and 0.8 equivalents of acetic anhydride in the presence of 1.2 equivalents of 2,4,6-collidine in $CHCl_3$ at -60 °C for 37 hours. As a result, 15 mg of topologically chiral rotaxane **13** was successfully isolated with perfect enantiopurity (>99.9% ee) in 30% yield with a selectivity factor of >16 (Figure 53B, 53C). CD spectrum of isolated rotaxane (-)-**13** in this kinetic resolution showed exactly opposite behavior to that of the other separated enantiomer (+)-**13** (Figure 53D, 53E).

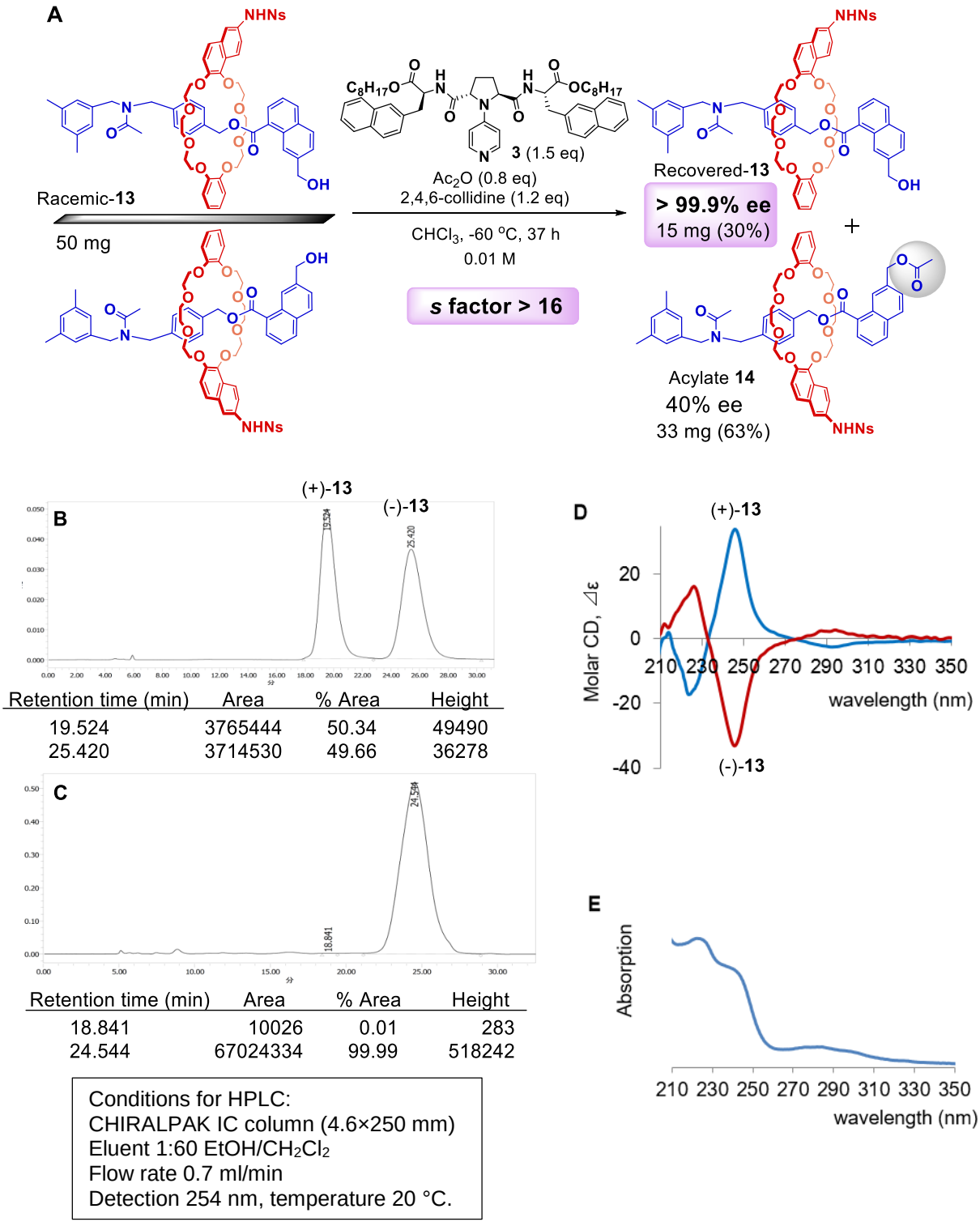

Figure 53 | Preparative scale production of enantiomerically pure rotaxane 13. (**A**) Kinetic resolution of **13** on preparative scale. The absolute structure of **13** is not determined, so the stereochemistry is tentatively shown. (**B**) Chiral HPLC chromatograms of racemic-**13** (**C**) Chiral HPLC chromatograms of isolated enantiopure recovered-**13**. (**D**) CD spectra of rotaxane **13**. Recorded in 0.5×10^{-5} M MeOH. (**E**) UV/Vis spectrum of rotaxane **13**. Recorded in 0.5×10^{-5} M MeOH.

4.7 Kinetic resolution of rotaxane with a typical catalyst

I also performed kinetic resolution of rotaxane **13** in the presence of Birman's catalyst **71** instead of catalyst **3**. Acylative kinetic resolution of racemic alcohols has been extensively developed, and Birman's catalyst has been well recognized as one of the most efficient catalysts for the purpose. Actually selectivity factor reaching 355 has been reported for the acylative kinetic resolution of a racemic alcohol **72** with Birman's catalyst **71** (Figure 54A) (*79*). However, Birman's catalyst **71** was totally ineffective for the kinetic resolution of rotaxane **13**, which afford acylate **14** and recovered **13** as the racemate with selectivity factor of 1.0 (Figure 54B).

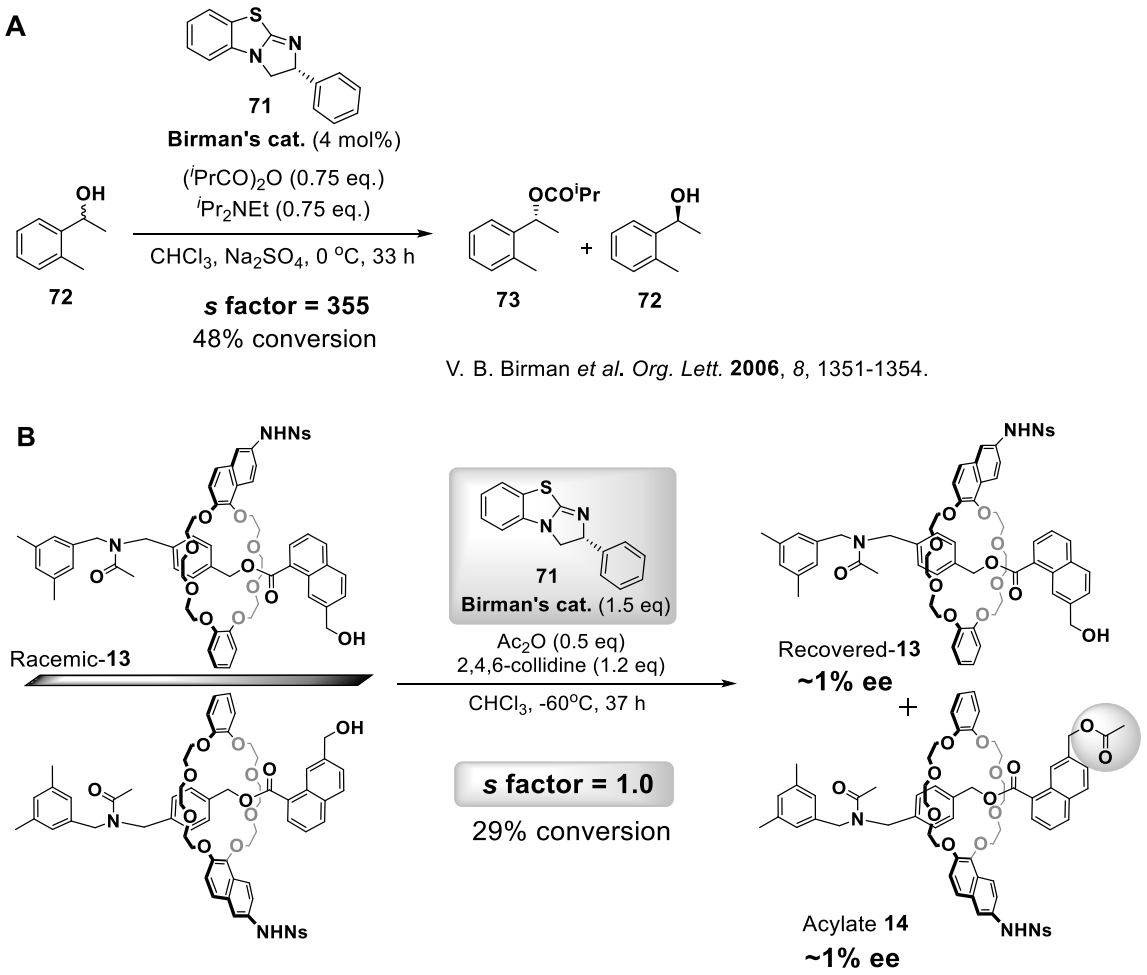

Figure 54 | Acylative kinetic resolution of alcohols with Birman's catalyst 71. (**A**) Highly selective acylative kinetic resolution of alcohols **72** with Birman's catalyst **71**. (**B**) Kinetic resolution of topologically chiral racemic rotaxane **13** with Birman's catalyst **71**.

4.8 Effects of acidic hydrogens of NHNs groups

In order to gain some mechanistic insights, I investigated the effects of NHNs group of **13** on discrimination of mobile supramolecular chirality by catalyst **3** (Figure 55). Kinetic resolution of rotaxane **62**, bearing the NMeNs group instead of the NHNs group, was performed under the optimum conditions. As the result, much less selectivity (s = 1.3) than that for **13** (s = 16.1) was observed, indicating that the NHNs group of **13** plays an important role for achieving highly efficient discrimination of mobile supramolecular chirality. Formation of a hydrogen bond between the NHNs group and catalyst **3** may be the possible origin of the observed phenomena.

Notably, in the kinetic resolution of **30**, conversion was also reduced (11%, 37 hours) as well as the selectivity factor compared to that of **13** (44%, 6 hours). This result indicates that the NHNs group in **13** is responsible for the accelerative acylation as well as the high enantioselectivity.

I also performed kinetic resolution of **29** with the benzylic NHNs group. Modest enantioselectivity was observed, but the selectivity factor was lower (s = 3.6) than that for **13** (s = 16.1). The more acidic hydrogen of the NHNs group in **13** than that in **29** appears to work as a more efficient hydrogen bond donor for the interaction with catalyst **3**.

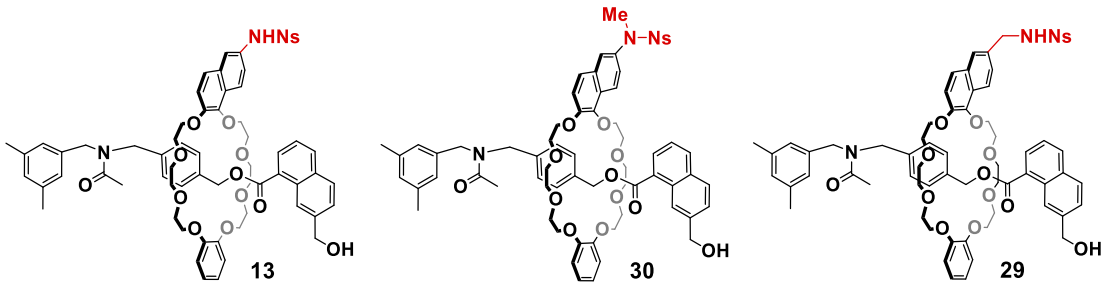

	13	30	29
s factor	16.1	1.3	3.6
conversion (time)	44% (6 h)	11% (37 h)	47% (6 h)
(acylate, SM)	79% ee, 63% ee	11% ee, 1% ee	43% ee, 39% ee

Figure 55 | Effects of acidic hydrogens of NHNs groups. Reaction conditions: catalyst **3** (1.5 equivalents), acetic anhydride (0.5 equivalents), 2,4,6-collidine (1.2 equivalents), $CHCl_3$, -60 °C, 0.01 M.

4.9 A proposal of a model for chiral discrimination

Catalyst **3** worked as a highly effective catalyst for discrimination of topological chirality of rotaxane **13**. In contrast, Birman's catalyst **71** was totally ineffective in the kinetic resolution although Birman's catalyst **71** has been known to be one of the best catalysts for acylative kinetic resolution of alcohols. Difference in the modes for the chiral discrimination between Figure 54A and Figure 53A is shown in Figure 56A. On the case of chiral discrimination of alcohol **72**, the chiral center is located adjacent to the reacting center, so that high performance in the discrimination of chirality of the molecule on acylation of the hydroxy group is expected. On the other hand, the discrimination of the chirality of rotaxane **13**, whose alcohol located at the edge of the molecule, is expected to be extremely difficult.

Birman's catalyst **71** and other typical catalysts generally favor the sterically least congested conformer (Figure 56B, gray-colored conformer). In this conformer, the ring component locates far from the reaction center of hydroxy group, thereby the hydroxy group is located in the least asymmetric microenvironments. Therefore, acylation of the hydroxy group of this conformer hardly result in effective kinetic resolution.

On the other hand, catalyst **3** discriminate the mobile supramolecular chiral environments probably at the moment when a NHNs group and a hydroxy group approach each other by around 5 Å distance (Figure 56B, red-colored conformer). In this conformer, the rotaxane has the sterically most congested conformation, however, the chiral environment becomes much more obvious because ring component is located close to catalyst **3**. Thus, the hydroxy group in the active conformer for catalyst **3** is located in the highly asymmetric microenvironments, although this conformer is the sterically least accessible conformer for typical catalysts. In this way, catalyst **3** utilize the mobile nature of supramolecular chirality for molecular recognition, and the highly efficient discrimination of mobile supramolecular chirality has been achieved.

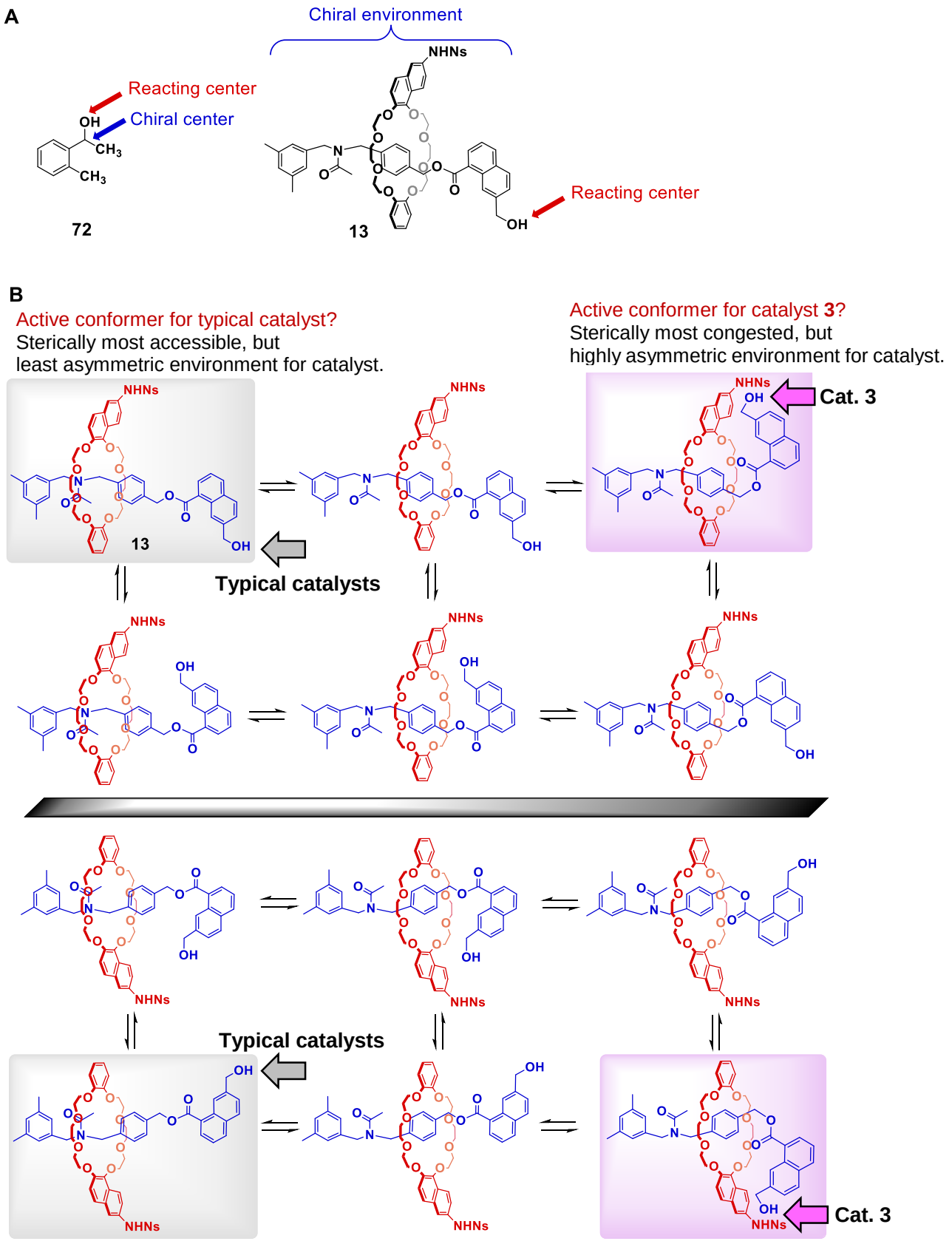

Figure 56 | Modes for the chiral discrimination. (**A**) Difference in the mode for the chiral discrimination between central chirality and topological chirality. (**B**) Difference in the mode for the chiral discrimination between typical catalyst and catalyst **3**.

4.10 Conclusion

The first highly efficient discrimination of mobile supramolecular chirality has been achieved by the kinetic resolution promoted with catalyst **3**. An acylative kinetic resolution of a racemic rotaxane **13** afforded a topologically chiral rotaxane with perfect enantiopurity (>99% ee) in excellent selectivity (*s* >16). The concept of dynamic molecular recognition enabled asymmetric synthetic chemistry to set foot into the fields of mobile supramolecular chemistry linked a non-covalent system, beyond the conventional fixed covalent system.

Conclusion and perspective

Discrimination of mobile supramolecular chirality was successfully achieved by using organocatalysts. The chiral PPY catalysts described in this thesis discriminated the dynamic structures of the large supramolecules in a highly selective manner by fine molecular recognition. Although the catalysts can form various transient complexes with the substrate at a similar energy level to each other, the reaction seems to proceed at the moment when the complex reaches the particular productive recognition mode. The chiral PPY catalysts adapt themselves to various transformations by flexibly changing their molecular recognition modes depending on the substrate structures.

Such dynamic and flexible recognition mode of the chiral PPY catalysts, without depending on the steric effect, is a contrast to the traditional static and rigid recognition mode of the typical conventional catalysts. Considering the high interest in the applications of supramolecules to catalysts (*46-48*), the application of the obtained topologically chiral supramolecule to the chiral catalyst might realize further dynamic and flexible recognition process in asymmetric synthesis because the topologically chiral supramolecule has mobility in the chiral environment itself.

The dynamic and flexible recognition modes of the chiral PPY catalysts are somewhat similar to the mode for protein-protein interactions (*80*, *81*). Protein-protein interactions are crucial interactions for signaling cascades and regulation of biological events in the cell. Proteins with conformational variability have been known to form complexes with various different kinds of proteins, repeating the association/dissociation process and finding the suitable interaction for its partner protein structure. In a similar manner to protein-protein interactions, these chiral PPY catalysts promote the reaction in an accelerative manner at the moment when the complexes reaches the most suitable recognition mode for the reaction among various possible interaction modes. From such a viewpoint, the concept of dynamic molecular recognition by the chiral PPY catalysts could be applied not only to recognition of supramolecules but to controlling other giant molecules like proteins. For example, the concept of dynamic molecular recognition has the possibility for contributing to the development of low-molecular-weight drugs which control the functions of proteins via protein-drug interactions in a highly selective manner.

The concept of dynamic molecular recognition discussed in this thesis is expected to be adopted as a novel concept in a wide range of fields including organic chemistry, biochemistry and medicinal chemistry.

Experimental Section

1. General Information

Reagents and solvents

Anhydrous toluene, *N*,*N*-dimethylformamide (DMF), tetrahydrofuran (THF), pyridine, dimethylsulfoxide (DMSO), methanol (MeOH), dichloromehthane (CH_2Cl_2) and chloroform ($CHCl_3$) were purchased from commercial suppliers and stored over activated molecular sieves. $CHCl_3$ for the kinetic resolution of rotaxanes was purchased from Kanto Chemical Co., Inc. and stored over aluminium oxide. Acetic anhydride, isobutyric anhydride and 2,4,6-collidine were distilled before use.

Reaction

All reactions, sensitive to air or moisture, were carried out in an argon atmosphere under anhydrous conditions. Thin-layer chromatography (TLC) was performed on Silica gel 60 F_{254} precoated plates (0.25 mm, Merck). Visualization of developed chromatogram was accomplished with UV light and *p*-anysaldehyde (conc. H_2SO_4 in ethanol) or phosphomolybdic acid (5 w/v% in ethanol) stain followed by heating.

Purification

Chromatographic purification of products was accomplished by using Silica gel 60 N (63-210 μm, Kanto Chemical Co., Inc.). Preparative TLC (PTLC) was carried out by using Silica gel 60N F_{254} (0.5 mm, Merck).

Analysis

Analytical HPLC was run on Waters 1525 Binary HPLC Pump, equipped with Waters 2998 Photodiode Array Detector. ^1H and ^{13}C NMR spectra were recorded on JEOL ECX-400 (400 and 100 MHz), JEOL ECA-600 (600 and 150 MHz) and Bruker Avance Ⅲ 600 (600 MHz). Chemical shifts are reported relative to the solvent ($CHCl_3$: δ (^1H) = 7.26 ppm, δ (^{13}C) = 77.0 ppm, benzene-d6: δ (^1H) = 7.16 ppm) as reference. Data for ^1H NMR are reported as follows: chemical shift (δ ppm), integration, multiplicity (s = singlet, d = doublet, t = triplet, dd = double doublet, ddd = double double doublet, dt = double triplet, m = multiplet, br = broad, brt = broad triplet) and coupling constant (Hz). Data for proton-decoupled ^{13}C NMR are reported in terms of chemical shift. Infrared (IR) spectra were recorded on a JASCO FT-IR 4200 spectrometer and are reported in terms of frequency of absorption (cm^{-1}). High resolution mass spectra (HRMS) were obtained using JEOL JMS-700 mass spectrometer and Bruker Impact HD mass spectrometer. Melting points (m.p.) were recorded using Yanagimoto Micro Melting Point Apparatus PM-500. Specific rotations were measured with JASCO P-2200 polarimeter and HORIBA SEPA-200 automatic digital polarimeter, and are reported as follows: $[\alpha]_D^t$ (*c* = 10 mg/ml, solvent, enantiomeric excess (ee)). UV/Vis absorption spectra were recorded with a JASCO V-550 UV/Vis spectrophotometer. Circular dichroism (CD) spectra were recorded with a JASCO J-720W spectropolarimeter and a JASCO J-820-L spectropolarimeter equipped with a JASCO PTC-423L Peltier Controller.

2. Chapter 2

2.1 General procedures for acylation of 1,*n*-diols

General procedure for the acylation of 1,*n*-diol (Figure 16, 17, 18)

To a stirred solution of 1,*n*-diol (0.2 mmol, 1.0 equivalents), catalyst (0.05 equivalents) and 2,4,6-collidine (1.5 equivalents) in $CHCl_3$ (2.9 mL, 0.07 M for 1,*n*-diol) at -60 °C was added cooled isobutyric anhydride (1.03 equivalents). After stirring at -60 °C for 24 h, the reaction mixture was quenched with MeOH (10 mL), and the solution was stirred for 10 min. Then the solvent was carefully evaporated. Yields of monoacylate, diacylate and recovered 1,*n*-diol were determined by NMR in $CDCl_3$ or benzene-d6.

Procedure for the competitive acylation (Figure 19)

To a stirred solution of 1,5-pentanediol (**4**) (0.16 mmol, 0.5 equivalents), 1,2-ethanediol (**7**) (0.16 mmol, 0.5 equivalents), catalyst (0.05 equivalents) and 2,4,6-collidine (1.5 equivalents) in $CHCl_3$ (4.6 mL, 0.07 M for the total amount of diols) at -60 °C was added cooled isobutyric anhydride (1.03 equivalents). After stirring at -60 °C for 24 h, the reaction mixture was quenched with MeOH (16 mL), and the solution was stirred for 10 min. Then the solvent was carefully evaporated. Yields of monoacylates, diacylates and recovered diols were determined by NMR in $CDCl_3$ and benzene-d6. Chemoselectivity of the acylation of 1,5-pentanediol (**4**) versus 1,2-ethanediol (**7**) ($k_{\text{(acylation of 4)}} / k_{\text{(acylation of 7)}}$) were determined according to the following equation: $k_{\text{(acylation of 4)}} / k_{\text{(acylation of 7)}} = \ln[(1\text{-conversion})(1-|(\mathbf{8}+\mathbf{9})-(\mathbf{5}+\mathbf{6})|/\{(\mathbf{8}+\mathbf{9})+(\mathbf{5}+\mathbf{6})\}]/\ln[(1\text{-conversion})(1+|(\mathbf{8}+\mathbf{9})-(\mathbf{5}+\mathbf{6})|/\{(\mathbf{8}+\mathbf{9})+(\mathbf{5}+\mathbf{6})\})]$. Conversion was calculated based on the total amount of the two diols.

2.2 Synthetic procedures and characterization details

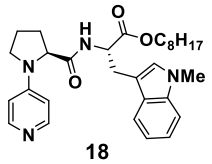

18

18: To a solution of *N*-(4-pyridyl)-L-proline (23 mg, 0.1 mmol), 1-methyl-L-tryptophan octyl ester hydrochloride (55 mg, 0.15 mmol) in CH_2Cl_2 (1.1 mL) were added 1-ehtyl-3-(3-dimethylaminopropyl)carbodiimide hydrochloride (EDCI) (29 mg, 0.15 mmol), 1-hydroxybenzotriazole (HOBt) (20 mg, 0.15 mmol) and *N*-methylmorpholine (44 μL, 0.4 mmol). After stirring at room temperature for 12 h, the mixture was diluted with AcOEt and washed wish sat. $NaHCO_3$ aq. and brine, dried over Na_2SO_4, filtered, and concentrated *in vacuo*. The crude product was purified by preparative TLC (SiO_2, 1:19 MeOH/ $CHCl_3$) to afford **18** (50 mg, 96% yield) as a white solid. m.p. 85-86 °C. $[\alpha]_D^{20}$ -103 (*c* 0.35, $CHCl_3$). ^{1}H NMR (600 MHz, $CDCl_3$): δ 8.15 (d, *J* = 5.5 Hz, 2H), 7.43 (d, *J* = 7.9 Hz, 1H), 7.26-7.21 (m, 2H), 7.11-7.08 (m, 1H), 6.68 (s, 1H), 6.44 (d, *J* = 7.6 Hz, 1H), 6.27-6.25 (m, 2H), 4.76-4.73 (m, 1H), 4.09 (dt, *J* = 5.8, 1.7 Hz, 2H), 3.98 (dd, *J* = 9.1, 1.7 Hz, 1H), 3.64 (s, 3H), 3.30 (dd, *J* = 15.0, 5.9 Hz, 1H), 3.23 (dd, *J* = 15.0, 5.9 Hz, 1H), 3.12-3.07 (m, 1H), 3.05-3.00 (m, 1H), 2.20-2.07 (m, 2H), 1.87-1.81 (m, 1H), 1.61-1.47 (m, 3H), 1.31-1.22 (m, 10H), 0.88 (t, *J* = 6.8 Hz, 3H). ^{13}C NMR (150 MHz, $CDCl_3$): δ 172.0, 171.2, 151.7, 149.0, 136.7, 128.2, 127.2, 121.9, 119.3, 118.0, 109.6, 108.0, 107.7, 65.7, 63.0, 53.1, 48.3, 32.7, 31.8, 30.9, 29.2, 28.5, 26.4, 25.8, 23.4, 22.6, 14.1. IR (neat): 3189, 2925, 1739, 1673, 1598, 1516, 1379, 1255, 1224, 999, 805, 743 cm^{-1}. HRMS (ESI): *m*/*z* calcd for $C_{30}H_{40}N_4O_3$ $[M+H]^+$: 505.3173 found: 505.3162.

3. Chapter 3

3.1 Formation of acylpyridinium ion pairs

Acylpyridinium ion pair 20 generated from acetic anhydride (Figure 28)

The formation of acylpyridinium ion **20** from PPY and acetic anhydride was monitored by variable-temperature ^{1}H NMR. A sealed NMR tube containing 0.1 M PPY and 0.15 M acetic anhydride in $CDCl_3$ was prepared. The position of the equilibrium was directly determined from the ratio of 4-pyrrolidinopyridine to **20** in the temperature range of -30 ~ -65 °C (Figure 28).

Acylpyridinium ion pair 21 generated from benzoic anhydride (Figure 29)

The formation of acylpyridinium ion **21** from PPY and benzoic anhydride was monitored by variable-temperature ^{1}H NMR. A sealed NMR tube containing 0.3 M PPY and 0.465 M benzoic anhydride in $CDCl_3$ was prepared. The position of the equilibrium was directly determined from the ratio of 4-pyrrolidinopyridine to **21** in the temperature range of -45 ~ -70 °C (Figure 29).

Acylpyridinium ion pair 22 generated from acetyl chloride (Figure 30)

The formation of acylpyridinium ion **22** from PPY and acetyl chloride was monitored by ^{1}H NMR. A NMR tube containing 0.07 M PPY and 0.07 M acetyl chloride in $CDCl_3$ was prepared. ^{1}H NMR spectra was obtained at 20 °C (Figure 30).

Acylpyridinium ion pair 23 generated from benzoyl chloride (Figure 31)

The formation of acylpyridinium ion **23** from PPY and benzoyl chloride was monitored by ^{1}H NMR. A NMR tube containing 0.07 M PPY and 0.07 M benzoyl chloride in $CDCl_3$ was prepared. ^{1}H NMR spectra was obtained at 20 °C (Figure 31).

3.2 General procedure of synthesis of rotaxanes

To a stirred solution of $AgPF_6$ (42 mg, 0.165 mmol), DMAP (1 mg, 0.0075 mmol) and 1-adamantaneacetyl chloride (23.4 mg, 0.11 mmol) in $CHCl_3$ (0.10 ml), a solution of axis component **10** (20 mg, 0.050 mmol), dibenzo-24-crown-8-ether **11** (33 mg, 0.074 mmol) and pivalic acid (11 mg, 0.11 mmol) in $CHCl_3$ (0.15 ml) was added at 0 °C. The reaction mixture was stirred at 0 °C for 2 h. The reaction mixture was diluted with $CHCl_3$, washed with 1M HCl aq. and water, dried over Na_2SO_4, filtered and concentrated *in vacuo*. The crude product was purified by preparative TLC (SiO_2, 1:19 MeOH/$CHCl_3$) to afford **12** (49 mg, 94% yield) as a white solid.

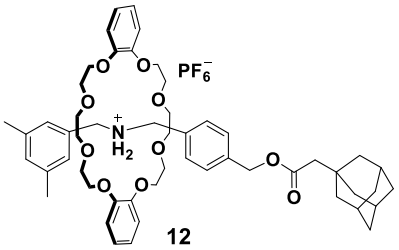

12

Rotaxane 12: A white solid. m.p. 161-163 °C. ^{1}H NMR (400 MHz, $CDCl_3$): δ 7.57 (br, 2H), 7.34 (d, *J* = 12.0 Hz, 2H), 7.20 (d, *J* = 12.0 Hz, 2H), 6.92-6.77 (m, 11H), 5.00 (s, 2H), 4.63 (t, *J* = 10.3 Hz, 2H), 4.44 (t, *J* = 10.3 Hz, 2H), 4.12-4.06 (m, 8H), 3.81-3.73 (m, 8H), 3.50-3.41 (m, 8H), 2.14 (s, 6H), 2.13 (s, 2H), 1.95 (br, 3H), 1.64-1.57 (m, 12H). ^{13}C NMR (100 MHz, $CDCl_3$): δ 171.45, 147.31, 138.26, 137.33, 131.42, 131.27, 130.58, 129.39, 127.91, 126.53, 121.56, 112.51, 70.55, 70.05, 68.02, 64.94, 52.57, 52.11, 48.71, 42.26, 36.58, 32.76, 28.47, 21.10. IR (neat): 3150, 3063, 2904, 2848, 1729, 1593, 1504, 1454, 1254, 1214, 1127, 1104, 1057, 954, 843, 751, 558 cm^{-1}. HRMS (ESI): *m*/*z* calcd for $C_{53}H_{70}NO_{10}$ $[M\text{-}PF_6]^+$: 880.4994, found: 880.4972.

4. Chapter 4

4.1 General procedures of kinetic resolution

Kinetic resolution on an analytical scale (Figure 51, entry 5)

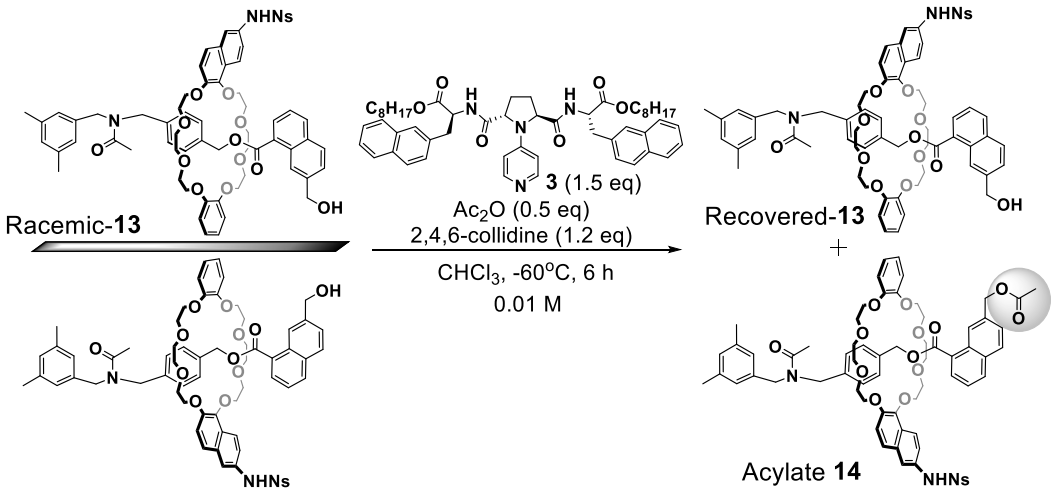

To a solution of catalyst **3** (1.087 mg, 0.01271 mmol, 1.5 equivalents) in $CHCl_3$ (15 µl) at room temperature was added $CHCl_3$ (31 µl), a solution of 2,4,6-collidine (0.134 µl, 0.0010166 mmol, 1.2 equivalents) in $CHCl_3$ (13.4 µl) and a solution of rotaxane **13** (1 mg, 0.0008472 mmol, 1.0 equivalents) in $CHCl_3$ (20 µl). The solution was cooled to -60 °C. Acetic anhydride (0.04 µl, 0.0004236 mmol, 0.5 equivalents) in $CHCl_3$ (4.0 µl) was added to the solution dropwise and the reaction mixture was kept at -60 °C for 6 h. MeOH (300 µl) was added to the reaction mixture at -60 °C and the solution was kept at room temperature for 30 min. The solvent was removed *in vacuo*. The resulting product was analyzed by chiral stationary phase HPLC with CHIRALPAK-IC column eluted by 1:60 EtOH/CH_2Cl_2 (0.7ml/min) at 20 °C to determine the enantiomeric enrichment of the recovered rotaxane **13** (63% ee) and the acylate **14** (79% ee). Conversion (C) and selectivity factor (*s*) were determined according to the following equation: conversion $C = ee_{\text{recovered SM}} / (ee_{\text{recovered SM}} + ee_{\text{product}})$ and selectivity factor $s = \ln[(1-C)(1-ee_{\text{recovered SM}})]/\ln[(1-C)(1+ee_{\text{recovered SM}})] = \ln[1-C(1+ee_{\text{product}})]/\ln[1-C(1-ee_{\text{product}})]$.

Kinetic resolution on a preparative scale (Figure 53)

To a stirred solution of catalyst **3** (54.34 mg, 0.06354 mmol, 1.5 equivalents) in $CHCl_3$ (2.25 ml) at room temperature was added a solution of 2,4,6-collidine (6.72 µl, 0.05083 mmol, 1.2 equivalents) in $CHCl_3$ (672 µl) and a solution of rotaxane **13** (50 mg, 0.04236 mmol, 1.0 equivalents) in $CHCl_3$ (1 ml). The solution was cooled to -60 °C. A solution of acetic anhydride (3.2 µl, 0.03389 mmol, 0.8 equivalents) in $CHCl_3$ (320 µl) was added to the solution dropwise and the reaction mixture was stirred at -60 °C for 37 h. MeOH (15 ml) was added to the reaction mixture at -60 °C and the solution was stirred at room temperature for 30 min. The solvent was removed *in vacuo*. The crude product was analyzed by chiral HPLC with CHIRALPAK-IC column eluted by 1:60 EtOH/CH_2Cl_2 (0.7ml/min) at 20 °C. The crude product was purified by preparative TLC (SiO_2, 1:19 MeOH/ $CHCl_3$) to afford recovered **13** (15.1 mg, 30% yield) and acylate **14** (32.7 mg, 65% yield). Enantiomeric enrichment of the recovered rotaxane **13** (99% ee) and the acylate **14** (40% ee) was determined by chiral HPLC with CHIRALPAK-IC column eluted by 1:60 EtOH/CH_2Cl_2 (0.7ml/min) at 20 °C.

4.2 HPLC charts for kinetic resolution

A Racemic-**13**

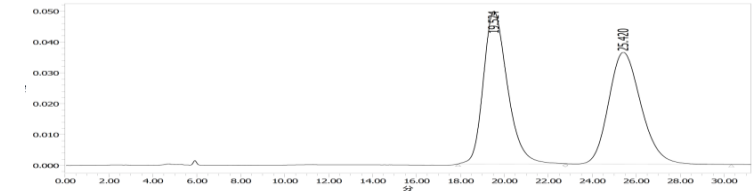

Retention time (min)	Area	% Area	Height
19.524	3765444	50.34	49490
25.420	3714530	49.66	36278

B Racemic-**14**

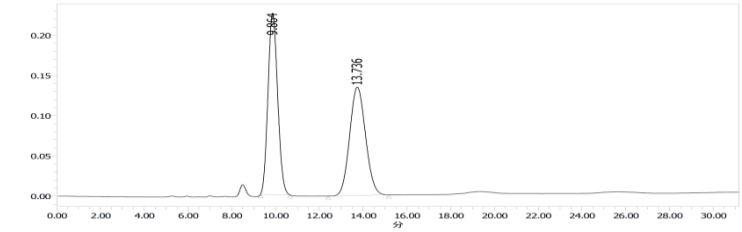

Retention time (min)	Area	% Area	Height
9.864	6906524	50.37	225649
13.736	6806010	49.63	134949

C Crude product of a kinetic resolution of racemic-**13** on an analytical scale (Figure 51, entry 5)

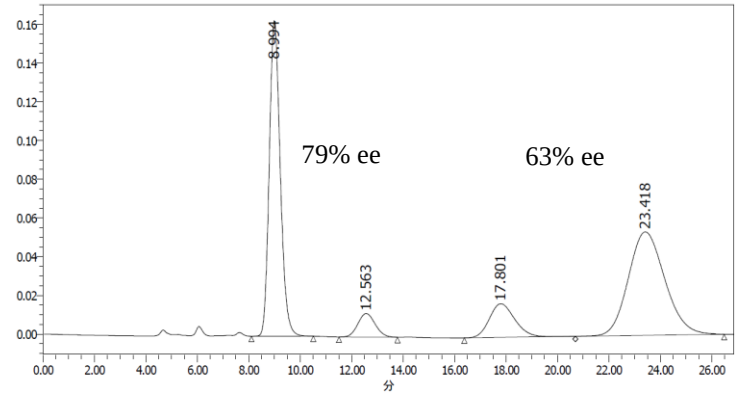

Retention time (min)	Area	% Area	Height
8.994	4826739	40.71	163015
12.563	569000	4.80	12157
17.801	1191675	10.05	17398
23.418	5267915	44.43	53443

Figure S1 | Chiral HPLC chromatograms of kinetic resolution of racemic-4 on an analytical scale (Figure 50, entry 5). Conditions for HPLC: CHIRALPAK IC column (4.6×250 mm); eluent 1:60 EtOH/CH_2Cl_2; flow rate 0.7 ml/min; detection 254 nm, temperature 20 °C. (**A**) Racemic-**13**. (**B**) Racemic-**14**. (**C**) Crude product of a kinetic resolution of racemic-**13** on an analytical scale (Figure 51, entry 5).

A Crude product of a kinetic resolution of racemic-**13** on a preparative scale (Figure 53)

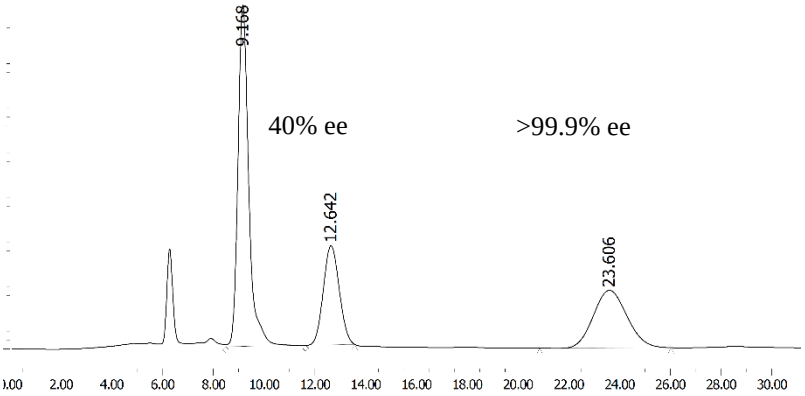

Retention time (min)	Area	% Area	Height
9.168	11240033	51.09	382326
12.642	4831686	21.96	111155
23.606	5928000	26.95	64541

B Isolated recovered-**13** (Figure 53)

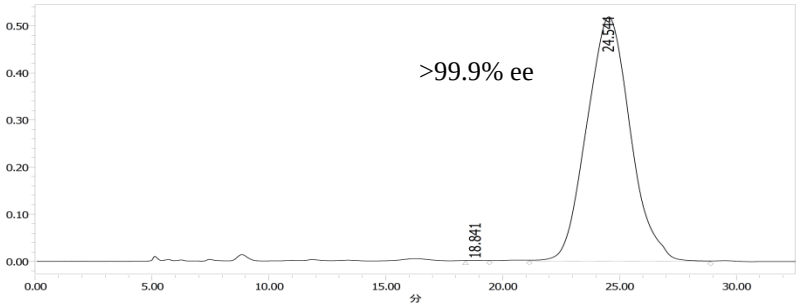

Retention time (min)	Area	% Area	Height
18.841	10026	0.01	283
24.544	67024334	99.99	518242

C Isolated acylate **14** (Figure 53)

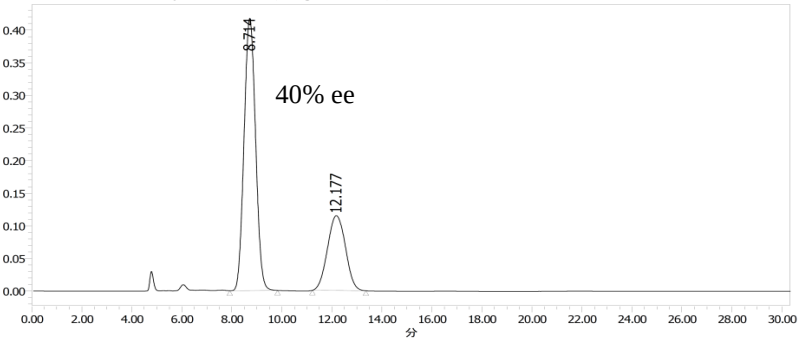

Retention time (min)	Area	% Area	Height
8.714	13329617	69.98	417417
12.177	5719404	30.02	114747

Figure S2 | **Chiral HPLC chromatograms of kinetic resolution of racemic-13 on a preparative scale (Figure 53).** Conditions for HPLC: CHIRALPAK IC column (4.6×250 mm); eluent 1:60 EtOH/CH_2Cl_2; flow rate 0.7 ml/min; detection 254 nm, temperature 20 °C. (**A**) Crude product of a kinetic resolution of racemic-**13** on a preparative scale. (**B**) Isolated recovered-**13**. (**C**) Isolated acylate **14**.

A Racemic-**74**

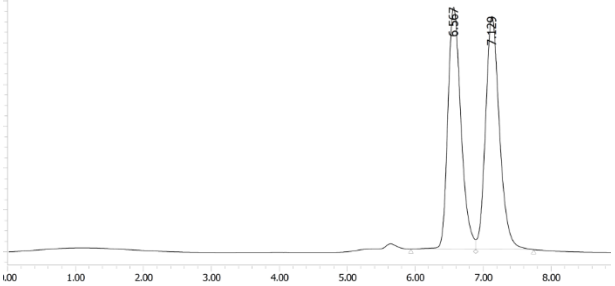

Retention time (min)	Area	% Area	Height
6.567	15496078	49.37	1156685
7.129	15888699	50.63	1114357

B Recovered-**30** (Figure 55), ee of recovered-**30** was determined after converting to acylate **74**.

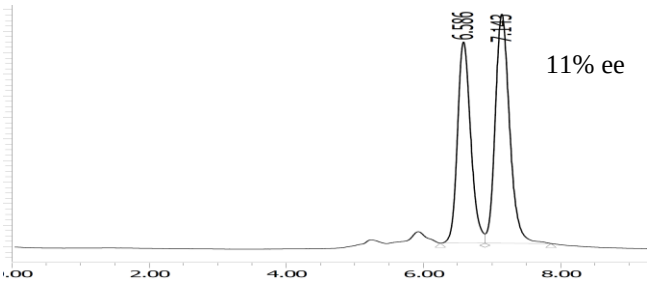

Retention time (min)	Area	% Area	Height
6.586	2505506	44.72	186822
7.413	3097666	55.28	212654

C Acylate-**74** (Figure 55)

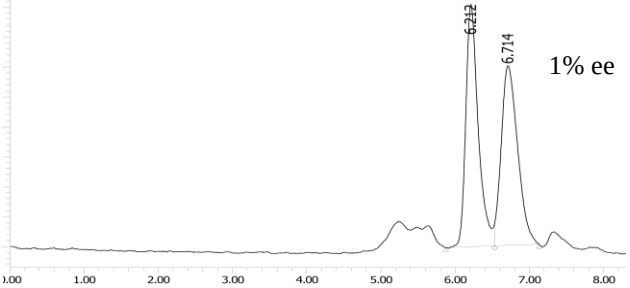

Retention time (min)	Area	% Area	Height
6.212	94705	50.68	8092
6.714	92180	49.32	6001

Figure S3 | Chiral HPLC chromatograms of kinetic resolution of racemic-30 (Figure 55). Conditions for HPLC: CHIRALPAK ID column (4.6×250 mm); eluent 1:540 EtOH/$CHCl_3$; flow rate 0.7 ml/min; temperature 20 °C. (**A**) Racemic-**74**. (**B**) Recovered-**30**. (**C**) Acylate-**74**.

A Racemic-**29**

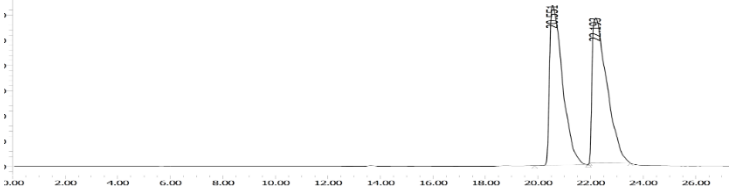

Retention time (min)	Area	% Area	Height
20.551	108720926	49.17	3171302
22.193	112404403	50.83	2868755

B Racemic-**75**

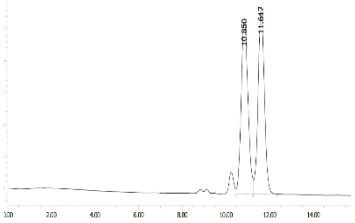

Retention time (min)	Area	% Area	Height
10.850	5923032	50.26	274097
11.617	5862701	49.74	293396

C Crude product of a kinetic resolution of racemic-**29** (Figure 55)

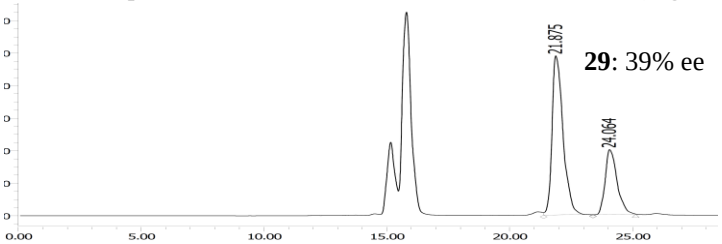

Retention time (min)	Area	% Area	Height
21.875	30492692	69.54	978281
24.064	13354707	30.46	397782

D Crude product of a kinetic resolution of racemic-**29** (Figure 55)

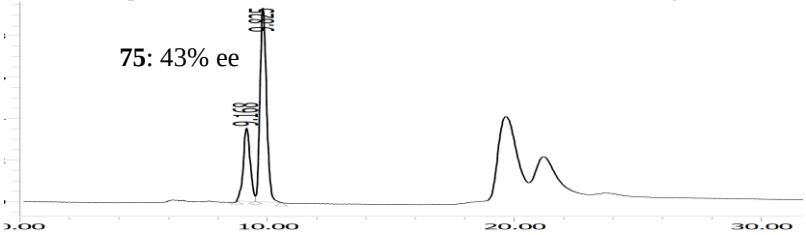

Retention time (min)	Area	% Area	Height
9.168	686190	28.46	35269
9.825	1725002	71.54	93382

Figure S4 | Chiral HPLC chromatograms of kinetic resolution of racemic-29. Conditions for HPLC (**A**, **C**) : CHIRALPAK ID column (4.6×250 mm); eluent 1:40 EtOH/CH_2Cl_2; flow rate 0.5 ml/min; temperature 20 °C. Conditions for HPLC (**B**, **D**): CHIRALPAK ID column (4.6×250 mm); eluent 1:80 EtOH/CH_2Cl_2; flow rate 1.0 ml/min; temperature 20 °C. (**A**) Racemic-**29**. (**B**) Racemic-**75**. (**C**, **D**) Crude product of a kinetic resolution of racemic-**29**.

4.3 Synthetic procedures and characterization details

4.3.1 Purification of catalyst 3

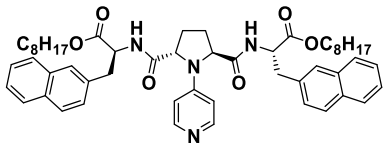

3

3: Catalyst **3** was prepared according to the reported method (*37*), then purified further in the following way. After extraction and evaporation of the reaction mixture, the crude product was subjected to column chromatography (SiO_2, 2:1 AcOEt/Hexane to 1:99 to 1:50 MeOH/$CHCl_3$) to afford crude **1** as a pale yellow residue. The pale yellow residue was dissolved in MeOH and the solution was concentrated *in vacuo*. Then the residue was dissolved in AcOEt and the solution was concentrated *in vacuo*. The pale yellow residue was recrystallized from hot AcOEt by cooling and adding a small amount of hexane to give a slightly pale yellow residue. To the slightly pale yellow residue was added a small amount of MeOH, which was filtered to afford completely pure catalyst **3** (7.02 g) as a white solid.

4.3.2 Synthesis of ring components (Figure 44)

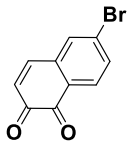

38

6-Bromonaphthalene-1,2-dione (38): To a stirred solution of 6-bromo-2-naphthol (35.6 g, 160 mmol) in THF (960 ml) at room temperature was added IBX (50 g, 178 mmol), which changed its color to bright orange within 1 h. The reaction mixture was stirred at room temperature for 16 h in the dark. The solvent was removed *in vacuo* and the residue was diluted with $CHCl_3$, washed with sat. $NaHCO_3$ aq. and brine, dried over Na_2SO_4, filtered and concentrated *in vacuo*. The crude product was obtained as a bright orange solid, which was directly used for the next step.

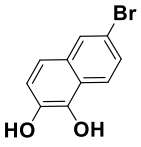

39

6-Bromonaphthalene-1,2-diol (39): The following steps were carried out under Ar atmosphere. All solvents and reaction vessels were degassed by flushing with Ar gas. The crude 6-bromonaphthalene-1,2-dione (**38**) was dissolved in degassed THF (245 ml) at room temperature under Ar. To the stirred solution was added a solution of $Na_2S_2O_4$ (145 g, 835 mmol) in degassed water (222 ml), which changed its color to pale orange within a few minutes. The reaction mixture was stirred under Ar atmosphere at room temperature for 15 min. The solvent was removed *in vacuo* under Ar atmosphere. The crude product was directly used for the next step.

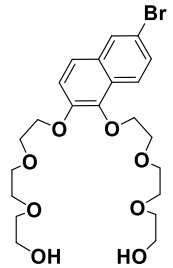

40

40: The following steps were carried out under Ar atmosphere. All solvents and reaction vessels were degassed by flushing with Ar gas. To a solution of triethylene glycol monotosylate (52 g, 171 mmol) and powdered K_2CO_3 (66.4 g, 480 mmol) in degassed MeCN (50 ml) at reflux temperature under Ar atmosphere was added a solution of the crude 6-bromonaphthalene-1,2-diol (**39**) in degassed MeCN (300 ml). The reaction mixture was stirred at reflux temperature under Ar atmosphere for 37 h. The reaction mixture was cooled to room temperature, filtered through a celite pad and the filtrate was concentrated *in vacuo*. The crude product was purified by column chromatography (SiO_2, 1:1 Hexane/Acetone) to afford **40** (20.9 g, 26% yield, 3 steps) as a pale yellow oil. ^{1}H NMR (600 MHz, $CDCl_3$): δ 8.09 (d, *J* = 8.9 Hz, 1H), 7.90 (d, *J* = 1.4 Hz, 1H), 7.50 (dd, *J* = 8.9, 2.0 Hz, 1H), 7.45 (d, *J* = 8.9 Hz, 1H), 7.27 (d, *J* = 9.6 Hz, 1H), 4.35 (t, *J* = 4.8 Hz, 2H), 4.29 (t, *J* = 4.8 Hz, 2H), 3.88 (t, *J* = 4.8 Hz, 2H), 3.86 (t, *J* = 4.8 Hz, 2H), 3.74-3.67 (m, 12H), 3.61-3.58 (m, 4H), 2.95 (br, 2H). ^{13}C NMR (150 MHz, $CDCl_3$): δ 147.38, 142.57, 130.86, 129.24, 129.15, 127.88, 123.71, 123.05, 118.25, 118.18, 72.52, 72.49, 72.45, 70.64, 70.47, 70.44, 70.32, 70.28, 69.80, 69.43, 61.54. IR (neat): 3384, 2873, 1587, 1496, 1456, 1348, 1272, 1105, 1070 cm^{-1}. HRMS (EI): *m*/*z* calcd for $C_{22}H_{31}{}^{79}BrO_8$ $[M]^+$: 502.1202, found: 502.1206; calcd for $C_{22}H_{31}{}^{81}BrO_8$ $[M]^+$: 504.1185, found: 504.1186.

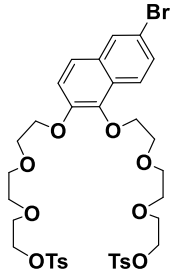

41

41: To a stirred solution of **40** (20.1 g, 40 mmol), triethylamine (56 ml, 400 mmol) and *N*,*N*-dimethyl-4-aminopyridine (970 mg, 8.0 mmol) in CH_2Cl_2 (100 ml) at room temperature was added a solution of *p*-toluenesulfonyl chloride (33.6 g, 176 mmol) in CH_2Cl_2 (250 ml) dropwise over 2 h. The reaction mixture was stirred at room temperature for 26 h, which changed its color to reddish brown. 5 M HCl aq. was carefully added to the reaction mixture and the aqueous layer was extracted with CH_2Cl_2. The organic layer was separated and washed with 2 M HCl aq., water and brine, dried over Na_2SO_4, filtered and concentrated *in vacuo*. The crude product was purified by column chromatography (SiO_2, 1:1 to 0:1 Hexane/AcOEt) to afford **41** (22.0 g, 68% yield) as an orange oil. ^{1}H NMR (600 MHz, $CDCl_3$): δ 8.08 (d, *J* = 8.9 Hz, 1H), 7.89 (d, *J* = 1.4 Hz, 1H), 7.79-7.75 (m, 4H), 7.47-7.44 (m, 2H), 7.32-7.29 (m, 4H), 7.27 (d, *J* = 8.9 Hz, 1H), 4.31 (t, *J* = 4.8 Hz, 2H), 4.27 (t, *J* = 4.8 Hz, 2H), 4.15-4.12 (m, 4H), 3.84 (t, *J* = 4.8 Hz, 2H), 3.77 (t, *J* = 4.8 Hz, 2H), 3.69-3.59 (m, 12H), 2.41 (s, 3H), 2.40 (s, 3H). ^{13}C NMR (150 MHz, $CDCl_3$): δ 147.42, 144.70, 144.67, 142.46, 132.72, 130.76, 129.69, 129.14, 128.99, 127.91, 127.76, 123.80, 122.94, 118.28, 118.07, 72.31,

70.61, 70.50, 70.36, 70.30, 69.84, 69.39, 69.16, 69.13, 68.56, 21.45. IR (neat): 2875, 1589, 1496, 1453, 1354, 1176, 1127, 1098 cm^{-1}. HRMS (FAB): *m*/*z* calcd for $C_{36}H_{43}{}^{79}BrO_{12}S_2$ $[M]^+$: 810.1379, found: 810.1408; calcd for $C_{36}H_{43}{}^{81}BrO_{12}S_2$ $[M]^+$: 812.1365, found: 812.1371.

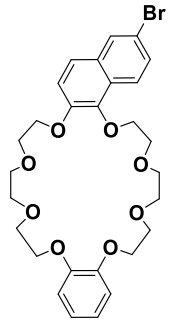

42

42: A solution of catechol (3.0 g, 27 mmol) and Cs_2CO_3 (44.0 g, 135 mmol) in MeCN (1000 ml) was stirred at reflux temperature for 15 min. To the stirred solution at reflux temperature was added a solution of **41** (21.9 g, 27 mmol) in MeCN (268 ml) dropwise over 1 h. The reaction mixture was stirred at reflux temperature for 7 days. The solvent was removed *in vacuo* and the residue was diluted with $CHCl_3$, washed with sat. $NaHCO_3$ aq. and brine, dried over Na_2SO_4, filtered and concentrated *in vacuo*. The crude product was subjected to column chromatography (SiO_2, 1:99 MeOH/$CHCl_3$) to afford an oil product. The oil product was purified by column chromatography (SiO_2, 1:1:4 $CHCl_3$/Hexane/AcOEt) to afford **42** (10.0 g, 64% yield) as a pale yellow solid. m.p. 58-61 °C. ^{1}H NMR (600 MHz, $CDCl_3$): δ 8.02 (d, *J* = 8.9 Hz, 1H), 7.90 (d, *J* = 1.4 Hz, 1H), 7.49 (dd, *J* = 8.9, 2.1 Hz, 1H), 7.45 (d, *J* = 8.9 Hz, 1H), 7.25 (d, *J* = 8.9 Hz, 1H), 6.90-6.87(m, 4H), 4.34 (t, *J* = 4.8 Hz, 2H), 4.29 (t, *J* = 4.4 Hz, 2H), 4.16-4.14 (m, 4H), 3.95 (t, *J* = 4.8 Hz, 2H), 3.93-3.90 (m, 6H), 3.86-3.83 (m, 4H), 3.82-3.79 (m, 4H). ^{13}C NMR (150 MHz, $CDCl_3$): δ 148.91, 148.84, 147.60, 142.51, 130.70, 129.35, 129.18, 127.77, 123.58, 123.01, 121.47, 121.39, 118.01, 117.46, 114.35, 114.08, 72.39, 71.09, 71.06, 70.62, 70.58, 69.99, 69.89, 69.83, 69.51, 69.32, 69.10. IR (KBr): 3427, 2922, 2886, 1622, 1589, 1501, 1450, 1360, 1329, 1269, 1206, 1135, 1070, 745 cm^{-1}. HRMS (FAB): *m*/*z* calcd for $C_{28}H_{33}{}^{79}BrO_8$ $[M]^+$: 576.1359, found: 576.1351; calcd for $C_{28}H_{33}{}^{81}BrO_8$ $[M]^+$: 578.1343, found: 578.1341.

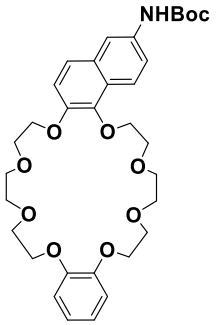

43

43: To a stirred solution of **42** (7.97 g, 13.8 mmol) in degassed toluene (55 ml) at room temperature was added successively $Pd_2(dba)_3$ (885 mg, 0.97 mmol), ^{t}BuXPhos (1.39 g, 2.9 mmol), NaO^{t}Bu (1.86 g, 19.3 mmol) and *tert*-butyl carbamate (1.94 g, 16.6 mmol). After stirring at room temperature for 8 h, the reaction mixture was filtered through a celite pad and the solvent was removed *in vacuo*. The crude product was purified by column chromatography (SiO_2, 1:99 MeOH/$CHCl_3$) to afford **43** (9.5 g, 99% yield) as a red oil.

^{1}H NMR (600 MHz, $CDCl_3$): δ 8.05 (d, *J* = 8.9 Hz, 1H), 7.96 (br, 1H), 7.46 (d, *J* = 8.9 Hz, 1H), 7.24 (dd, *J* = 8.9, 2.0 Hz, 1H), 7.20 (d, *J* = 8.9 Hz, 1H), 6.90-6.87 (m, 4H), 6.64 (br, 1H), 4.32 (t, *J* = 4.8 Hz, 2H), 4.27 (t, *J* = 4.1 Hz, 2H), 4.16-4.14 (m, 4H), 3.95 (t, *J* = 4.8 Hz, 2H), 3.93-3.91 (m, 6H), 3.85-3.84 (m, 4H), 3.82-3.79 (m, 4H), 1.54 (s, 9H). ^{13}C NMR (150 MHz, $CDCl_3$): δ 152.84, 148.88, 148.81, 146.26, 142.48, 134.45, 130.33, 125.66, 123.29, 122.45, 121.41, 121.34, 119.44, 117.34, 114.34, 114.10, 80.34, 72.26, 70.98, 70.57, 70.52, 70.03, 69.80, 69.74, 69.63, 69.27, 69.09, 28.25. IR (neat): 3319, 2929, 2873, 1719, 1604, 1543, 1502, 1454, 1369, 1250, 1158, 1128, 1058, 750 cm^{-1}. HRMS (FAB): *m*/*z* 636.2781 $[M+Na]^+$, 613.2893 $[M]^+$.

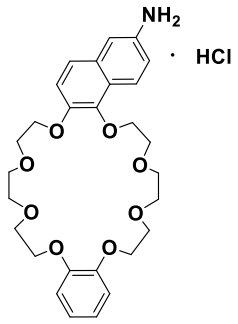

44

44: 4M HCl in dioxane (80 ml) was added to a reaction vessel containing **43** (9.9 g, 16.1 mmol) at room temperature. After stirring at room temperature for 7 h, the solvent was removed *in vacuo*. The crude product was directly used for the next step.

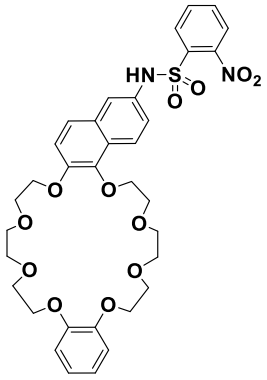

34

Ring component 34: To a stirred solution of **44** and NaOAc (7.4 g, 90 mmol) in MeOH (161 ml) and water (161 ml) at room temperature was added 2-nitrobenzenesulfonyl chloride (12.5 g, 56 mmol). The reaction mixture was stirred at 50 °C for 12 h. The reaction mixture was diluted with $CHCl_3$ and washed with sat. $NaHCO_3$ aq. and brine, dried over Na_2SO_4, filtered and concentrated *in vacuo*. The crude product was purified by column chromatography (SiO_2, 1:99 MeOH/AcOEt) to afford **34** (9.69 g, 86% yield, 2 steps) as a pale yellow amorphous. ^{1}H NMR (600 MHz, $CDCl_3$): δ 8.04 (d, *J* = 8.9 Hz, 1H), 7.85 (d, *J* = 7.6 Hz, 1H), 7.78 (dd, *J* = 7.5, 1.3 Hz, 1H), 7.66-7.62 (m, 1H), 7.57 (d, *J* = 2.0 Hz, 1H), 7.51-7.47 (m, 1H), 7.44 (d, *J* = 8.9 Hz, 1H), 7.36 (br, 1H), 7.25-7.22 (m, 2H), 6.90-6.86 (m, 4H), 4.31 (t, *J* = 4.8 Hz, 2H), 4.27 (t, *J* = 4.8 Hz, 2H), 4.15-4.12 (m, 4H), 3.93 (t, *J* = 5.5 Hz, 2H), 3.91-3.89 (m, 6H), 3.84-3.82 (m, 4H), 3.80-3.77 (m, 4H). ^{13}C NMR (150 MHz, $CDCl_3$): δ 148.84, 148.72, 148.02, 147.46, 142.24, 133.85, 132.48, 131.99, 131.66, 131.36, 129.55, 127.55, 125.09, 123.58, 123.30, 122.26, 121.44, 121.31, 120.77, 117.40, 114.34, 113.96,

72.30, 70.94, 70.51, 70.46, 69.87, 69.78, 69.69, 69.44, 69.24, 68.98. IR (neat): 2927, 2874, 1600, 1543, 1503, 1453, 1370, 1255, 1124, 748 cm^{-1}. HRMS (FAB): *m/z* calcd for $C_{34}H_{38}N_2O_{12}SNa$ $[M+Na]^+$: 721.2043, found: 721.2037.

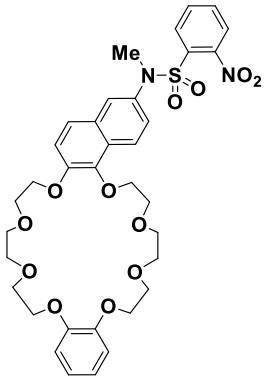

36

Ring component 36: To a stirred solution of ring component **34** (132 mg, 0.189 mmol) in DMF (0.66 ml) at room temperature was added NaH (9.5 mg, 0.395 mmol), then the mixture was stirred at room temperature for 15 min. To the resulting mixture was added methyl iodide (25 µl, 0.395 mmol) and the mixture was stirred at room temperature for another 1 h. The reaction was quenched with water and the aqueous layer was extracted with AcOEt. The organic extract was washed with water, dried over Na_2SO_4, filtered and concentrated *in vacuo*. The crude product was purified by column chromatography (SiO_2, 1:25:25 MeOH/AcOEt/Hexane to 1:50 MeOH/$CHCl_3$) to afford **36** (130 mg, 96% yield) as a yellow oil. ^{1}H NMR (400 MHz, $CDCl_3$): δ 8.09 (d, *J* = 9.2 Hz, 1H), 7.66-7.58 (m, 3H), 7.48-7.34 (m, 3H), 7.27-7.24 (m, 2H), 6.89-6.86 (m, 4H), 4.35-4.33 (m, 2H), 4.31-4.29 (m, 2H), 4.16-4.14 (m, 4H), 3.96-3.90 (m, 8H), 3.85-3.79 (m, 8H), 3.45 (s, 3H). ^{13}C NMR (100 MHz, $CDCl_3$): δ 148.83, 148.73, 148.18, 148.04, 142.22, 136.04, 133.60, 131.55, 130.95, 130.91, 129.39, 128.32, 126.08, 124.99, 123.99, 123.59, 123.14, 121.42, 121.31, 117.19, 114.32, 113.98, 72.32, 70.96, 70.54, 70.48, 69.87, 69.80, 69.72, 69.41, 69.21, 68.98, 39.40.IR (neat): 2925, 2874, 1597, 1545, 1502, 1454, 1353, 1256, 1123, 752 cm^{-1}. HRMS (FAB): *m/z* calcd for $C_{35}H_{40}N_2O_{12}S$ $[M]^+$: 712.2302, found: 712.2302.

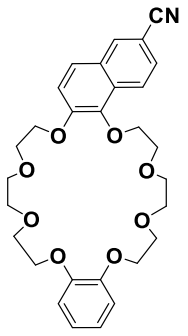

45

45: To a stirred solution of **42** (4.1 g, 6.9 mmol) in DMF (30 ml) at room temperature was added CuCN (12.4 g, 138 mmol). The reaction mixture was stirred at 120 °C for 70 h. The reaction was quenched with brine and the aqueous layer was extracted with AcOEt. The organic extract was washed with $NaHCO_3$ aq., dried over Na_2SO_4, filtered and concentrated *in vacuo*. The crude product was subjected to a short column

(SiO_2, 1:1 Hexane/AcOEt to 1:9 MeOH/$CHCl_3$) to afford a crude **45** as a brown oil, which was directly used for the next step.

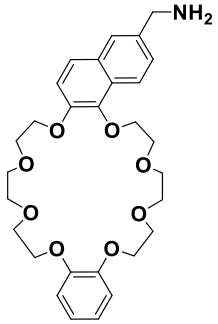

46

46: To a stirred solution of $LiAlH_4$ (410 mg, 10.8 mmol) in THF (12.5 ml) at 0 °C was added a solution of crude **45** (1.88 g) in THF (12.5 ml). The reaction mixture was stirred at room temperature for 10 h. The reaction mixture was quenched by adding water, followed by 15% NaOH aq. and water. The resulting precipitate was filtered through celite and a part of solvent was removed *in vacuo*. The aqueous layer was extracted with $CHCl_3$. The organic extract was washed with brine, dried over Na_2SO_4, filtered and concentrated *in vacuo*. The crude product was directly used for the next step.

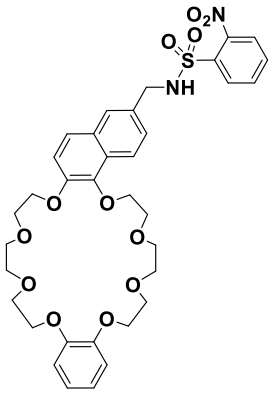

35

Ring component 35: To a stirred solution of **46** and triethylamine (550 μl, 3.95 mmol) in CH_2Cl_2 (10 ml) at room temperature was added 2-nitrobenzenesulfonyl chloride (875 mg, 3.95 mmol). The reaction mixture was stirred at room temperature for 1 h. The reaction mixture was diluted with $CHCl_3$ and washed with 1 M HCl aq. and brine, dried over Na_2SO_4, filtered and concentrated *in vacuo*. The crude product was purified by column chromatography (SiO_2, 1:99 MeOH/$CHCl_3$) to afford **35** (2.05 g, 42% yield, 3 steps) as a reddish brown amorphous. ^{1}H NMR (400 MHz, $CDCl_3$): δ 7.95 (d, *J* = 8.7 Hz, 1H), 7.89 (dd, *J* = 7.3, 0.9 Hz, 1H), 7.74 (d, *J* = 7.8 Hz, 1H), 7.56-7.51 (m, 2H), 7.44-7.39 (m, 2H), 7.23-7.21 (m, 2H), 6.89-6.86 (m, 4H), 5.84 (brt, *J* = 6.0 Hz, 1H), 4.44 (d, *J* = 6.0 Hz, 2H), 4.30-4.27 (m, 4H), 4.17-4.13 (m, 4H), 3.95-3.89 (m, 8H), 3.86-3.78 (m, 8H). ^{13}C NMR (100 MHz, $CDCl_3$): δ 148.82, 148.72, 147.64, 147.44, 142.09, 133.75, 133.13, 132.34, 131.16, 130.76, 129.08, 128.53, 126.65, 125.47, 124.92, 123.77, 122.23, 121.43, 121.32, 116.65, 114.29, 113.98, 72.25, 70.96, 70.52, 70.44, 69.92, 69.77, 69.71, 69.32, 69.21, 68.97, 47.85. IR (neat): 3012, 2927, 2875, 1600, 1541, 1502, 1345, 1255, 1125, 751 cm^{-1}. HRMS (FAB): *m*/*z* calcd for $C_{35}H_{40}N_2O_{12}S$ $[M]^+$: 712.2302, found: 712.2304.

4.3.3 Synthesis of an endcap component (Figure 45)

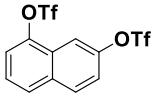

47

1,7-Naphthyl bis(trifluoromethanesulfonate) (47): To a stirred solution of 1,7-dihydroxynaphthalene (23.4 g, 146 mmol) in pyridine (200 ml) at 0 °C was added trifluoromethanesulfonic anhydride (49 ml, 292 mmol) dropwise. The reaction mixture was allowed to warm to room temperature and stirred for 3 h. The reaction mixture was partitioned between water and AcOEt. The organic extract was washed with 1M HCl aq., water and brine, dried over Na_2SO_4, filtered and concentrated *in vacuo*. The crude product was purified by column chromatography (SiO_2, 5:1 Hexane/AcOEt) to afford 1,7-naphthylbis(trifluoromethanesulfonate) **47** (61.3 g, 99% yield) as a colorless oil. ^{1}H NMR (600 MHz, $CDCl_3$): δ 8.04 (d, *J* = 8.9 Hz, 1H), 7.94-7.97 (m, 2H), 7.63-7.60 (m, 2H), 7.53 (dd, *J* = 8.9, 2.7 Hz, 1H). ^{13}C NMR (150 MHz, $CDCl_3$): δ 148.43, 145.12, 133.59, 131.07, 128.33, 126.65, 126.42, 121.38, 119.61, 118.85 (q, *J* = 318.8 Hz), 118.76 (q, *J* = 318.8 Hz), 112.89. IR (neat): 1606, 1510, 1428, 1215, 1138, 1204 cm^{-1}. HRMS (EI): *m*/*z* calcd for $C_{12}H_6F_6O_6S_2$ $[M]^+$: 423.9510, found: 423.9494.

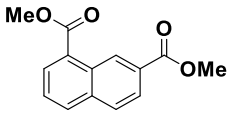

48

Dimethyl naphthalene 1,7-dicarboxylate (48): To a stirred solution of 1,7-naphthylbis(trifluoromethanesulfonate) (**47**) (18.6 g, 43.8 mmol) in DMSO (153 ml) and MeOH (153 ml) at room temperature was added triethylamine (92 ml, 660 mmol) followed by $Pd(OAc)_2$ (1.1 g, 4.38 mmol) and 1,3-Bis(diphenylphosphino)propane (1.8 g, 4.38 mmol). A stream of CO was passed into the solution for 2-3 min then the reaction vessel and contents were placed in a 55~65 °C oil bath under a CO balloon. After stirring for 36 h, the reaction mixture was filtered through a celite pad and a part of solvent was removed *in vacuo*. The solution was diluted with AcOEt and washed with 1 M HCl aq., water and brine, dried over Na_2SO_4, filtered and concentrated *in vacuo*. The crude product was purified by column chromatography (SiO_2, 5:1 Hexane/AcOEt) to afford dimethyl naphthalene 1,7-dicarboxylate (**48**) (3.47 g, 32% yield) as a yellow solid. m.p. 83-85 °C. ^{1}H NMR (600 MHz, $CDCl_3$): δ 9.65 (s, 1H), 8.23 (d, *J* = 6.2 Hz, 1H), 8.13 (dd, *J* = 8.9, 1.4 Hz, 1H), 8.04 (d, *J* = 8.3 Hz, 1H), 7.92 (d, *J* = 8.3 Hz, 1H), 7.60 (t, *J* = 8.3 Hz, 1H), 4.03 (s, 3H), 3.99 (s, 3H). ^{13}C NMR (150 MHz, $CDCl_3$): δ 167.27, 167.08, 135.56, 132.87, 130.69, 130.23, 128.84, 128.60, 128.00, 126.58, 125.52, 52.21. IR (KBr): 2949, 1717, 1457, 1435, 1272, 1242, 1196, 1146 cm^{-1}. HRMS (EI): *m*/*z* calcd for $C_{14}H_{12}O_4$ $[M]^+$: 244.0736, found: 244.0740.

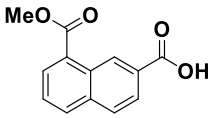

49

1,7-Naphthalenedicarboxylic acid, 1-methyl ester (49): To a stirred solution of dimethyl naphthalene 1,7-dicarboxylate (**48**) (20.0 g, 81.9 mmol) in dioxane (360 ml) at room temperature was added a solution of KOH (4.73 g, 84.3 mmol) in MeOH (17 ml). The reaction mixture was stirred at room temperature for 2 h.

The reaction mixture was partitioned between water and AcOEt. The organic layer containing dimethyl naphthalene 1,7-dicarboxylate (**48**) was washed with water and concentrated. This recovered dimethyl naphthalene 1,7-dicarboxylate (**48**) was again used for the above reaction. After repeating above reaction three times, the combined aqueous layers were acidified with 1 M HCl aq. to pH 3. The aqueous layer was extracted with AcOEt and the combined organic extracts were washed with brine, dried over Na_2SO_4, filtered and concentrated *in vacuo*. The crude product was subjected to column chromatography (SiO_2, 1:99 MeOH/$CHCl_3$) to afford a mixture of 1,7-naphthalenedicarboxylic acid, 1-methyl ester (**49**) and 1,7-naphthalenedicarboxylic acid, 7-methyl ester. The mixture was recrystallized from $CHCl_3$ to give 1,7-naphthalenedicarboxylic acid, 1-methyl ester (**49**) (5.9 g, 31% yield) as a white solid. m.p. 229-231 °C. ^{1}H NMR (600 MHz, $CDCl_3$): δ 9.77 (s, 1H), 8.27 (dd, *J* = 6.8, 1.4 Hz, 1H), 8.18 (dd, *J* = 8.9, 1.4 Hz, 1H), 8.09 (d, *J* = 8.3 Hz, 1H), 7.98 (d, *J* = 8.9 Hz, 1H), 7.65 (t, *J* = 6.8 Hz, 1H), 4.06 (s, 3H). ^{13}C NMR (150 MHz, $CDCl_3$): δ 170.15, 167.46, 136.16, 133.03, 130.95, 130.38, 129.99, 128.95, 128.59, 127.97, 127.19, 125.87, 52.47. IR (neat): 3411, 2950, 1713, 1510, 1454, 1436, 1281, 1251, 1226, 1136 cm^{-1}. HRMS (EI): *m*/*z* calcd for $C_{13}H_{10}O_4$ $[M]^+$: 230.0579, found: 230.0579.

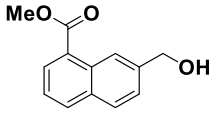

50

1-Naphthalenecarboxylic acid, 7-(hydroxymethyl)-, methyl ester (50): To a stirred solution of 1,7-naphthalenedicarboxylic acid, 1-methyl ester (**49**) (5.8 g, 25.3 mmol) in THF (50 ml) at 0 °C was added 1.0 M borane tetrahydrofuran complex in THF. The reaction mixture was stirred at 0 °C for 6 h. After 1 M HCl aq. was added dropwise, the mixture was extracted with AcOEt. The organic layer was washed with water and brine, dried over Na_2SO_4, filtered and concentrated *in vacuo*. The crude product was purified by column chromatography (SiO_2, 1:50 to 1:20 MeOH/$CHCl_3$) to afford 1-naphthalenecarboxylic acid, 7-(hydroxymethyl)-, methyl ester (**50**) **(**4.6 g, 83% yield) as a colorless oil. ^{1}H NMR (600 MHz, $CDCl_3$): δ 8.86 (s, 1H), 8.17 (d, *J* = 7.6 Hz, 1H), 8.00 (d, *J* = 8.3 Hz, 1H), 7.87 (d, *J* = 8.2 Hz, 1H), 7.56 (d, *J* = 8.2 Hz, 1H), 7.48 (t, *J* = 8.2 Hz, 1H), 4.88 (s, 2H), 3.99 (s, 3H), 2.12 (br, 1H). ^{13}C NMR (150 MHz, $CDCl_3$): δ 167.98, 140.41, 133.07, 131.10, 130.29, 128.74, 126.66, 125.42, 124.24, 123.05, 65.39, 52.08. IR (KBr): 3411, 3056, 2950, 1711, 1685, 1622, 1461, 1300, 1274, 1249, 1196, 1157, 1111 cm^{-1}. HRMS (EI): *m*/*z* calcd for $C_{13}H_{12}O_3$ $[M]^+$: 216.0786, found: 216.0785.

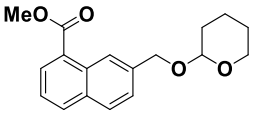

51

51: To a stirred solution of 1-naphthalenecarboxylic acid, 7-(hydroxymethyl)-, methyl ester (**50**) (4.54 g, 21 mmol) and 3,4-dihydro-2*H*-pyran (14.0 ml, 154 mmol) in CH_2Cl_2 (200 ml) at room temperature was added pyridinium *p*-toluenesulfonate (503 mg, 2.0 mmol). The reaction mixture was stirred at room temperature for 3 h. The reaction mixture was partitioned between sat. $NaHCO_3$ aq. and CH_2Cl_2. The organic extract was washed with washed with water and brine, dried over Na_2SO_4, filtered and concentrated *in vacuo*. The crude product was purified by column chromatography (SiO_2, 5:1 Hexane/AcOEt) to afford **51** (6.3 g, 99% yield)

as a colorless oil. ^{1}H NMR (600 MHz, $CDCl_3$): δ 8.88 (s, 1H), 8.18 (dd, *J* = 7.6, 1.4 Hz, 1H), 8.01 (d, *J* = 8.2 Hz, 1H), 7.88 (d, *J* = 8.3 Hz, 1H), 7.59 (dd, *J* = 8.3, 1.4 Hz, 1H), 7.48 (t, *J* = 7.6 Hz, 1H), 4.99 (d, *J* = 12.4 Hz, 1H), 4.78 (t, *J* = 3.4 Hz, 1H), 4.72 (d, *J* = 12.4 Hz, 1H), 4.00 (s, 3H), 4.00-3.95 (m, 1H), 3.61-3.56 (m, 1H), 1.93-1.87 (m, 1H), 1.80-1.75 (m, 1H), 1.73-1.68 (m, 1H), 1.64-1.53 (m, 3H). ^{13}C NMR (150 MHz, $CDCl_3$): δ 167.81, 137.78, 133.18, 132.99, 131.11, 130.25, 128.61, 126.80, 126.09, 124.25, 97.73, 69.05, 62.01, 51.96, 30.46, 25.35, 19.68. IR (neat): 2947, 1717, 1510, 1455, 1437, 1281, 1251, 1135, 1034 cm^{-1}. HRMS (EI): *m*/*z* calcd for $C_{18}H_{20}O_4$ $[M]^+$: 300.1362, found: 300.1366.

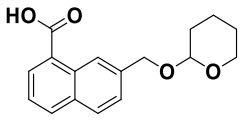

37

Endcap component 37: To a stirred solution of **51** (6.3 g, 20.8 mmol) in THF (210 ml) and MeOH (84 ml) at room temperature was added a solution of KOH (5.3 g, 94 mmol) in water (42 ml). The reaction mixture was stirred at room temperature for 12 h. A part of solvent was removed *in vacuo* and the mixture was partitioned between water and $CHCl_3$. The aqueous layer was neutralized with citric acid aq. and extracted with $CHCl_3$. The organic extract was washed with washed with water and brine, dried over Na_2SO_4, filtered and concentrated *in vacuo*. The crude product was purified by column chromatography (SiO_2, 1:99 MeOH/AcOEt) to afford **37** (5.0 g, 84% yield) as a white solid. m.p. 86-89 °C. ^{1}H NMR (600 MHz, $CDCl_3$): δ 9.06 (s, 1H), 8.39 (dd, *J* = 8.2, 1.4 Hz, 1H), 8.07 (d, *J* = 8.4 Hz, 1H), 7.90 (d, *J* = 8.3 Hz, 1H), 7.61 (dd, *J* = 8.9, 1.4 Hz, 1H), 7.53 (t, *J* = 7.6 Hz, 1H), 5.02 (d, *J* = 12.4 Hz, 1H), 4.81 (t, *J* = 3.4 Hz, 1H), 4.76 (d, *J* = 12.4 Hz, 1H), 3.99 (ddd, *J* = 11.0, 8.9, 3.4 Hz, 1H), 3.59 (dt, *J* = 11.0, 4.8 Hz, 1H), 1.95-1.89 (m, 1H), 1.81-1.76 (m, 1H), 1.75-1.70 (m, 1H), 1.65-1.54 (m, 3H). ^{13}C NMR (150 MHz, $CDCl_3$): δ 172.91, 138.27, 134.31, 133.40, 131.95, 131.56, 128.89, 126.26, 125.57, 124.48, 124.44, 97.84, 69.16, 62.17, 30.56, 25.47, 19.28. IR (KBr): 2934, 2870, 2630, 1689, 1593, 1571, 1511, 1458, 1286, 1256, 1124, 1066, 1039 cm^{-1}. HRMS (EI): *m*/*z* calcd for $C_{17}H_{18}O_4$ $[M]^+$: 286.1205, found: 286.1199.

4.3.4 Synthesis of rotaxanes (Figure 47)

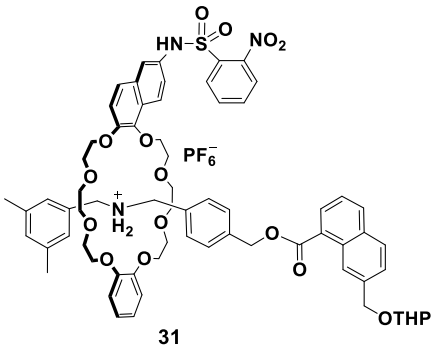

31

Racemic rotaxane 31 (as a mixture of diastereomers): To a stirred solution of ring component **34** (7.2 g, 10.3 mmol) in $CHCl_3$ (20 ml) was added axis component **10** (2.8 g, 7.0 mmol) and the mixture was stirred at 0 °C for 45 min, which turned to a transparent solution. Endcap component **37** (2.8 g, 9.8 mmol), *N*,*N*'-dicyclohexylcarbodiimide (5.8 g, 27.9 mmol) and tributylphosphine (345 µl, 1.4 mmol) were added to the solution successively. The solution was stirred at 0 °C for 15 h. The reaction mixture was partitioned between water and $CHCl_3$ and the organic extract was washed with water and brine, dried over Na_2SO_4, filtered and concentrated *in vacuo*. The crude product was subjected to a short column (SiO_2, 1:99 to 1:20 MeOH/$CHCl_3$) to afford a mixture of rotaxane **31** and recovered ring component **34**, which was directly used for the next step.

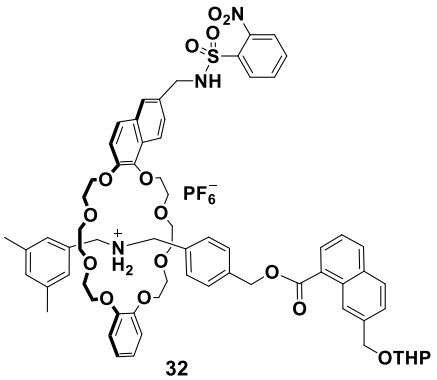

32

Racemic rotaxane 32 (as a mixture of diastereomers): According to the synthetic procedure of racemic rotaxane **31**, preparation of racemic rotaxane **32** was performed.

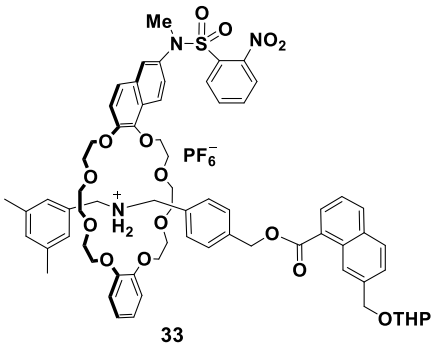

33

Racemic rotaxane 33 (as a mixture of diastereomers): To a stirred solution of ring component **36** (120 mg, 0.168 mmol) in $CHCl_3$ (5.2 ml) was added axis component **10** (94.3 mg, 0.235 mmol) and the mixture

was stirred at 0 °C for 5 h. Endcap component **37** (67.3 mg, 0.235 mmol), tributylphosphine (83 µl, 0.336 mmol) and *N*,*N*'-dicyclohexylcarbodiimide (139 mg, 0.672 mmol) were added to the solution successively. The solution was stirred at 0 °C for 14 h. The reaction mixture was filtered and concentrated *in vacuo*. The residue was subjected to a preparative TLC (SiO_2, 1:19 MeOH/$CHCl_3$) in order to separate rotaxane **33** from ring component **36**. The crude **33** was directly used for the next step.

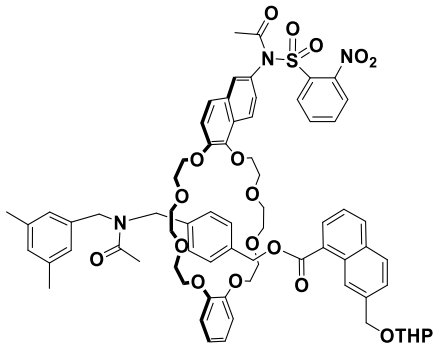

58

Racemic rotaxane 58 (as a mixture of diastereomers): To a stirred solution of **31** in MeCN (70 ml) at room temperature was added triethylamine (19.4 ml, 139 mmol) and acetic anhydride (6.6 ml, 70 mmol). The reaction mixture was stirred at 40 °C for 3 h. The solvent was removed *in vacuo* and the residue was diluted with AcOEt, washed with water and brine, dried over Na_2SO_4, filtered and concentrated *in vacuo*. The crude product was purified by column chromatography (SiO_2, 1:2 hexane/AcOEt to 1:199 MeOH/AcOEt) to afford **58** (4.8 g, 53% yield, 2 steps) as a yellow amorphous, which is a mixture of diastereomers derived from a topological chirality and a chirality of THP group. ^{1}H NMR (600 MHz, $CDCl_3$): δ 9.01 (s, 1H), 8.86-8.83 (m, 1H), 8.43-8.42 (m, 1H), 8.05-8.03 (m, 2H), 7.97-7.95 (m, 2H), 7.78-7.70 (m, 5H), 7.66-7.65 (m, 1H), 7.52-7.50 (m, 1H), 7.46-7.43 (m, 1H), 7.35-7.34 (m, 1H), 7.08-7.02 (m, 2H), 6.99-6.98 (m, 1H), 6.87-6.85 (m, 1H), 6.79-6.77 (m, 3H), 6.74-6.69 (m, 3H), 6.27-6.22 (m, 2H), 4.97-4.93 (m, 1H), 4.78-4.76 (m, 1H), 4.70-4.61 (m, 2H), 4.49 (s, 1H), 4.42-4.37 (m, 2H), 4.28-4.26 (m, 2H), 4.22 (s, 1H), 4.19-4.15 (m, 1H), 4.10-4.02 (m, 4H), 3.99-3.90 (m, 2H), 3.89-3.85 (m, 1H), 3.83-3.79 (m, 1H), 3.71-3.62 (m, 4H), 3.59-3.37 (m, 7H), 3.35-3.31 (m, 1H), 3.28-3.24 (m, 1H), 2.25-2.22 (m, 6H), 2.13-2.12 (m, 3H), 1.99-1.98 (m, 3H), 1.92-1.85 (m, 1H), 1.79-1.66 (m, 2H), 1.63-1.59 (m, 1H), 1.57-1.52 (m, 2H). ^{13}C NMR (150 MHz, $CDCl_3$): δ 170.89, 170.83, 170.81, 167.81, 149.58, 149.55, 148.28, 148.25, 148.22, 148.18, 147.99, 141.70, 141.66, 138.34, 137.88, 137.80, 137.43, 137.20, 136.98, 136.96, 136.89, 136.86, 136.39, 134.86, 134.65, 134.61, 133.92, 132.90, 132.87, 132.54, 131.84, 131.75, 131.60, 131.23, 130.06, 130.02, 129.95, 129.76, 129.61, 129.53, 129.00, 128.97, 128.92, 128.79, 128.40, 128.36, 127.71, 127.16, 126.90, 126.85, 125.89, 125.56, 125.52, 125.33, 124.85, 124.81, 124.15, 123.99, 123.93, 123.48, 122.61, 120.19, 118.00, 115.91, 115.86, 111.30, 111.11, 97.78, 97.72, 71.85, 71.55, 70.98, 70.85, 70.69, 70.25, 70.16, 69.72, 69.63, 69.56, 69.50, 69.35, 69.32, 69.21, 68.15, 68.13, 67.75, 67.66, 62.03, 61.97, 50.45, 49.97, 47.47, 47.34, 30.53, 30.51, 25.39, 24.68, 21.67, 21.15, 21.11, 19.30, 19.26. IR (neat): 3009, 2925, 2874, 1708, 1639, 1597, 1545, 1504, 1452, 1419, 1366, 1252, 1172, 1126, 1061, 1035, 755 cm^{-1}. HRMS (ESI): *m*/*z* calcd for $C_{72}H_{79}N_3O_{18}SNa$ $[M+Na]^+$: 1328.4972, found: 1328.4988.

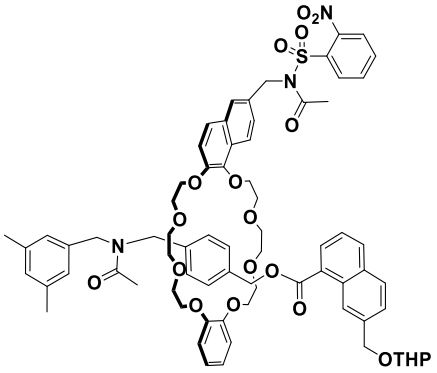

59

Racemic rotaxane 59 (as a mixture of diastereomers): According to the synthetic procedure of racemic rotaxane **58**, acylative neutralization of **32** was performed. Pale yellow oil (26 mg, 25%, 2 steps). ^{1}H NMR (400 MHz, $CDCl_3$): δ 9.01 (s, 1H), 8.89-8.87 (m, 1H), 8.44-8.40 (m, 1H), 8.03 (d, *J* = 7.8 Hz, 1H), 7.97-7.93 (m, 2H), 7.79-7.70 (m, 6H), 7.60-7.58 (m, 1H), 7.52-7.49 (m, 1H), 7.39-7.36 (m, 1H), 7.30-7.27 (m, 1H), 7.11-7.04 (m, 2H), 6.98-6.96 (m, 1H), 6.86-6.84 (m, 1H), 6.80-6.72 (m, 5H), 6.65 (s, 1H), 6.25-6.23 (m, 2H), 5.16 (s, 2H), 4.95-4.92 (m, 1H), 4.77-4.75 (m, 1H), 4.69-4.65 (m, 1H), 4.58-4.47 (m, 2H), 4.41-4.36 (m, 2H), 4.25-4.16 (m, 4H), 4.10-4.03 (m, 4H), 3.99-3.78 (m, 4H), 3.72-3.23 (m, 14H), 2.23-2.22 (m, 6H), 2.15-2.10 (m, 6H), 1.94-1.83 (m, 1H), 1.79-1.51 (m, 4H). ^{13}C NMR (100 MHz, $CDCl_3$): δ 171.05, 170.99, 170.96, 167.88, 148.57, 148.50, 148.37, 148.35, 148.31, 148.28, 147.86, 141.69, 138.46, 137.99, 137.84, 137.46, 137.27, 137.08, 137.01, 136.46, 134.92, 134.60, 134.57, 133.99, 132.97, 132.02, 131.93, 131.50, 131.46, 131.39, 130.07, 129.65, 129.30, 129.27, 129.02, 128.90, 128.79, 128.49, 127.62, 127.25, 126.00, 125.66, 125.63, 125.43, 125.32, 124.93, 124.63, 124.56, 124.33, 123.99, 122.58, 120.30, 115.47, 115.41, 111.39, 111.24, 97.90, 97.82, 71.84, 70.90, 70.79, 70.29, 70.20, 69.82, 69.77, 69.48, 69.46, 69.24, 68.27, 67.86, 67.78, 62.15, 62.08, 51.25, 50.52, 50.00, 47.55, 47.41, 30.62, 30.61, 29.68, 25.49, 24.30, 21.73, 21.23, 21.20, 19.39, 19.34. IR (neat): 3009, 2925, 2875, 1707, 1642, 1543, 1504, 1452, 1366, 1251, 1172, 1126, 1061, 1034, 753 cm^{-1}. HRMS (ESI): *m*/*z* calcd for $C_{73}H_{81}N_3O_{18}SNa$ $[M+Na]^+$: 1342.5128, found: 1342.5146.

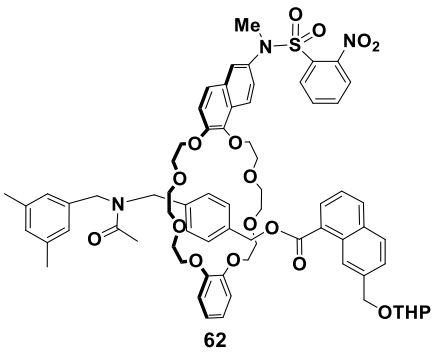

62

Racemic rotaxane 62 (as a mixture of diastereomers): To a stirred solution of **33** in MeCN (940 μl) at room temperature was added triethylamine (940 μl, 6.72 mmol) and acetic anhydride (320 μl, 3.36 mmol). The reaction mixture was stirred at 40 °C for 1 h. The solvent was removed *in vacuo*. The crude product was purified by preparative TLC (SiO_2, 1:19 MeOH/$CHCl_3$) then preparative TLC (SiO_2, 1:50:50 MeOH/AcOEt/Hexane) to afford **62** (67.6 mg, 34% yield, 2 steps) as a pale yellow amorphous, which is a mixture of diastereomers derived from a topological chirality and a chirality of THP group. ^{1}H NMR (400 MHz, $CDCl_3$): δ 9.01-8.99 (m, 1H), 8.88-8.85 (m, 1H), 8.02 (d, *J* = 8.3 Hz, 1H), 7.95 (d, *J* = 7.8 Hz, 1H),

7.88-7.85 (m, 1H), 7.76-7.71 (m, 2H), 7.63-7.56 (m, 3H), 7.53-7.49 (m, 2H), 7.44-7.42 (m, 1H), 7.39-7.35 (m, 1H), 7.30-7.27 (m, 1H), 7.19-7.17 (m, 1H), 7.11-7.02 (m, 2H), 6.97-6.95 (m, 1H), 6.88-6.85 (m, 1H), 6.79-6.76 (m, 2H), 6.73-6.68 (m, 3H), 6.66 (s, 1H), 6.23-6.22 (m, 2H), 4.96-4.91 (m, 1H), 4.78-4.75 (m, 1H), 4.69-4.64 (m, 1H), 4.59-4.45 (m, 2H), 4.40-4.33 (m, 2H), 4.25-4.13 (m, 4H), 4.08-3.77 (m, 8H), 3.71-3.22 (m, 17H), 2.25-2.22 (m, 6H), 2.12-2.09 (m, 3H), 1.92-1.83 (m, 1H), 1.78-1.51 (m, 5H). ^{13}C NMR (100 MHz, $CDCl_3$): δ 170.99, 170.89, 167.86, 148.90, 148.27, 141.61, 138.44, 137.96, 137.78, 137.40, 137.21, 137.07, 137.00, 136.41, 135.87, 135.82, 134.90, 133.96, 133.56, 132.99, 132.95, 131.95, 131.83, 131.64, 131.34, 131.08, 130.99, 130.11, 129.66, 129.18, 129.14, 129.02, 128.88, 128.44, 127.67, 127.62, 127,16, 126.31, 125.94, 125.66, 125.60, 125.35, 125.11, 125.08, 124.88, 124.40, 124.34, 124.26, 123.96, 123.63, 122.93, 120.26, 115.73, 115.67, 111.34, 111.19, 97.88, 97.81, 71.79, 70.89, 70.70, 70.33, 70.23, 69.78, 69.72, 69.43, 69.40, 69.26, 68.20, 67.82, 67.76, 62.12, 62.05, 50.47, 50.02, 47.52, 47.36, 39.43, 30.59, 25.45, 21.68, 21.21, 21.17, 19.36, 19.32. IR (neat): 3008, 2924, 2875, 1704, 1641, 1598, 1547, 1504, 1452, 1367, 1252, 1063, 755 cm^{-1}. HRMS (ESI): *m*/*z* calcd for $C_{71}H_{79}N_3O_{17}SNa$ $[M+Na]^+$: 1300.5022, found: 1300.5046.

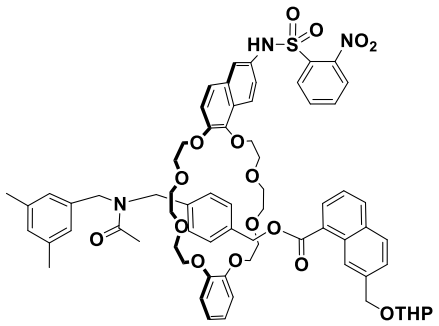

60

Racemic rotaxane 60 (as a mixture of diastereomers): To a stirred solution of rotaxane **58** (4.6 g, 3.5 mmol) in THF (85 ml) at room temperature was added a solution of KOH (0.48 g, 8.4 mmol) in water (25 ml). The reaction mixture was stirred at 40 °C for 4 h. A part of solvent was removed *in vacuo* and the mixture was partitioned between water and $CHCl_3$. The organic extract was washed with water and brine, dried over Na_2SO_4, filtered and concentrated *in vacuo*. The crude product was directly used for the next step.

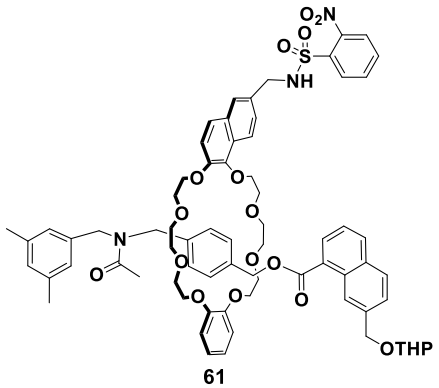

61

Racemic rotaxane 61 (as a mixture of diastereomers): According to the synthetic procedure of racemic rotaxane **60**, hydrolysis of **59** was performed.

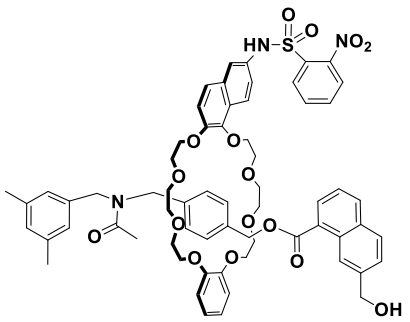

13

Racemic rotaxane 13: To a stirred solution of rotaxane **60** in EtOH (35 ml) and THF (35 ml) at 30 °C was added pyridinium *p*-toluenesulfonate (17.6 g, 70 mmol). The reaction mixture was stirred at 30 °C for 19 h. The solvent was removed *in vacuo* and the residue was diluted with $CHCl_3$, washed with water and brine, dried over Na_2SO_4, filtered and concentrated *in vacuo*. The crude product was subjected to a short column (SiO_2, 1:5 to 0:1 hexane/AcOEt), then purified by preparative TLC (SiO_2, 1:19 MeOH/$CHCl_3$) to afford **13** (1.53 g, 37% yield, 2 steps) as a yellow amorphous. HPLC conditions: CHIRALPAK IC column, eluent 1:60 EtOH/CH_2Cl_2, flow rate 0.7 ml/min, temperature 20 °C, 18.8 min (minor), 24.5 min (major). $[\alpha]_D^{23}$ -23.4 (major enantiomer, 99% ee, *c* 0.72, $CHCl_3$). ^{1}H NMR (600 MHz, $CDCl_3$): δ 8.83-8.80 (m, 1H), 8.70-8.66 (m, 1H), 8.03 (d, *J* = 7.9 Hz, 1H), 7.96 (d, *J* = 7.9 Hz, 1H), 7.83-7,81 (m, 2H), 7.77-7.74 (m, 1H), 7.71-7.64 (m, 2H), 7.62-7.59 (m, 1H), 7.55 (s, 1H), 7.46-7.42 (m, 4H), 7.22-7.18 (m, 2H), 7.10-7.03 (m, 2H), 6.97 (d, *J* = 8.2 Hz, 1H), 6.88-6.85 (m, 1H), 6.77-6.74 (m, 3H), 6.66-6.63 (m, 3H), 6.25-6.20 (m, 2H), 4.80-4.78 (m, 2H), 4.55-4.44 (m, 2H), 4.37-4.35 (m, 1H), 4.33-4.29 (m, 1H), 4.26-4.24 (m, 1H), 4.22-4.18 (m, 2H), 4.14-4.08 (m, 1H), 4.02-3.96 (m, 4H), 3.90-3.76 (m, 3H), 3.72-3.68 (m, 1H), 3.63-3.59 (m, 3H), 3.54-3.43 (m, 5H), 3.40-3.33 (m, 2H), 3.29-3.26 (m, 1H), 3.21-3.17 (m, 1H), 2.25-2.22 (m, 6H), 2.11-2.07 (m, 3H), 1.74 (br, 1H). ^{13}C NMR (150 MHz, $CDCl_3$): δ 171.06, 170.96, 168.24, 148.30, 148.26, 148.17, 148.15, 148.10, 141.59, 141.58, 139.56, 139.49, 138.47, 137.98, 137.76, 137.37, 137.19, 136.37, 134.91, 133.98, 133.81, 132.79, 132.75, 132.49, 132.19, 131.70, 131.57, 131.42, 131.18, 131.14, 131.11, 131.10, 131.07, 130.06, 129.61, 129.28, 129.25, 129.04, 128.90, 128.50, 128.46, 128.33, 128.24, 127.68, 127.64, 127.12, 125.93, 125.32, 125.12, 124.98, 124.95, 124.26, 123.94, 123.89, 123.77, 123.73, 123.08, 122.47, 122.44, 121.02, 120.22, 115.87, 115.82, 111.30, 111.17, 71.79, 70.87, 70.63, 70.30, 70.21, 69.87, 69.83, 69.79, 69.73, 69.68, 69.63, 69.17, 68.07, 67.89, 67.77, 65.64, 50.52, 50.03, 47.58, 47.46, 21.66, 21.64, 21.22, 21.17. IR (neat): 3011, 2922, 2876, 1705, 1626, 1603, 1543, 1505, 1451, 1369, 1251, 1127, 753 cm^{-1}. HRMS (ESI): *m*/*z* calcd for $C_{65}H_{69}N_3O_{16}SNa$ $[M+Na]^+$: 1202.4291, found: 1202.4322.

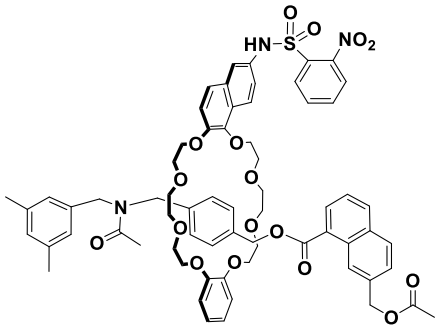

14

Acylate 14: Yellow amorphous. HPLC conditions: CHIRALPAK IC column, eluent 1:60 EtOH/CH_2Cl_2, flow rate 0.7 ml/min, temperature 20 °C, 9.2 min (major), 12.6 min (minor). $[\alpha]_D^{23}$ +9.89 (major enantiomer, 40% ee, *c* 1.16, $CHCl_3$). ^{1}H NMR (600 MHz, $CDCl_3$): δ 9.02-9.00 (m, 1H), 8.88-8.86 (m, 1H), 8.02 (d, *J* = 8.2 Hz, 1H), 7.94 (d, *J* = 7.9 Hz, 1H), 7.83-7.81 (m, 2H), 7.75-7.69 (m, 3H), 7.63-7.59 (m, 1H), 7.56-7.55 (m, 1H), 7.48-7.42 (m, 3H), 7.35 (br, 1H), 7.25-7.24 (m, 1H), 7.20-7.18 (m, 1H), 7.12-7.07 (m, 1H), 7.03-7.01 (m, 1H), 6.97-6.95 (m, 1H), 6.89-6.86 (m, 1H), 6.76-6.73 (m, 3H), 6.68-6.66 (m, 3H), 6.24-6.20 (m, 2H), 5.26-5.24 (m, 2H), 4.55-4.44 (m, 2H), 4.38-4.33 (m, 2H), 4.25-4.12 (m, 4H), 4.07-4.00 (m, 4H), 3.92-3.77 (m, 3H), 3.71-3.68 (m, 1H), 3.63-3.60 (m, 3H), 3.54-3.36 (m, 6H), 3.33-3.29 (m, 1H), 3.25-3.22 (m, 1H), 2.25-2.22 (m, 6H), 2.13-2.07 (m, 6H). ^{13}C NMR (150 MHz, $CDCl_3$): δ 171.01, 170.89, 167.77, 148.35, 148.27, 148.21, 148.16, 141.68, 138.49, 138.01, 137.78, 137.40, 137.38, 137.26, 136.46, 134.99, 134.45, 134.36, 134.05, 133.83, 133.14, 132.54, 132.23, 132.07, 131.88, 131.79, 131.24, 131.18, 131.14, 130.21, 129.77, 129.33, 129.05, 128.91, 128.67, 128.64, 127.82, 127.78, 127.17, 125.96, 125.85, 125.82, 125.54, 125.51, 125.32, 125.19, 124.75, 123.95, 123.16, 122.49, 121.13, 120.25, 115.93, 115.86, 111.30, 111.15, 71.82, 70.95, 70.69, 70.41, 70.32, 69.83, 69.77, 69.28, 68.20, 67.98, 67.85, 66.94, 50.52, 50.04, 47.58, 47.45, 21.70, 21.25, 21.20, 21.05. IR (neat): 2958, 2926, 2874, 1731, 1631, 1602, 1543, 1506, 1453, 1370, 1252, 1170, 1125, 1065, 753 cm^{-1}. HRMS (ESI): *m/z* calcd for $C_{67}H_{71}N_3O_{17}SNa$ $[M+Na]^+$: 1244.4396, found: 1244.4416.

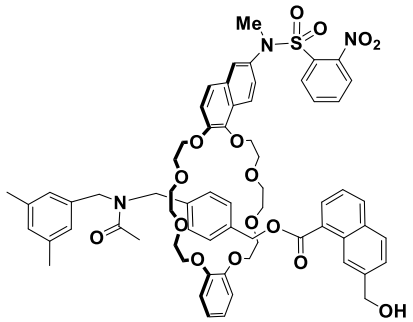

30

Rotaxane 30: According to the synthetic procedure of racemic rotaxane **13**, preparation of racemic rotaxane **30** was performed. Pale yellow amorphous (42 mg, 96%). HPLC conditions: After the kinetic resolution of racemic **30**, the recovered rotaxane **30** was purified by HPLC and converted to acylate **74** by DMAP for ease of chiral HPLC analysis. $[\alpha]_D^{20}$ -20.12 (major enantiomer, 68% ee, *c* 0.43, $CHCl_3$). ^{1}H NMR (400 MHz, $CDCl_3$): δ 8.85-8.82 (m, 1H), 8.72-8.67 (m, 1H), 8.04 (d, *J* = 7.8 Hz, 1H), 7.97 (d, *J* = 8.2 Hz, 1H), 7.89-7.86 (m, 1H), 7.74-7.67 (m, 2H), 7.63-7.57 (m, 3H), 7.52-7.36 (m, 4H), 7.26-7.18 (m, 2H), 7.12-7.04 (m, 2H), 7.00-6.98 (m, 1H), 6.88-6.85 (m, 1H), 6.77-6.74 (m, 3H), 6.67-6.63 (m, 3H), 6.27-6.24 (m, 2H), 4.81-4.79 (m, 2H), 4.61-4.53 (m, 1H), 4.50-4.30 (m, 3H), 4.27-4.18 (m, 3H), 4.15-4.07 (m, 1H), 4.04-3.94 (m, 4H), 3.91-3.77 (m, 3H), 3.73-3.60 (m, 4H), 3.57-3.33 (m, 10H), 3.30-3.26 (m, 1H), 3.22-3.17 (m, 1H), 2.25-2.21 (m, 6H), 2.12-2.10 (m, 3H). ^{13}C NMR (100 MHz, $CDCl_3$): δ 171.07, 170.93, 168.37, 168.34, 148.87, 148.30, 148.19, 141.62, 139.61, 139.53, 138.49, 138.01, 137.78, 137.37, 137.19, 136.39, 135.92, 135.86, 134.98, 134.05, 133.58, 132.84, 132.79, 131.68, 131.50, 131.16, 131.01, 130.07, 129.63, 129.21, 129.18, 129.07, 128.93, 128.57, 128.53, 128.47, 128.44, 128.39, 128.29, 127.17, 126.34, 125.96, 125.40, 125.18, 125.12, 125.01, 124.97, 124.43, 124.37, 124.31, 123.98, 123.76, 123.72, 123.68, 122.95, 120.26, 115.76, 115.70, 111.33, 111.19, 71.85, 70.91, 70.66, 70.33, 70.24, 69.90, 69.86, 69.70, 69.22, 68.09, 67.96, 67.81,

65.71, 50.52, 50.09, 47.59, 47.43, 39.48, 21.70, 21.24, 21.18. IR (neat): 3418, 3012, 2925, 2877, 1704, 1631, 1600, 1547, 1504, 1453, 1367, 1252, 1128, 1061, 755 cm^{-1}. HRMS (ESI): *m/z* calcd for $C_{66}H_{71}N_3O_{16}SNa$ $[M+Na]^+$: 1216.4447, found: 1216.4479.

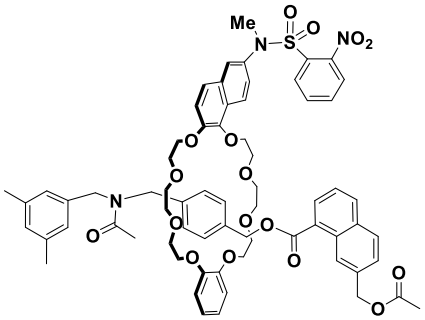

74

Acylate 74: Pale yellow amorphous. HPLC conditions: CHIRALPAK ID column, eluent 1:540 EtOH/$CHCl_3$, flow rate 0.7 ml/min, temperature 20 °C, 6.6 min (minor), 7.1 min (major). $[\alpha]_D^{20}$ +19.07 (major enantiomer, 62% ee, *c* 1.17, $CHCl_3$). ^{1}H NMR (400 MHz, $CDCl_3$): δ 9.02-9.00 (m, 1H), 8.90-8.86 (m, 1H), 8.03 (d, *J* = 8.2 Hz, 1H), 7.96 (d, *J* = 8.2 Hz, 1H), 7.88-7.86 (m, 1H), 7.77-7.71 (m, 2H), 7.62-7.56 (m, 3H), 7.51-7.49 (m, 1H), 7.45-7.42 (m, 2H), 7.40-7.35 (m, 1H), 7.29-7.26 (m, 1H), 7.20-7.17 (m, 1H), 7.14-7.07 (m, 1H), 7.04 (d, *J* = 7.8 Hz, 1H), 6.98 (d, *J* = 7.8 Hz, 1H), 6.88-6.85 (m, 1H), 6.76-6.73 (m, 3H), 6.70-6.67 (m, 3H), 6.25-6.22 (m, 2H), 5.26-5.24 (m, 2H), 4.60-4.52 (m, 1H), 4.49-4.46 (m, 1H), 4.40-4.34 (m, 2H), 4.27-4.12 (m, 4H), 4.07-4.00 (m, 4H), 3.94-3.78 (m, 3H), 3.72-3.61 (m, 4H), 3.53-3.36 (m, 10H), 3.33-3.29 (m, 1H), 3.26-3.22 (m, 1H), 2.25-2.22 (m, 6H), 2.12-2.09 (m, 6H). ^{13}C NMR (100 MHz, $CDCl_3$): δ 171.06, 170.92, 167.84, 148.93, 148.90, 148.31, 148.26, 148.19, 141.65, 141.63, 138.50, 138.01, 137.79, 137.40, 137.22, 136.42, 135.92, 135.88, 135.00, 134.46, 134.38, 134.06, 133.57, 133.14, 133.12, 132.11, 131.95, 131.83, 131.69, 131.26, 131.16, 131.00, 130.20, 129.76, 129.23, 129.19, 129.07, 128.93, 128.70, 128.67, 128.50, 128.47, 127.81, 127.76, 127.19, 126.35, 125.97, 125.84, 125.81, 125.58, 125.54, 125.39, 125.17, 125.11, 124.77, 124.45, 124.39, 123.99, 123.67, 122.96, 120.27, 115.74, 115.68, 111.31, 111.16, 71.85, 70.96, 70.70, 70.41, 70.31, 69.84, 69.75, 69.29, 68.21, 68.00, 67.85, 66.95, 50.51, 50.08, 47.59, 47.42, 39.48, 21.71, 21.24, 21.19, 21.04. IR (neat): 2925, 2855, 1738, 1706, 1641, 1599, 1547, 1504, 1454, 1369, 1254, 1124, 757 cm^{-1}. HRMS (ESI): *m/z* calcd for $C_{68}H_{73}N_3O_{17}SNa$ $[M+Na]^+$: 1258.4553, found: 1258.4569.

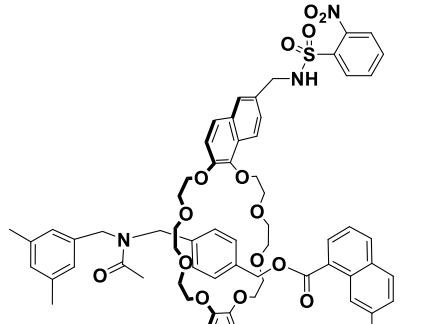

29

Rotaxane 29: According to the synthetic procedure of racemic rotaxane **13**, preparation of racemic rotaxane **29** was performed. Pale yellow amorphous (8.4 mg, 36%, 2 steps). HPLC conditions: CHIRALPAK ID column, eluent 1:40 EtOH/CH_2Cl_2, flow rate 0.5 ml/min, temperature 20 °C, 21.9 min (major), 24.1 min

(minor). $[\alpha]_D^{20}$ -27.37 (major enantiomer, 63% ee, *c* 1.21, $CHCl_3$). ^1H NMR (400 MHz, $CDCl_3$): δ 8.85-8.84 (m, 1H), 8.77-8.73 (m, 1H), 8.02 (d, *J* = 8.3 Hz, 1H), 7.94 (d, *J* = 8.3 Hz, 1H), 7.89-7.85 (m, 1H), 7.74-7.66 (m, 4H), 7.57-7.54 (m, 1H), 7.45-7.30 (m, 4H), 7.22-7.09 (m, 3H), 7.03-6.95 (m, 2H), 6.88-6.85 (m, 1H), 6.79-6.72 (m, 3H), 6.69-6.66 (m, 3H), 6.25-6.22 (m, 2H), 6.03-5.92 (m, 1H), 4.79-4.77 (m, 2H), 4.52-4.33 (m, 6H), 4.26-4.11 (m, 4H), 4.06-3.99 (m, 4H), 3.90-3.80 (m, 3H), 3.73-3.68 (m, 1H), 3.65-3.45 (m, 8H), 3.40-3.21 (m, 4H), 2.25-2.22 (m, 6H), 2.12-2.09 (m, 3H). ^{13}C NMR (100 MHz, $CDCl_3$): δ 171.20, 170.96, 168.17, 148.41, 148.24, 148.20, 148.18, 148.16, 147.58, 141.53, 141.44, 139.65, 139.59, 138.48, 138.00, 137.78, 137.36, 137.17, 136.34, 134.92, 134.00, 133.91, 133.09, 133.06, 132.84, 132.82, 132.34, 132.30, 131.73, 131.61, 131.36, 131.19, 130.96, 130.84, 129.99, 129.59, 129.05, 128.92, 128.88, 128.82, 128.67, 128.64, 128.56, 128.54, 128.20, 128.10, 127.13, 126.95, 126.89, 125.95, 125.62, 125.39, 124.97, 124.93, 124.29, 124.16, 124.07, 123.96, 123.71, 123.67, 122.03, 120.27, 115.14, 111.34, 111.22, 71.75, 70.86, 70.67, 70.26, 70.21, 69.91, 69.77, 69.70, 69.12, 69.10, 68.13, 67.91, 67.78, 65.65, 50.49, 50.04, 47.93, 47.89, 47.53, 47.41, 21.67, 21.23, 21.18. IR (neat): 3441, 3011, 2925, 2877, 1702, 1630, 1541, 1504, 1452, 1344, 1251, 1128, 1061, 753 cm^{-1}. HRMS (ESI): *m/z* calcd for $C_{66}H_{71}N_3O_{16}SNa$ $[M+Na]^+$: 1216.4447, found: 1216.4475.

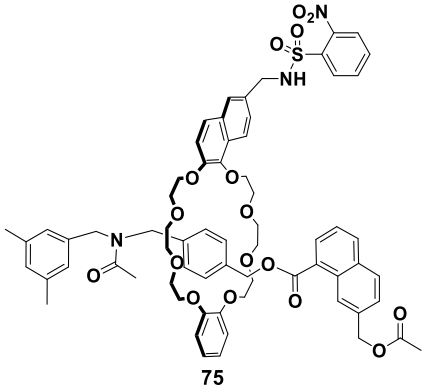

75

Acylate 75: Pale yellow amorphous. HPLC conditions: CHIRALPAK ID column, eluent 1:80 EtOH/CH_2Cl_2, flow rate 1.0 ml/min, temperature 20 °C, 9.2 min (minor), 9.8 min (major). $[\alpha]_D^{20}$ +19.13 (major enantiomer, 64% ee, *c* 0.79, $CHCl_3$). ^1H NMR (600 MHz, $CDCl_3$): δ 9.02 (s, 1H), 8.93-8.90 (m, 1H), 8.01 (d, *J* = 8.3 Hz, 1H), 7.92 (d, *J* = 8.3 Hz, 1H), 7.87-7.82 (m, 1H), 7.78-7.65 (m, 4H), 7.57-7.55 (m, 1H), 7.47-7.21 (m, 5H), 7.17-7.13 (m, 2H), 7.01-6.95 (m, 2H), 6.88-6.85 (m, 1H), 6.77-6.66 (m, 6H), 6.27-6.18, (m, 2H), 6.01-5.88 (m, 1H), 5.26-5.20 (m, 2H), 4.50-4.32 (m, 6H), 4.28-4.00 (m, 8H), 3.92-3.80 (m, 3H), 3.73-3.68 (m, 1H), 3.64-3.26 (m, 12H), 2.25-2.22 (m, 6H), 2.12-2.08 (m, 6H). ^{13}C NMR (150 MHz, $CDCl_3$): δ 171.11, 170.93, 167.74, 167.73, 148.49, 148.37, 148.32, 148.29, 148.26, 147.66, 141.54, 141.51, 138.50, 138.02, 137.82, 137.40, 137.25, 136.44, 135.00, 134.55, 134.48, 134.08, 134.02, 133.18, 133.09, 133.05, 132.33, 132.28, 132.18, 131.96, 131.87, 131.32, 131.00, 130.96, 130.89, 130.14, 129.75, 129.07, 128.93, 128.77, 128.71, 128.69, 128.58, 127.85, 127.79, 127.18, 127.01, 126.94, 126.00, 125.86, 125.80, 125.64, 125.59, 125.41, 124.99, 124.94, 124.80, 124.17, 124.08, 124.00, 121.11, 120.33, 120.30, 120.28, 115.21, 111.37, 111.24, 71.79, 70.95, 70.75, 70.38, 70.34, 69.97, 69.83, 69.79, 69.74, 69.68, 69.24, 69.20, 68.26, 68.01, 67.88, 66.94, 50.54, 50.09, 48.02, 47.97, 47.56, 47.46, 21.69, 21.25, 21.21, 21.05. IR (neat): 3012, 2924, 2878, 1738, 1707, 1633, 1603, 1541, 1452, 1346, 1251, 1128, 1062, 754 cm^{-1}. HRMS (ESI): *m/z* calcd for $C_{68}H_{73}N_3O_{17}SNa$ $[M+Na]^+$: 1258.4553, found: 1258.4613.

Ring component 34

^{1}H NMR (600 MHz, $CDCl_3$)

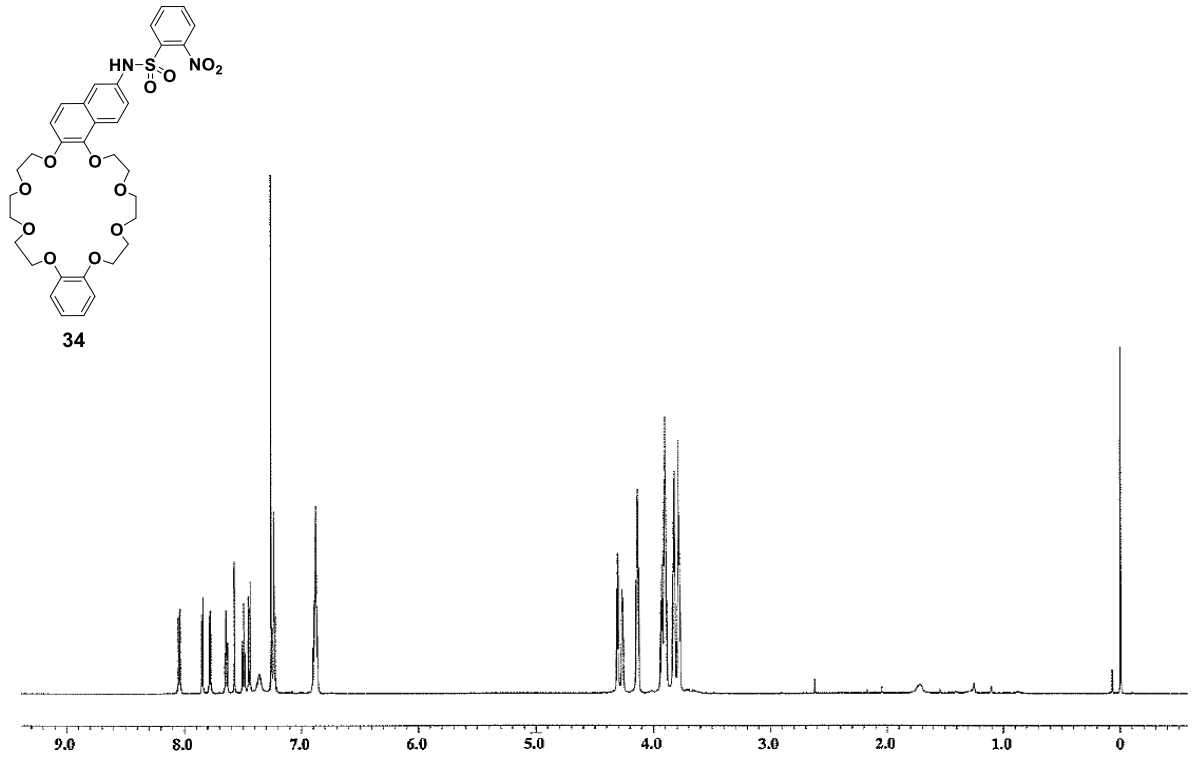

Rotaxane 13

^{1}H NMR (600 MHz, $CDCl_3$)

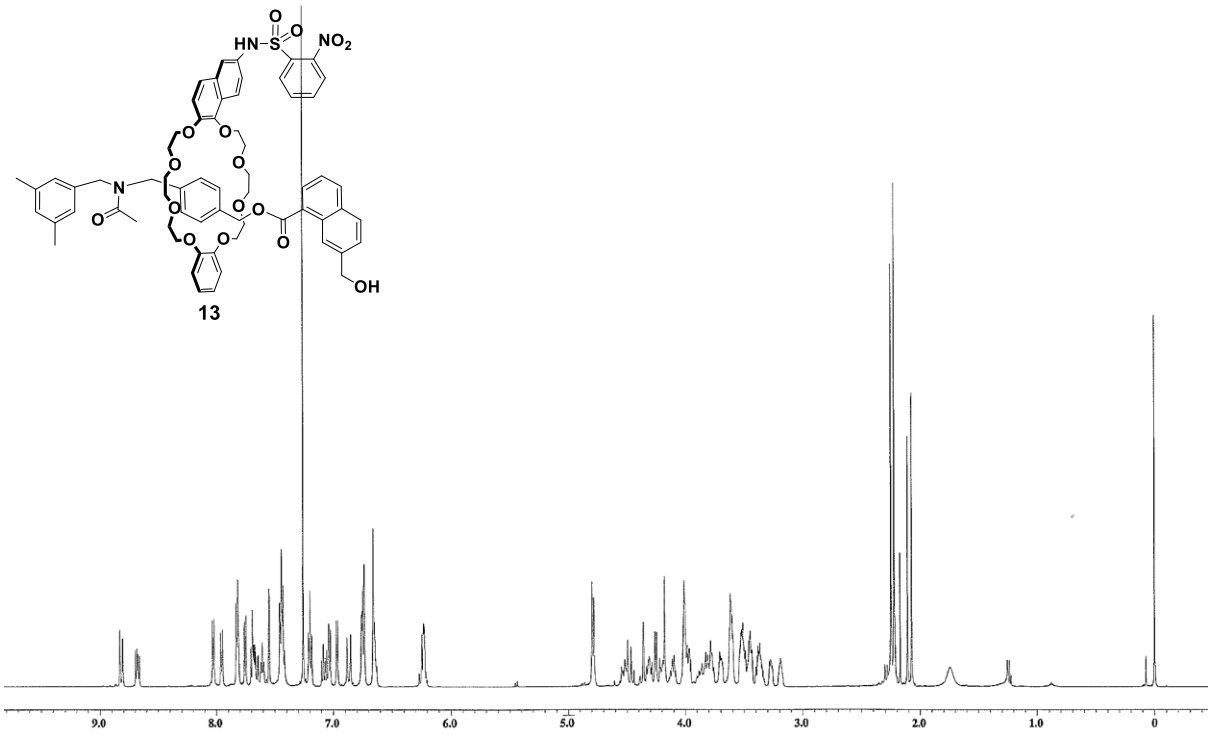

Ring component 36

^{1}H NMR (400 MHz, $CDCl_3$)

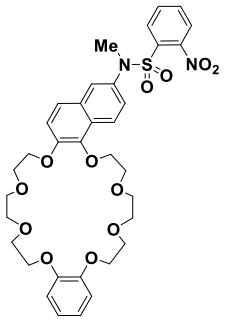

36

Rotaxane 30

^{1}H NMR (400 MHz, $CDCl_3$)

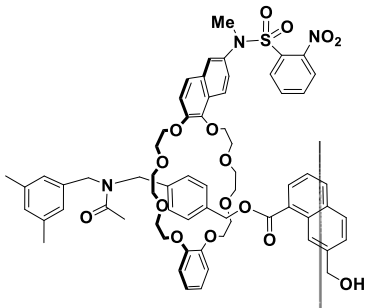

30

Ring component 35

^{1}H NMR (400 MHz, $CDCl_3$)

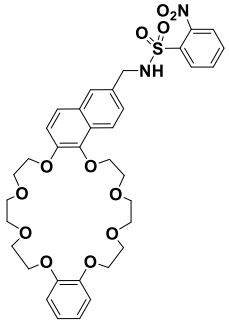

35

Rotaxane 29

^{1}H NMR (400 MHz, $CDCl_3$)

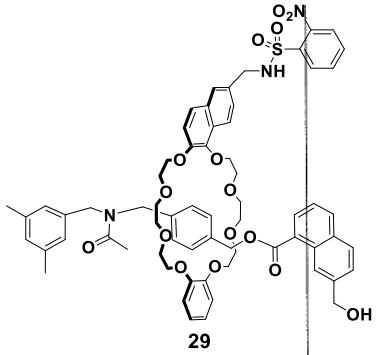

29

Acylate 14

^{1}H NMR (600 MHz, $CDCl_3$)

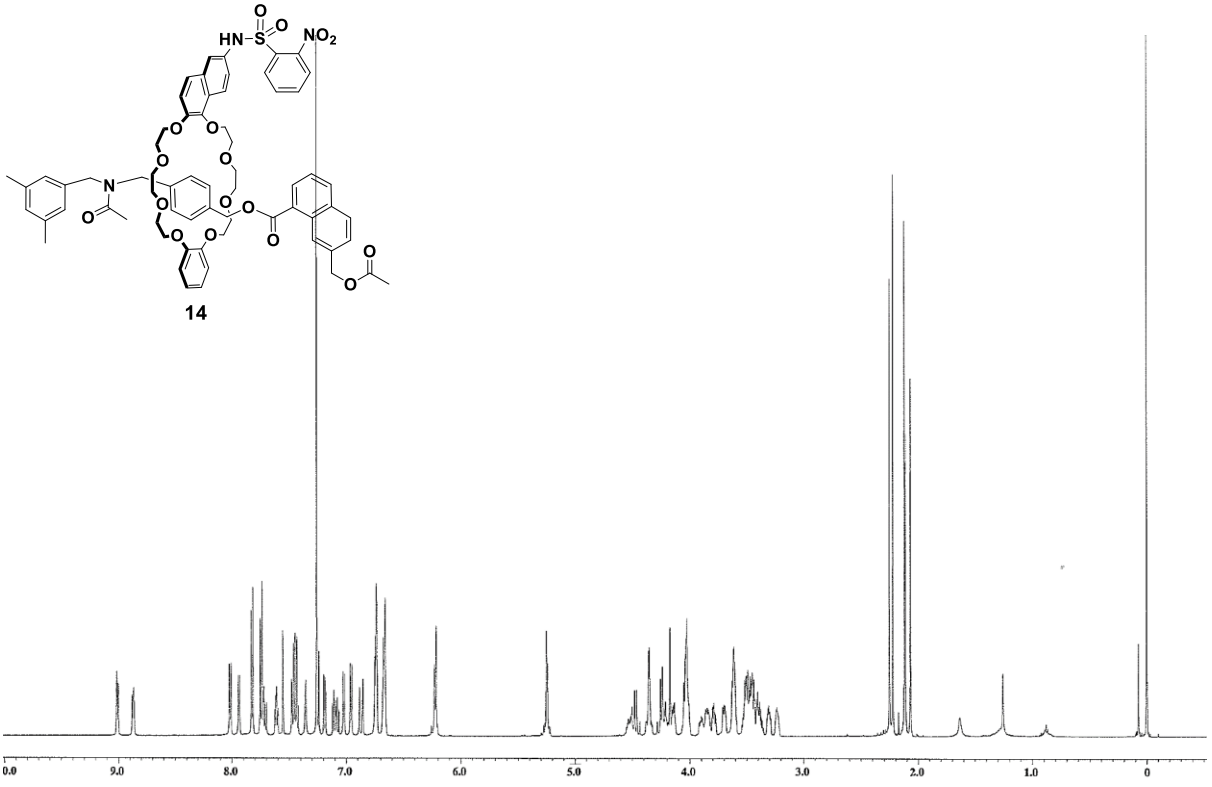

Acylate 14

^{1}H NMR (600 MHz, CD_3CN)

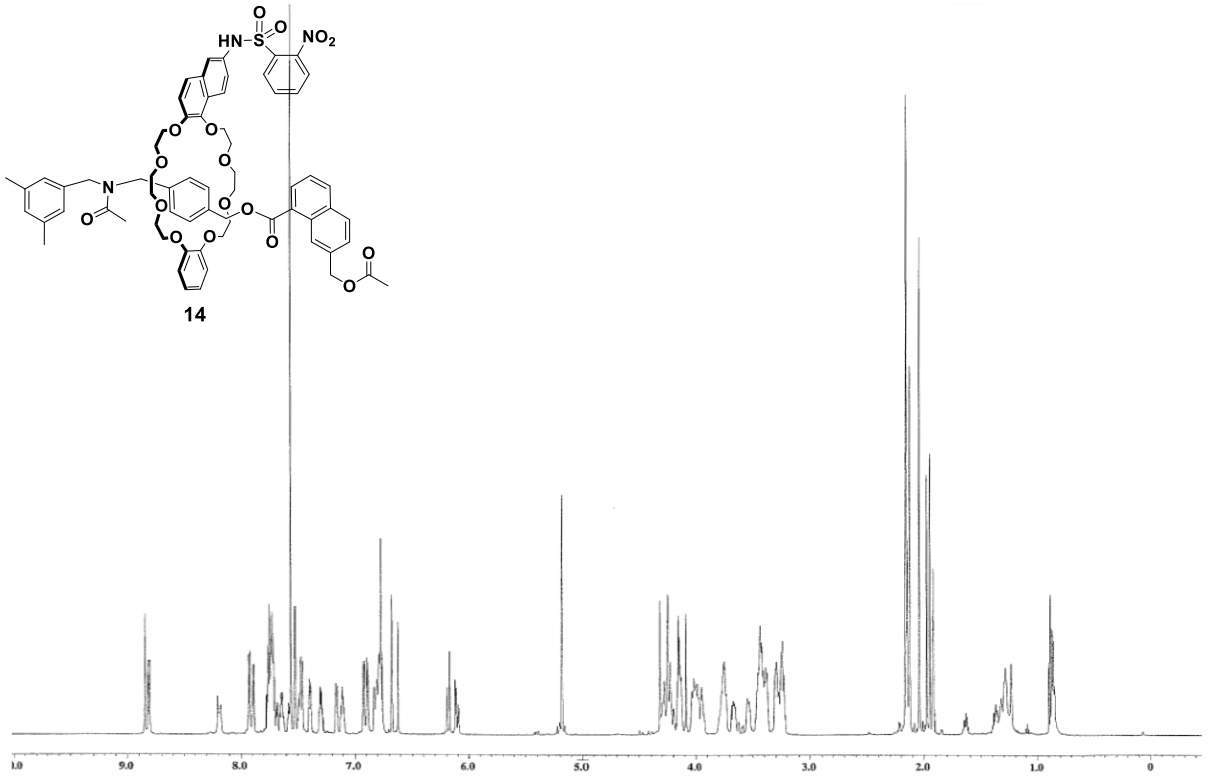

References and Notes

1. K. Boyack, D. Klavans, W. B. Paley, K. Börner, SCIENTIFIC METHOD: RELATIONSHIPS AMONG SCIENTIFIC PARADIGMS. *SEED* (2007).
2. K. W. Boyack, R. Klavans, K. Börner, Mapping the backbone of science. *Scientometrics* **64**, 351-374 (2005).
3. U. Eder, G. Sauer, R. Wiechert, New Type of Asymmetric Cyclization to Optically Active Steroid CD Partial Structures. *Angewandte Chemie-International Edition* **10**, 496-497 (1971).
4. Z. G. Hajos, D. R. Parrish, Asymmetric Synthesis of Bicyclic Intermediates of Natural Product Chemistry. *Journal of Organic Chemistry* **39**, 1615-1621 (1974).
5. B. List, R. A. Lerner, C. F. Barbas III, Proline-Catalyzed Direct Asymmetric Aldol Reactions. *Journal of the American Chemical Society* **122**, 2395-2396 (2000).
6. W. Notz, B. List, Catalytic Asymmetric Synthesis of *anti*-1,2-Diols. *Journal of the American Chemical Society* **122**, 7386-7387 (2000).
7. B. List, P. Pojarliev, C. Castello, Proline-Catalyzed Asymmetric AldolReactions between Ketones and α-Unsubstituted Aldehydes. *Organic Letters* **3**, 573-575 (2001).
8. E. R. Jarvo, S. J. Miller, Amino acids and peptides as asymmetric organocatalysts. *Tetrahedron*, **58**, 2481-2495 (2002).
9. A. Forni, I. Moretti, A. V. Prosyanik, G. Torr, Optically Active Trifluoromethylcarbinols as Chiral Solvating Agents for Asymmetric Transformations at a Ring -nitrogen Atom. *Journal of the Chemical Society, Chemical Communications*, 588-590 (1981).
10. G. H. Christie, J. Kenner, The Molecular Configurations of Polynuclear Aromatic Compounds. Part I. The Resolution of γ-6:6'-Dinitro- and 4:6:4':6'-Tetranitro-diphenic Acids into Optically Active Components. *Journal of Chemical Society, Transactions*, **121**, 614-620 (1922).
11. A. C. Cope, C. R. Ganellin, H. W. Jhonson, T. V. Van Auken, H. J. S. Winkler, Molecular Asymmetry of Olefins. I. Resolution of *trans*-Cycloctene, *Journal of the American Chemical Society* **85**, 3276-3279 (1963).
12. A. C. Cope, B. A. Pawson, Molecular Asymmetry of Olefins. IV. Kinetics of Racemization of (+ or -)-*trans*-Cyclooctene. *Journal of the American Chemical Society* **87**, 3649-3651 (1965).
13. M. S. Newman, W. B. Lutz, D. Lednicer, A NEW REAGENT FOR RESOLUTION BY COMPLEX FORMATION; THE RESOLUTION OF PHENANTHRO[3,4-*c*]PHENANTHRENE. *Journal of the American Chemical Society* **77**, 3420-3421 (1955).
14. M. S. Newman, D. Lednicer, The Synthesis and Resolution of Hexahelicene. *Journal of the American Chemical Society* **78**, 4765-4770 (1956).
15. G. Gottarelli, H. J. Hansen, G. P. Spada, R. H. Weber, 50. A Liquid-Crystal Study of Heptalene. *Helvetica Chimica Acta*, **70**, 430-435 (1987).
16. P. Finocchiaro, D. Gust, K. Mislow, Structure and Dynamic Stereochemistry of Trimesitylmethane. I. Synthesis and Nuclear Magnetic Resonance Studies. *Journal of the American Chemical Society* **96**, 2165-2167 (1974).
17. J. D. Andose, K. Mislow, Structure and Dynamic Stereochemistry of Trimesitylmethane. 1. Empirical Force Field Calculations. *Journal of the American Chemical Society* **96**, 2168-2176 (1974).
18. P. Finocchiaro, D. Gust, K. Mislow, Stereochemistry of Dimesityl-9-anthrylmethane and Bis(2,6-

xylyl)-1-(2-methylnaphthyl)methane. Evidence for the Two-Ring Flip Mechanism in Triarylmethanes. *Journal of the American Chemical Society* **96**, 2176-2182 (1974).

19. K. S. Hayes, M. Nagumo, J. F. Blount, K. Mislow, Structure, Optical Resolution, and Conformational Stability of Perchlorotriphenylamine. *Journal of the American Chemical Society* **102**, 2773-2776 (1980).
20. C. Thilgen, A. Herrmann, F. Diederieh, 16. Configurational Description of Chiral Fullerenes and Fullerene Derivatives with a Chiral Functionalization Pattern, *Helvetica Chimica Acta*, **80**, 183-199 (1997).
21. S. Shirakawa, S. Liu, S. Kaneko, Organocatalyzed Asymmetric Synthesis of Axially, Planar, and Helical Chiral Compounds. *Chemistry - An Asian Journal* (2015). DOI: 10.1002/asia.201500951.
22. D.-J. Cheng, L. Yan, S.-K. Tian, M.-Y. Wu, L.-X. Wang, Z.-L. Fan, S.-C. Zheng, X.-Y. Liu, B. Tan, Highly Enantioselective Kinetic Resolution of Axially Chiral BINAM Derivatives Catalyzed by a Brønsted Acid. *Angewandte Chemie-International Edition* **53**, 3684-3687 (2014).
23. R. Miyaji, K. Asano, S. Matsubara, Bifunctional Organocatalysts for the Enantioselective Synthesis of Axially Chiral Isoquinoline *N*-Oxides. *Journal of the American Chemical Society* **137**, 6766-6769 (2015).
24. A. Link, C. Sparr, Organocatalytic Atroposelective Aldol Condensation: Synthesis of Axially Chiral Biaryls by Arene Formation. *Angewandte Chemie-International Edition* **53**, 5458-5461 (2014).
25. N. Di Iorio, P. Righi, A. Mazzanti, M. Mancinelli, A. Ciogli, G. Bencivenni, Remote Control of Axial Chirality: Aminocatalytic Desymmetrization of *N*-Arylmaleimides via Vinylogous Michael Addition. *Journal of the American Chemical Society* **136**, 10250-10253 (2014).
26. L. Kötzner, M. J. Webber, A. Martínez, C. De Fusco, B. List, Asymmetric Catalysis on the Nanoscale: The Organocatalytic Approach to Helicenes. *Angewandte Chemie-International Edition* **53**, 5202-5205 (2014).
27. J. M. Hawkins, A. Meyer, Optically Active Carbon: Kinetic Resolution of C_{76} by Asymmetric Osmylation. *Science*, **260**, 1918-1920 (1993).
28. Y. Shoji, K. Tashiro, T. Aida, One-Pot Enantioselective Extraction of Chiral Fullerene C_{76} Using a Cyclic Host Carrying an Asymmetrically Distorted, Highly π-Basic Porphyrin Module. *Journal of the American Chemical Society* **132**, 5928-5929 (2010).
29. A. Ikeda, M. Ishikawa, J. Kikuchi, K. Nobusawa, Enantioselective Recognition of [60]Fullerene-Bisadducts by Cyclodextrin: Kinetic Control of a Mechanochemical High-Speed Vibration Milling Process. *Chemistry Letters*, **42** 1137-1139 (2013).
30. E. M. Pérez, N. Martín, Chiral recognition of carbon nanoforms. *Organic & Biomolecular Chemistry*, **10**, 3577-3583 (2012).
31. H. L. Frisch, E. Wasserman, CHEMICAL TOPOLOGY. *Journal of the American Chemical Society* **83**, 3789-3795 (1961).
32. C. Liang, K. Mislow, Topological chirality and achirality of links. *Journal of Mathematical Chemistry* **18**, 1-24 (1995).
33. C. Wolf, Dynamic stereochemistry of chiral compounds: principles and applications. *RSC (Royal*

Society of Chemistry) Publishing, Cambridge (2008).

34. Y. Makita, N. Kihara, N. Nakakoji, T. Takata, S. Inagaki, C. Yamamoto, Y. Okamoto, Catalytic asymmetric synthesis and optical resolution of planar chiral rotaxane. *Chemistry Letters* **36**, 162-163 (2007).
35. K. Yoshida, T. Furuta, T. Kawabata, Organocatalytic Chemoselective Monoacylation of 1,*n*-Linear Diols. *Angewandte Chemie-International Edition* **50**, 4888-4892 (2011).
36. K. Yoshida, T. Shigeta, T. Furuta, T. Kawabata, Catalyst-controlled reversal of chemoselectivity in acylation of 2-aminopentane-1,5-diol derivatives. *Chemical Communications* **48**, 6981-6983 (2012).
37. T. Kawabata, W. Muramatsu, T. Nishio, T. Shibata, H. Schedel, A Catalytic One-Step Process for the Chemo- and Regioselective Acylation of Monosaccharides. *Journal of the American Chemical Society* **129**, 12890-12895 (2007).
38. K. Yoshida, K. Mishiro, Y. Ueda, T. Shigeta, T. Furuta, T. Kawabata, Non-Enzymatic Geometry-Selective Acylation of Tri- and Tetrasubstituted α,α'-Alkenediols. *Advanced Synthesis & Catalysis* **354**, 3291-3298 (2012).
39. T. Shigeta, PhD thesis, Kyoto University (2014).
40. E. R. Kay, D. A. Leigh, F. Zerbetto, Synthetic molecular motors and mechanical machines. *Angewandte Chemie-International Edition* **46**, 72-191 (2007).
41. E. A. Neal, S. M. Goldup, Chemical consequences of mechanical bonding in catenanes and rotaxanes: isomerism, modification, catalysis and molecular machines for synthesis. *Chemical Communications* **50**, 5128-5142 (2014).
42. K. Ito, Novel Cross-Linking Concept of Polymer Network: Synthesis, Structure, and Properties of Slide-Ring Gels with Freely Movable Junctions. *Polymer Journal*, **39**, 489-499 (2007)
43. Y. Okumura, K. Ito, The Polyrotaxane Gel: A Topological Gel by Figure-of-Eight Cross-links. *Advanced Material*, **13**, 485-487 (2001).
44. T. Takata, Y. Koyama, K. Nakazono, T. Hasegawa, Y. G. Lee, N. Ono, K. Nishio, Y. Fujita, Rotaxane compound and anticancer agent, Japan Patent WO2010047094 A1 (2010-04-29).
45. R. Barat, T. Legigan, I. Tranoy-Opalinski, B. Renoux, E. Péraudeau, J. Clarhaut, P. Poinot, A. E. Fernandes, V. Aucagne, D. A. Leigh, S. Papot, A mechanically interlocked molecular system programmed for the delivery of an anticancer drug. *Chemical Science*, **6**, 2608-2613 (2015).
46. Y. Tachibana, N. Kihara, T. Takata, Asymmetric Benzoin Condensation Catalyzed by Chiral Rotaxanes Tethering a Thiazolium Salt Moiety via the Cooperation of the Component: Can Rotaxane Be an Effective Reaction Field? *Journal of the American Chemical Society* **126**, 3438-3439 (2004).
47. G. Hattori, T. Hori, Y. Miyake, Y. Nishibayashi, Design and Preparation of a Chiral Ligand Based on a Pseudorotaxane Skeleton: Application to Rhodium-Catalyzed Enantioselective Hydrogenation of Enamides. *Journal of the American Chemical Society* **129**, 12930-12931 (2007).
48. J. Beswick, V. Blanco, G. De Bo, D. A. Leigh, U. Lewandowska, B. Lewandowski, K. Mishiro, Selecting reactions and reactants using a switchable rotaxane organocatalyst with two different active sites. *Chemical Science*, **6**, 140-143 (2015).
49. M. Yamanaka, U. Yoshida, M. Sato, T. Shigeta, K. Yoshida, T. Furuta, T. Kawabata, Origin of High *E*-Selectivity in 4-Pyrrolidinopyridine-Catalyzed Tetrasubstitutedα,α'-Alkenediols: A Computational and Experimental Study. *Journal of Organic Chemistry* **80**, 3075-3082 (2015).

50. C. A. Lewis, B. R. Sculimbrene, Y. Xu, S. J. Miller, Desymmetrization of Glycerol Derivatives with Peptide-Based Acylation Catalysts. *Organic Letters* **7**, 3021-3023 (2005).
51. S. Takahashi, T. Katagiri, K. Uneyama, A binary hydrogen bonding motif based on homochiral recognition: crystal structures and hydrogen bonding networks of meso-(R,S)-bis(trifluorolactate)s. *Chemical Communications* 3658-3660 (2005).
52. M. Iwashita, K. Makide, T. Nonomura, Y. Misumi, Y. Otani, M. Ishida, R. Taguchi, M. Tsujimoto, J. Aoki, H. Arai, T. Ohwada, Synthesis and Evaluation of Lysophosphatidylserine Analogues as Inducers of Mast Cell Degranulation. Potent Activities of Lysophosphatidylthreonine and Its 2-Deoxy Derivative. *Journal of Medicinal Chemistry* **52**, 5837-5863 (2009).
53. H. E. Giesbrecht, B. J. Knight, N. R. Tanguileg, C. R. Emerson, P. R. Blakemore, Thieme Chemistry Journal Awardees – Where Are They Now? Stereoselective Synthesis of *Z*-Configured a,b-Unsaturated Macrocyclic Lactones and Diolides by Intramolecular Julia–Kocienski Olefination. *Synlett* **3**, 374-378 (2010).
54. A. B. Hajjar, P. F. Nicks, C. J. Knowles, Preparation of monomeric acrylic ester intermediates using lipase catalyzed transesterifications in organic solvents. *Biotechnology Letters* **12**, 825-830 (1990).
55. V. Framis, F. Camps, P. Clapés, Lipase-catalysed selective monoacylation of 1,n-diols with vinyl acetate. *Tetrahedron Letters* **45**, 5031-5033 (2004).
56. The reproducibility was confirmed, see: Table 2, entry 7 of reference 32.
57. S. Xu, I. Held, B. Kempf, H. Mayr, W. Steglich, H. Zipse, The DMAP-Catalyzed Acetylation of Alcohols—A Mechanistic Study (DMAP=4-(Dimethylamino)pyridine). *Chemistry-A European Journal* **11**, 4751-4557 (2005).
58. E. Larionov, H. Zipse, Organocatalysis: acylation catalysts. *Wiley Interdisciplinary Reviews: Computational Molecular Science* **1**, 601-619 (2011).
59. H. Kawasaki, N. Kihara, T. Takata, High Yielding and Practical Synthesis of Rotaxanes by Acylative End-Capping Catalyzed by Tributylphohine. *Chemistry Letters* **28**, 1015-1016 (1999).
60. N. Kihara, J-I. Shin, Y. Ohga, T. Takata, Direct Preparation of Rotaxane from Aminoalcohol: Selective *O*-Acylation of Aminoalcohol in the Presence of Trifluoromethanesulfonic Acid and Crown Ether. *Chemistry Letters* **30**, 592-593 (2001).
61. N. Kihara, N. Nakakoji, T. Takata, Trbutylphosphine-catalyzed Acylation of Alcohol by Active Ester Directed toward Effective End-capping of Pseudorotaxane Consisting of Ammonium Group and Crown Ether. *Chemistry Letters* **31**, 924-925 (2002).
62. Y. Tachibana, H. Kawasaki, N. Kihara, T. Takata, Sequential O- and N-acylation protocol for high-yield preparation and modification of rotaxanes: Synthesis, functionalization, structure, and intercomponent interaction of rotaxanes. *Journal of Organic Chemistry* **71**, 5093-5104 (2006).
63. This condition is the optimized condition of kinetic resolution of rotaxanes discussed in Chapter 4 in this thesis (Figure 51A, entry 5).
64. M. Yanagi, PhD thesis, Kyoto University (2015).
65. C. Yamamoto, Y. Okamoto, T. Schmidt, R. Jager, F. Vogtle, Enantiomeric resolution of cycloenantiomeric rotaxane, topologically chiral catenane, and pretzel-shaped molecules: Observation of pronounced circular dichroism. *Journal of the American Chemical Society* **119**, 10547-10548 (1997).

66. R. Schmieder, G. Hubner, C. Seel, F. Vogtle, The first cyclodiasteromeric [3] rotaxane. *Angewandte Chemie-International Edition* **38**, 3528-3530 (1999).
67. E. A. Neal, S. M. Goldup, Chemical consequences of mechanical bonding in catenanes and rotaxanes: isomerism, modification, catalysis and molecular machines for synthesis. *Chemical Communications* **50**, 5128-5142 (2014).
68. A. Theil, C. Mauve, M. T. Adeline, A. Marinetti, J. P. Sauvage, Phosphorus-containing 2 catenanes as an example of interlocking chiral structures. *Angewandte Chemie-International Edition* **45**, 2104-2107 (2006).
69. M. Alvarez-Perez, S. M. Goldup, D. A. Leigh, A. M. Z. Slawin, A chemically-driven molecular information ratchet. *Journal of the American Chemical Society* **130**, 1836-1838 (2008).
70. Y. Tachibana, N. Kihara, T. Takata, Asymmetric benzoin condensation catalyzed by chiral rotaxanes tethering a thiazolium salt moiety via the cooperation of the component: Can rotaxane be an effective reaction field? *Journal of the American Chemical Society* **126**, 3438-3439 (2004).
71. G. Hattori, T. Hori, Y. Miyake, Y. Nishibayashi, Design and preparation of a chiral ligand based on a pseudorotaxane skeleton: Application to rhodium-catalyzed enantioselective hydrogenation of enamides. *Journal of the American Chemical Society* **129**, 12930-12931 (2007).
72. Y. Okada, Z. H. Miao, M. Akiba, J. Nishimura, Synthesis and characterization of chiral catenanes based on rigid calix 4 arene. *Tetrahedron Letters* **47**, 2699-2702 (2006).
73. P. Mobian, N. Banerji, G. Bernardinelli, J. Lacour, Towards the stereoselective synthesis of inherently chiral pseudorotaxanes. *Organic & Biomolecular Chemistry* **4**, 224-231 (2006).
74. R. J. Bordoli, S. M. Goldup, An Efficient Approach to Mechanically Planar Chiral Rotaxanes. *Journal of the American Chemical Society* **136**, 4817-4820 (2014).
75. P. E. Glen, J. A. T. O'Neill, A.-L. Lee, Synthesis of a C-1-symmetric Box macrocycle and studies towards active-template synthesis of mechanically planar chiral rotaxanes. *Tetrahedron* **69**, 57-68 (2013).
76. G. A. Breault, C. A. Hunter, P. C. Mayers, Supramolecular topology. *Tetrahedron* **55**, 5265-5293 (1999).
77. J. M. Keith, J. F. Larrow, E. N. Jacobsen, Practical considerations in kinetic resolution reactions. *Advanced Synthesis & Catalysis* **343**, 5-26 (2001).
78. E. Vedejs, M. Jure, Efficiency in nonenzymatic kinetic resolution. *Angewandte Chemie-International Edition* **44**, 3974-4001 (2005).
79. V. B. Birman, X. M. Li, Benzotetramisole: A remarkably enantioselective acyl transfer catalyst. *Organic Letters* **8**, 1351-1354 (2006).
80. S. E. A. Ozbabacan, H. B. Engin, A. Gursoy1, O. Keskin, Transient protein-protein interactions. *Protein Engineering, Design & Selection*, 1-14 (2011).
81. J. R. Perkins, I. Diboun, B. H. Dessailly, J. G. Lees, C. Orengo, Transient Protein-Protein Interactions: Structural, Functional, and Network Properties. *Structure* **18**, 1233-1243 (2010).

Acknowledgements

Firstly, I express my sincere gratitude to Professor Takeo Kawabata (Kyoto University) for his generous discussion, thoughtful guidance, support and help throughout the research. I am truly happy to have been able to lay the foundation as a researcher, learning his attractive research perspective and personality, over six years on the first stage of my research life.

I wish to thank Associate Professor Tomoyuki Yoshimura (Kanazawa University) for discussing my ideas, and sharing his sophisticated skills, knowledge and experience. I am thankful to Associate Professor Takumi Furuta (Kyoto University) for his valuable and useful discussions and suggestions. I am grateful to Assistant Professor Yoshihiro Ueda (Kyoto University) for useful discussion on a wide range of matters.

I am really grateful to Professor Masahiro Yamanaka (Rikkyo University) and Dr. Makoto Sato for their substantial contributions to DFT calculations and useful discussions. I would like to thank Lecturer Kazuto Takaishi (Okayama University) and Professor Kenji Monde (Hokkaido University) for calculations of supramolecules. I wish to thank Professor Kazunori Tsubaki (Kyoto Prefectural University) for helpful advice on NMR experiments.

I would like to thank Professor Shiro Futaki (Kyoto University) and Special Lecturer Ikuhiko Nakase (Osaka Prefecture University) for their kind guidance in measurement of MALDI mass spectrometry, Professor Masaharu Nakamura (Kyoto University) and Associate Professor Hikaru Takaya (Kyoto University) for their helpful guidance in measurement of ESI mass spectrometry, Ms. Kyoko Omine for measuring variable-temperature NMR spectra, and Ms. Akiko Fujihashi for mass spectrometry.

I would like to express my appreciation to Professor Kiyosei Takasu (Kyoto University) and Professor Yoshiji Takemoto (Kyoto University) for reviewing my thesis and for providing valuable comments.

I wish to thank Professor Jun Hiratake (Kyoto University) for his useful guidance in research ethics. I gratefully thank all members of the pocket seminar for enjoyable discussion.

I would like to thank Professor Ivan Huc (University of Bordeaux) and all members of Huc group for giving me the valuable opportunity to learn their excellent chemistry. My stay in France was supported by The Kyoto University Foundation.

I am grateful to Dr. Bhatraju Vasantha Lakshmi, Dr. Keisuke Yoshida, Dr. Keisuke Tomohara, Dr. Kenji Mishiro, Dr. Shohei Hamada, Dr. Takashi Shigeta and Mr. Masanori Yanagi for their valuable discussions and suggestions. I express my gratitude to Mr. Hironori Takeuchi, Mr. Ryuichi Hyakutake and Mr. Atsushi Hirata for their kind help and constant encouragement over several years. I am thankful to the secretary, Ms. Kaori Hashimoto, for her support. I gratefully thank all past and present members of Kawabata group for active discussions and sharing various experiences.

This study was supported by Japan Society for the Promotion of Science (15J10954).

I express my deep gratitude to my parents, sister and grandparents for their kind support, understanding and continuous encouragement.

Finally, I thank my husband, Ryuji, with all my heart. He has always made me happy and words cannot express how grateful I am. I would like to share many adventures and dreams together in the future too.

Ayumi Imayoshi